Max-Planck-Institut
für Meteorologie

MAX-PLANCK-GESELLSCHAFT

International Max Planck Research School
on Earth System Modelling

Estimation of evapotranspiration using satellite TOA radiances

Jian Peng

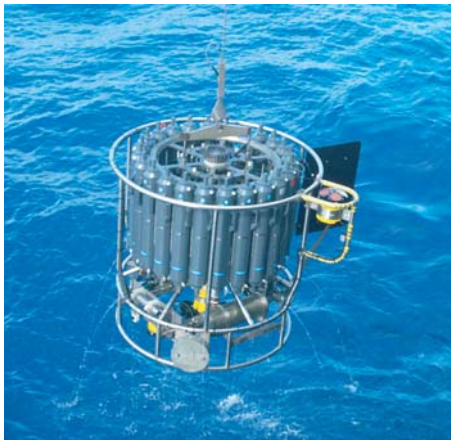

Berichte zur Erdsystemforschung 140/2013

Reports on Earth System Science

Hinweis

Die Berichte zur Erdsystemforschung werden vom Max-Planck-Institut für Meteorologie in Hamburg in unregelmäßiger Abfolge herausgegeben.

Sie enthalten wissenschaftliche und technische Beiträge, inklusive Dissertationen.

Die Beiträge geben nicht notwendigerweise die Auffassung des Instituts wieder.

Die "Berichte zur Erdsystemforschung" führen die vorherigen Reihen "Reports" und "Examensarbeiten" weiter.

Notice

The Reports on Earth System Science are published by the Max Planck Institute for Meteorology in Hamburg. They appear in irregular intervals.

They contain scientific and technical contributions, including Ph. D. theses.

The Reports do not necessarily reflect the opinion of the Institute.

The "Reports on Earth System Science" continue the former "Reports" and "Examensarbeiten" of the Max Planck Institute.

Anschrift / Address

Max-Planck-Institut für Meteorologie
Bundesstrasse 53
20146 Hamburg
Deutschland

Tel.: +49-(0)40-4 11 73-0
Fax: +49-(0)40-4 11 73-298
Web: www.mpimet.mpg.de

Layout:

Bettina Diallo, PR & Grafik

Titelfotos:
vorne:
Christian Klepp - Jochem Marotzke - Christian Klepp
hinten:
Clotilde Dubois - Christian Klepp - Katsumasa Tanaka

Berichte zur Erdsystemforschung 140/2013

Estimation of evapotranspiration using satellite TOA radiances

Jian Peng

aus Jiangsu, China

Hamburg 2013

Reports on Earth System Science 140/2013

ISSN 1614-1199

Jian Peng
Max-Planck-Institut für Meteorologie
Bundesstrasse 53
20146 Hamburg

Als Dissertation angenommen
vom Department Geowissenschaften der Universität Hamburg

auf Grund der Gutachten von
Prof. Dr. Martin Claußen
und
Dr. Alexander Löw

Hamburg, den 22. Oktober 2013
Prof. Dr. Christian Betzler
Leiter des Departments für Geowissenschaften

ISSN 1614-1199

Estimation of evapotranspiration using satellite TOA radiances

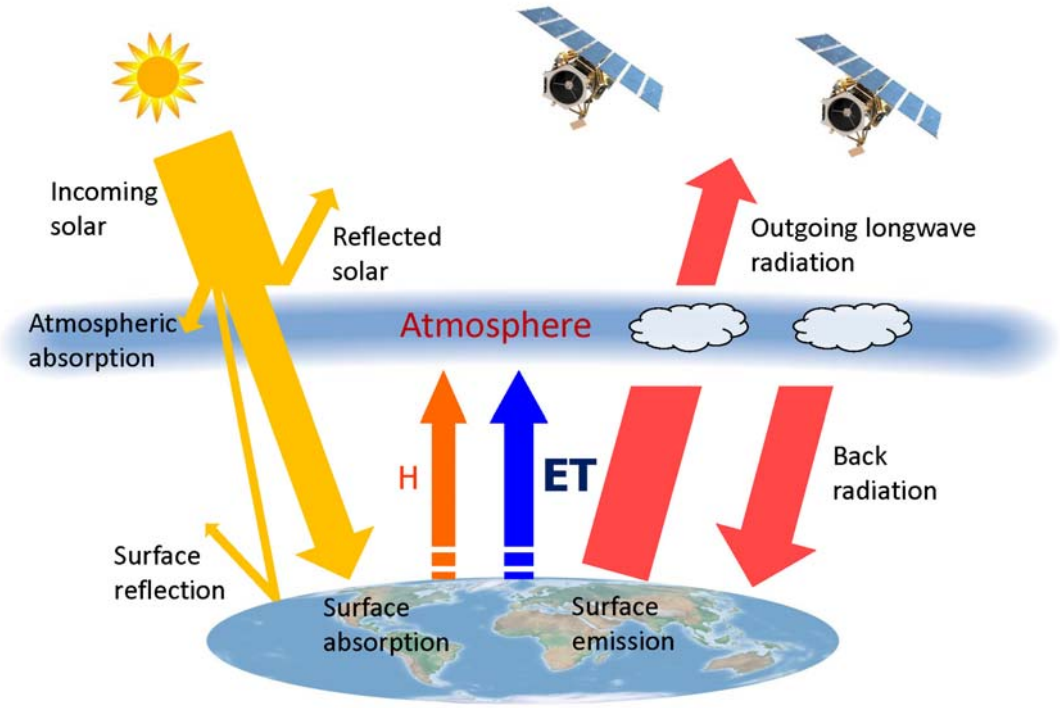

Jian Peng

Hamburg 2013

Abstract

ET (Evapotranspiration) is an important variable in the water and energy balance on the Earth's surface and a key process in the climate system. Accurate estimation of the temporal and spatial pattern of ET is of great significance for better understanding the mechanism of climate change and plays a crucial role in hydrological, agricultural and meteorological studies. A simplified single-source energy balance parameterization scheme, known as the LST/NDVI (Land Surface Temperature/Normalized Difference Vegetation Index) feature space method, has been applied successfully to estimate clear sky ET in many studies. Based on the LST/NDVI feature space method, a new method is proposed in this thesis to estimate ET directly using the TOA (Top of Atmosphere) radiances without performing atmospheric correction and other complicated processes.

Firstly, the feasibility and uncertainties in estimating NDTI (Normalized Difference Temperature Index, a key parameter in EF (evaporative fraction) estimation) from TOA radiances are investigated. Through a physical understanding of the Planck radiation law and radiative transfer equation, together with a detailed sensitivity analysis of NDTI on surface and atmosphere variability, it is found that the NDTI can be estimated from TOA radiances with an accuracy of 90% if the spatial variabilities of atmospheric parameters (water vapor, effective atmospheric temperature) and surface emissivity are below 10%, 4 K, and 0.05, respectively. A test study is performed using MODIS (Moderate Resolution Imaging Spectroradiometer) data at a regional scale. The TOA radiance-estimated NDTI value and LST-determined NDTI value are quite close, which indicates that the use of TOA radiances appears to be adequate for estimating NDTI in these case studies.

Then the applicability and robustness of the MODIS TOA radiances based EF estimation scheme are investigated using FLUXNET (a global network of eddy covariance stations) observations. From direct comparison with measured EF at different FLUXNET sites, the estimated EF from TOA radiances perform mostly well across a wide variety of climate and biome types. The accuracy level is also comparable with published results in the literature. Diagnostic analysis suggests that large error sources of EF estimates from TOA radiances are related to precipitation before satellite overpass.

Furthermore, the FLUXNET measurements are used to examine the assumption of EF self preservation, and the conditions under which it can hold. It is found that the instantaneous EF can represent daytime EF under clear sky conditions especially between 11:00 h LT (local time) and 14:00 h LT for all stations, and the midday (12:00 h LT to 13:00 h LT) EF is closest to daytime EF. However, the EF is more variable during cloudy skies so that an increase in cloud cover results in an increase in the variability of the EF during daytime.

Finally, a new parameterization scheme to estimate daytime ET directly using TOA radiances is proposed and evaluated over a regional scale. The instantaneous EF

and net radiation are derived respectively based entirely on MODIS TOA radiances. Then daytime ET maps are estimated from these EF and net radiation maps by using a sinusoidal temporal interpolation model. To evaluate the performance of the TOA radiances based estimates, the estimated EF, net radiation and ET are compared with field observations and MODIS products based estimates. The results indicate comparable accuracy to results of other current widely used satellite-based methods. Overall, the proposed algorithm requires fewer assumptions and can avoid complex atmospheric corrections associated with the satellite derived products. It provides a useful alternative for determining ET and relevant applications as well.

Zusammenfassung

ET (Evapotranspiration) ist eine wichtige Variable im Wasser- und Energiehaushalt der Erdoberfläche und ein Schlüsselprozess im Klimasystem. Die genaue Bestimmung der zeitlichen und räumlichen Muster von ET ist von großer Bedeutung für das Verständnis der Mechanismen des Klimawandels und spielt eine entscheidende Rolle in hydrologischen, landwirtschaftlichen und meteorologischen Studien. Eine vereinfachte Parametrisierung der Energiebilanz, bekannt als die LST/NDVI (Landoberflächentemperatur / normalisierter differenzierter Vegetationsindex) Methode, wurde vielfach erfolgreich zur Abschätzung von ET unter wolkenlosen Bedingungen angewendet. Auf dieser Basis wurde in der vorliegenden Arbeit eine neue Methode entwickelt, um ET direkt mit Hilfe von Strahldichten an der Atmosphärenobergrenze (TOA) ohne Atmosphärenkorrektur oder Berücksichtigung anderer komplizierter Prozesse abzuschätzen.

Zuerst wurden die Machbarkeit und die Unsicherheiten der Ableitung des NDTI (normalisierter differenzierter Temperaturindex, ein Schlüsselparameter in der Abschätzung des Verdunstungsanteils (EF)) aus den TOA-Strahldichten untersucht. Aus dem physikalischen Verständnis des Planck'schen Strahlungsgesetzes und der Strahlungstransportgleichung und einer detaillierten Sensitivitätsstudie des NDTI bezüglich Oberflächen- und Atmosphärenvariabilität ergab sich, dass der NDTI mit einer Genauigkeit von 90% abgeschätzt werden kann, wenn die räumliche Variabilität der atmosphärischen Wasserdampfsäule, der effektiven Atmosphärentemperatur und der Bodenemissivität kleiner als 10%, 4K und 0.05 sind. Dazu wurde eine Teststudie mit MODIS (Moderate Resolution Imaging Spectroradiometer) Daten auf einer regionalen Skala durchgeführt. Der NDTI Wert berechnet aus den Strahldichten gleicht beinahe dem NDTI Wert der aus LST bestimmt wurde, was darauf hindeutet, dass die Verwendung der TOA Radianzen zur Berechnung von NDTI in diesen Teststudien angebracht erscheint.

Dann wurde die Anwendbarkeit und Robustheit der Abschätzung von EF basierend auf den MODIS TOA-Strahldichten mit Hilfe von FLUXNET (ein globales Netzwerk aus Eddy-Kovarianz-Messstationen) Beobachtungen untersucht. Ein direkter Vergleich mit gemessenen EF Werten an verschiedenen FLUXNET Stationen ergab, dass der abgeschätzte EF Wert aus den TOA-Strahldichten über verschiedene Klimate und Biome hinweg den In-situ-Messwerten nahe kommt. Die Genauigkeit ist vergleichbar mit veröffentlichten Werten in der Literatur. Diagnostische Analysen legen nahe, dass die größten Abweichungen von Niederschlag aus dem Zeitraum vor dem verwendeten Satellitenüberflug stammen.

Zusätzlich wurden die FLUXNET Messungen zur Untersuchung der Annahme der Selbsterhaltung von EF und der Bedingungen für diese Annahme verwendet. Dabei zeigt sich, dass die Instantanwerte von EF an allen Stationen unter wolkenlosen Bedingungen insbesondere zwischen 11:00 und 14:00 h LT (Lokalzeit) den Tageswert (Mittelwert zwischen 8:00 und 17:00 h LT) gut repräsentieren, wobei der Mittagswert

von EF (zwischen 12:00 und 13:00 h LT) dem Tageswert am nächsten kommt. Allerdings schwankt EF bei Bewölkung stärker, so dass eine Zunahme der Bewölkung mit einer Zunahme der Variabilität von EF während des Tages einher geht.

Schließlich wurde ein neues Parameterisierungsschema für Tageswerte von ET aus TOA-Strahldichten entwickelt und auf einer regionalen Skala evaluiert. Die Instantanwerte von EF und Nettostrahlung werden dazu gänzlich aus den MODIS TOA-Strahldichten hergeleitet. Dann werden tägliche ET-Karten mit Hilfe einer sinusförmigen Zeitinterpolation berechnet. Zur Genauigkeitsabschätzung werden die aus den TOA-Strahldichten abgeschätzte EF, Nettostrahlung und ET mit Feldbeobachtungen und MODIS Produkten verglichen. Die Ergebnisse deuten darauf hin, dass die Genauigkeit vergleichbar ist mit anderen weit verbreiteten satellitenbasierten Methoden. Insgesamt benötigt der entwickelte Algorithmus weniger Annahmen und kommt ohne komplizierte atmosphärische Korrekturen aus, wie sie bei anderen Satellitenprodukten üblich sind. Somit stellt er eine nützliche Alternative zur Bestimmung von ET und für weitere relevante Anwendungen dar.

Contents

List of Figures

List of Tables

Chapter 1

Introduction

1.1 Motivation and Objectives

ET (Evapotranspiration[1]) is an important link of global water, energy and carbon cycles and a key process in the climate system through the mass and energy interactions between land and atmosphere (Jung et al., 2010). About two-thirds of the annual land precipitation is re-evaporated by ET (see Figure 1.1) (Chahine, 1992; Oki and Kanae, 2006). The energy used for ET is referred as LE (latent heat flux), where L is the latent heat of vaporization (J Kg^{-1}). As one important component of Earth's global energy balance (Figure 1.2), the LE helps to control surface temperatures, which has important implications for the occurrences of serious heat waves and droughts (Seneviratne et al., 2006; Teuling et al., 2013). It should be noted here that the terms LE and ET are used interchangeably in this thesis. The knowledge of ET is also essential for water resources management applications such as industrial water use, the provision of irrigation and drinking water (Oki and Kanae, 2006). Therefore, accurate estimation of temporal and spatial pattern of ET is of great significance for better understanding the mechanism of climate change and plays a crucial role in hydrological, agricultural and meteorology studies (Sellers et al., 1997).

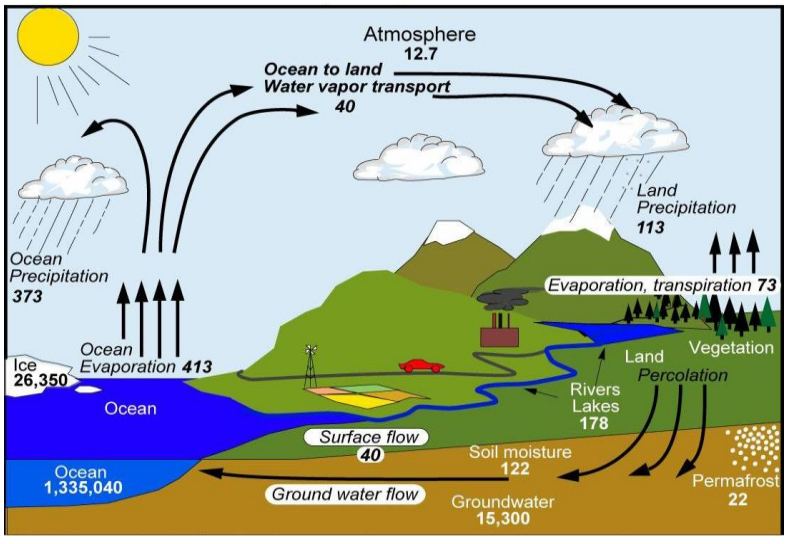

Figure 1.1: The illustration of the hydrological cycle for the Earth system (Trenberth et al., 2007).

[1] The term evapotranspiration describes the water transported from the land's surface to the atmosphere. The evapotranspiration includes direct evaporation from soil surface, small water surface and wet canopy surface, as well as vegetation transpiration.

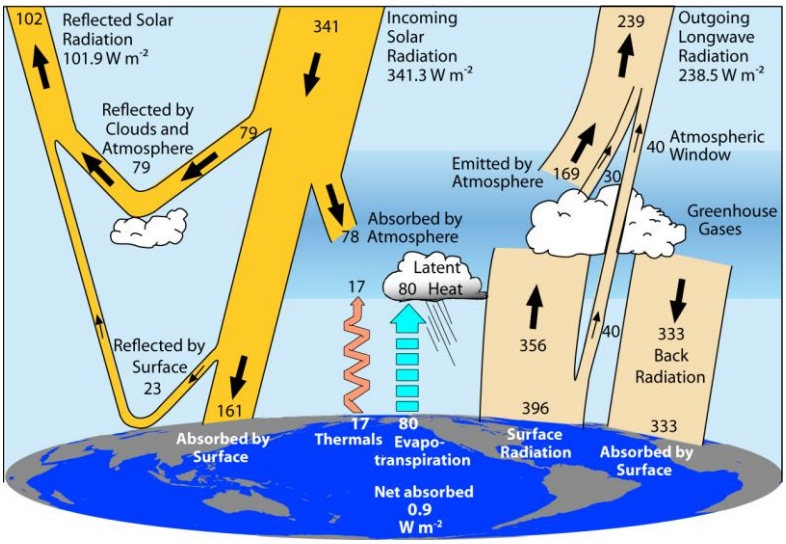

Figure 1.2: Earth's annual global mean energy budget (Trenberth et al., 2009).

Although ET itself is a simple concept, the complicated physical mechanisms of ET process including turbulent transport, biophysical characteristic of transpiration, the feedback in the soil–plant–atmosphere continuum and the heterogeneity of land surface all combine to make estimation of ET a challenge (McCabe et al., 2011; Lettau, 1969). Nevertheless, much theoretical progress has been made in ET modeling such as Penman equation and the subsequently modified P–M (Penman–Monteith) equation. These advances strengthened the confidence for ET estimation and provided bases for the widely used FAO–24 and FAO–56 approaches (Farahani et al., 2007). To facilitate application, a well recognized simplification of P-M equation was proposed by Priestley and Taylor (1972) for water unstressed conditions, in which the temperature and aerodynamic terms were replaced by an empirically derived constant factor. On the other hand, much effort has also been dedicated to measure ET using various micrometeorological techniques. In general, the ET could now be measured directly using evaporation pans, weighing lysimeters and EC (eddy covariance) technique on various spatial scales from hundreds to thousands of meters, due to the ability to measure surface energy exchange and near surface climate variables (Dugas et al., 1991). Today, EC systems have been deployed in hundreds of flux towers around the world for providing continuous measurements of surface water and carbon fluxes. All of these flux towers belong to the FLUXNET network, with excellent coverage over Europe and North America (Vinukollu et al., 2011).

Although ET is quantifiable at the small scale using ground-based techniques, larger-scale estimates require alternative measurements and estimation approaches. They need a variety of land surface and atmospheric variables, such as temperature, wind speed, and the amount of available energy. Such quantities, however, are difficult to obtain over large-scale heterogeneous areas and have to be extrapolated/interpolated to various temporal and spatial scales with limited accuracy (Wood, 1995). Therefore, it is important and necessary to develop other methods for

estimating spatially distributed regional ET.

Land surface model is one possible way for mapping spatial distribution of ET. Generally, these models need to be calibrated and evaluated using ground observations (Shuttleworth, 2007). However, these observations are of short durations.

Satellite remote sensing has been recognized as a promising technique to provide accurate estimations of diurnal, daily and annual variability of ET on local, regional and global scales, with a potential of providing reliable and long-term estimates of ET for land surface model evaluation (Jiménez et al., 2011). Remote sensing can provide unprecedented spatial distribution of critical land surface and atmospheric variables, such as land surface temperature, albedo, and vegetation indices, which are logistically and economically impossible to obtain from conventional observation networks. However, satellites do not directly measure ET. Therefore, a number of physical and empirical remote sensing based models that vary in complexity, from simplified empirical regression methods to energy balance based models, and finally to data assimilation techniques, have been proposed to estimate ET over the last few decades. For a review, see e.g. Kalma et al. (2008). Most of these methods require explicit characterization of numerous physical parameters like wind speed, aerodynamic resistance, and surface roughness, which cannot readily be measured through remote sensing techniques. Therefore, it is still challenging to routinely map regional and even global ET distribution using satellite remote sensing without ground measurements or reanalyzed meteorological data. To overcome this problem, some attempts have been made to develop new parameterizations for ET estimation that depend entirely on remote sensing.

One widely used approach among them is the LST/NDVI (land surface temperature/ Normalized Difference Vegetation Index) feature space method, which is based on the P–T (Priestley–Taylor) equation. Recent and detailed reviews of this method have been provided in terms of the theoretical basis, biophysical properties and limitations by Carlson (2007) and Petropoulos et al. (2009). A number of researchers have also demonstrated the applicability of this method for the estimation of regional ET from various satellite sensors, such as NOAA-AVHRR, TERRA/AQUA-MODIS, MSG-SEVIRI and FY-2C (Han et al., 2010; Sandholt et al., 2002; Tang et al., 2010). The assessment of ET derived by this method (Batra et al., 2006; Jiang and Islam, 2003; Jiang et al., 2004; Long et al., 2012; Stisen et al., 2008) shows that the RMSD (root mean square difference) and RE (relative error) are generally within 60 W m^{-2} and 30% at the hourly and daily timescales.

Generally, when satellite data are used to represent traditionally ground-based measurements, signal corrections based on radiative transfer theory are necessary to account properly for viewing angles and atmospheric variables (Li et al., 2013). This actually poses great challenges for the remote sensing community to develop different correction procedures to eliminate the atmospheric attenuation effects (Vermote et al., 1997). Although much effort has been devoted to establish sophisticated and streamlined data correction procedures, these procedures are troublesome and need

independent observation data to satisfy the mathematical and physical constrains. These limitations practically increase the operational difficulty.

Under this background, the main objective of this research is to develop an alternative scheme to estimate daytime ET by directly using the TOA (Top of Atmosphere) radiances without performing atmospheric correction and associated processes. Firstly, the general possibility of estimating NDTI (Normalized Difference Temperature Index, a key parameter for EF (evaporative fraction) estimation) from TOA radiances, and the associated uncertainties are investigated. Secondly, the assumption of EF self preservation during daytime is tested using global FLUXNET measurements. Then, the daytime EF retrieved from satellite TOA radiances is evaluated using FLUXNET measured daytime EF. Finally, a daytime ET parameterization based entirely on TOA radiances is developed and validated over a regional scale. The above studies are going to answer the following research questions:

1. What are the uncertainties in estimating NDTI from TOA radiances?
2. How accurate is the EF estimation scheme based on TOA radiances?
3. How representative are instantaneous evaporative fraction measurements for daytime fluxes?
4. Is it possible to estimate daily ET from TOA radiances?

1.2 Thesis outline

It should be noted here that different chapters of this thesis are based on published and drafted journal articles. Therefore, these chapters have their own individual abstracts, introductions and conclusions. Chapter 2, 4 and 5 have already been published, while Chapter 3 is in preparation for submission. The main contents of these chapters and the flowchart for the study are as follows:

- **In Chapter 2**, the feasibility of estimating NDTI from TOA radiances is examined through a physical understanding of Planck radiation law and radiative transfer equation. A detailed sensitivity analysis of NDTI on surface and atmosphere variability is performed. Furthermore, the proposed method is tested using MODIS (Moderate Resolution Imaging Spectroradiometer) data over a heterogeneous area of the Poyang Lake basin, China. This chapter has been published in *IEEE Transactions on Geoscience and Remote Sensing* (Peng et al., 2013a).

- **In Chapter 3**, the applicability and robustness of the TOA radiances based EF estimation scheme is evaluated through comparison with measurements from global FLUXNET observations. To study the influence of land cover or biome types on EF estimates, the performance of the EF estimates over different land

- covers is analyzed. Furthermore, the sources of uncertainties and errors associated with these EF estimates are also investigated. This chapter is currently prepared for submission.

- **In Chapter 4**, the EF variation during daytime is investigated using global FLUXNET measurements. The goal here is to figure out how representative instantaneous EF measurements are for daytime values. At the same time, the effects of different cloud cover on EF are also analyzed. This chapter has been published in *Hydrology and Earth System Sciences* (Peng et al., 2013b).

- **In Chapter 5**, a new method is proposed to estimate daily ET directly from TOA radiances without performing atmospheric correction. Firstly, the EF is estimated over a study area in Poyang Lake basin using the scheme proposed in chapter 4. Then the net radiation over the same study area is derived based entirely on MODIS TOA radiances as well. Finally, daily ET maps are estimated from these EF and net radiation maps by using a sinusoidal temporal interpolation model. To evaluate the performance of the estimates based on TOA radiances, the estimated EF, net radiation and ET are compared with field observations and estimates based on MODIS products. This chapter has been published in *Hydrology and Earth System Sciences* (Peng et al., 2013c).

- **In Chapter 6**, the main findings of this thesis are summarized, and some recommendations and opportunities for future research are put forward.

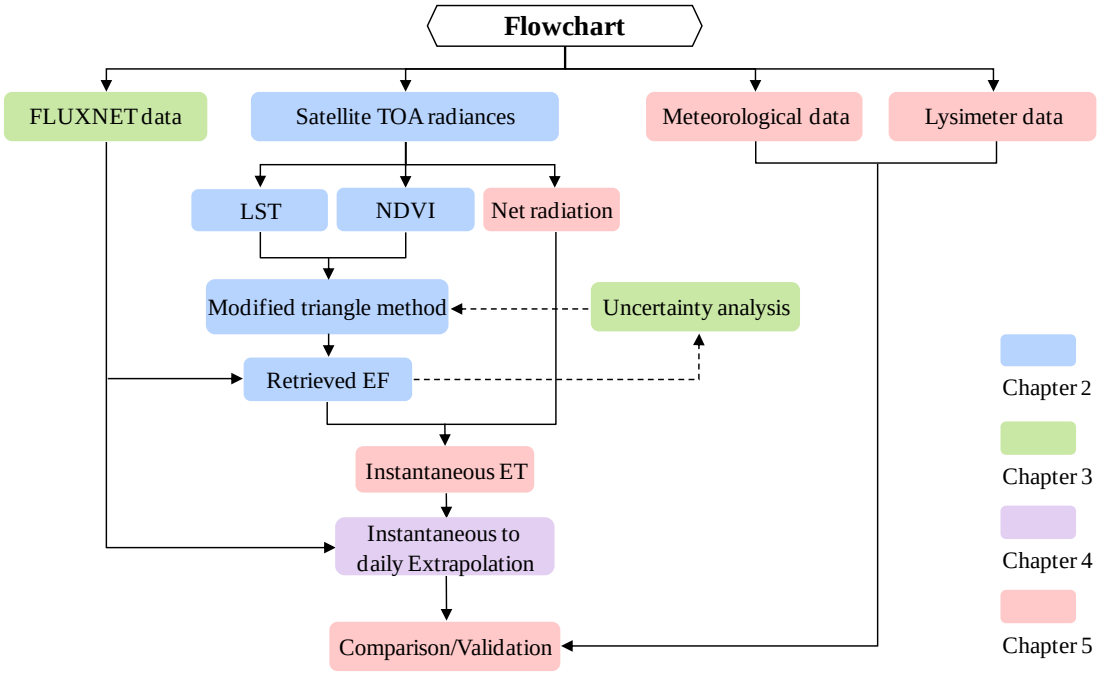

Figure 1.3: Flowchart of the study.

Chapter 2

Uncertainties in estimating Normalized Difference Temperature Index from TOA radiances[2]

Abstract

The widely used surface temperature/vegetation index (T_s/NDVI) triangle method provides an effective way to estimate surface turbulent energy fluxes and soil moisture. This type of method mainly relies on the Normalized Difference Temperature Index (NDTI), which is usually calculated from land surface temperature (LST). However, retrieval of LST from satellite data requires atmospheric correction procedures, which are often difficult and troublesome. Our study investigates the feasibility of determining NDTI using top of the atmosphere (TOA) radiances, instead of satellite-derived LST. A thorough assessment of the uncertainties in NDTI estimates for different atmospheric and surface conditions is performed. It is shown that NDTI can be estimated from TOA radiances with an accuracy of 90% if the spatial variabilities of atmospheric parameters (water vapor, effective atmospheric temperature) and surface emissivity are below 10 %, 4 K and 0.05, respectively. A test study is performed using Moderate Resolution Imaging Spectroradiometer (MODIS) data over a heterogeneous area of the Poyang Lake basin of China for six consecutive image acquisitions. When the spatial variations of the surface emissivity, effective atmospheric temperature and water vapor are respectively less than 0.01, 1 K and 0.2 g cm^{-2}, the TOA radiance-calculated NDTI value and LST-determined NDTI value are quite close with root mean square deviation (RMSD) values and biases varying from 0.033 to 0.051 and from -0.004 to 0.014. The high coefficient of determination (R^2) values, ranging from 0.904 to 0.939, indicated that the use of TOA radiances appears to be adequate for calculating NDTI in these studies. Overall, the proposed algorithm requires less prior information on the atmospheric state while providing NDTI estimates at a similar level of accuracy than obtained using atmospherically corrected LST data products.

[2] Peng, J., Liu, Y., and Loew, A.: Uncertainties in Estimating Normalized Difference Temperature Index From TOA Radiances, *IEEE Transactions on Geoscience and Remote Sensing*, 51(5):2487 – 2497, 2013.

2.1 Introduction

Accurate estimates of surface turbulent energy fluxes and soil moisture are of great significance to a wide range of environmental applications, including land surface climatology, hydrology, meteorology, and water resource management (Moran et al., 1994; Houser et al., 1998; Ryu et al., 2010). Over the last few decades, a large number of remote sensing based methods have been proposed to provide spatially distributed information about surface energy fluxes and soil moisture status (Courault et al., 2005; Gowda et al., 2008; Verstraeten et al., 2008; Glenn et al., 2010; Yang et al., 2006). The feature space of land surface temperature (LST) and vegetation index (e.g., the normalized difference vegetation index, NDVI) has been widely used for these purposes.

Negative correlation was found between LST and NDVI in numerous studies (Nemani and Running, 1989; Carlson et al., 1994; Goetz, 1997). The scatter plot of LST versus NDVI often results in a triangular shape (Gillies and Carlson, 1995; Gillies et al., 1997; Price, 1990b). Jiang and Islam (1999; 2001) made use of the LST/NDVI triangular space and the simplified Priestley-Taylor equation to estimate evapotranspiration over a large heterogeneous area. With the triangular space, Sandholt et al. (2002) proposed the Temperature–Vegetation Dryness Index (TVDI) to assess soil surface moisture status. Likewise, Wan et al. (2004) developed the Vegetation Temperature Condition Index (VTCI) for monitoring drought occurrence. Recently, Carlson (2007) and Petropoulos et al. (2009) provided comprehensive reviews on these studies relying on the triangular space. An important advantage of the approaches is that they are relatively insensitive to uncertainties associated with atmospheric corrections and land surface heterogeneity (Valor and Caselles, 1996a; Venturini et al., 2004; Petropoulos et al., 2009).

These approaches mainly used the Normalized Difference Temperature Index (NDTI) which determines the subsequent retrievals. The idea of NDTI was developed by McVicar and Jupp (McVicar and Jupp, 2002) and was often calculated from satellite retrieved LST instead of ground measurement of LST, because there is no spatially distributed map of ground-based LST measurement. Various techniques and algorithms have been proposed to retrieve LST from thermal infrared remote sensing data (Becker and Li, 1990; Wan and Li, 1997; Coll et al., 2006; Galve et al., 2008; Cristóbal et al., 2009; Jiménez-Muñoz and Sobrino, 2010; Coll et al., 2010; Moser and Serpico, 2009). All of them involve complicated atmospheric corrections based on radiative transfer theory (Dash et al., 2002). In practice, these correction procedures are often troublesome and increase the operational difficulty especially for the sensors with only one thermal band e.g. Landsat-7/ETM+. Moreover, accurate and robust estimation of LST remains a challenging problem because of the uncertainties introduced by residual atmospheric effects, insufficient correction of sun-target-satellite geometry and uncertainties in land surface emissivity (Jiang et al., 2004; Liu et al., 2007). The uncertainties associated with satellite-derived LST are on

the order of several degrees in K (Prata and Cechet, 1999; Peres and DaCamara, 2004; Yu et al., 2009; Jiménez-Muñoz et al., 2009), which may result in incorrect NDTI values. In addition, satellite-derived LST products often contain void values due to cloud contamination or mis-classification even under apparently clear-sky conditions.

An alternative to use LST data products for the estimation of NDTI is the use of top-of-atmosphere (TOA) radiances. This idea was proposed by Valor and Caselles (1996a) to monitor the land degradation. As NDTI is a relative index that is based on the identification of regional scale contrast of land surface conditions one might expect that robust estimates of NDTI can be obtained in case of homogeneous atmospheric conditions. The present paper investigates the general potential of estimating NDTI from TOA radiances and focuses on the sensitivity of NDTI estimates on surface and atmospheric variability. The paper is structured as follows: The theoretical framework for estimating NDTI from TOA radiances is introduced in Section 2.2. A sensitivity analysis of NDTI to key parameters is performed in Section 2.3. The method is then applied and verified in Section 2.4. The results of the sensitivity analysis and the effectiveness of the method are discussed in Section 2.5. The conclusion is given in Section 2.6.

2.2 Theory

The triangular shape of the LST/NDVI feature space formed by the scatter of LST against NDVI over a wide range of soil moisture content and fractional vegetation cover is shown in Figure 2.1. It may be noticed that as the vegetation fraction cover increases along the x-axis, surface temperature decreases. Actually, the sensitivity of LST to soil moisture over surfaces ranging from bare soil to full vegetation cover results in the emergence of the triangular shape (Carlson et al., 1990). The dry edge and wet edge, as shown in Figure 2.1, are defined as the locus of the highest surface temperature and the lowest surface temperature, respectively. While the dry edge reflects the status of limited soil moisture, the wet edge represents the conditions of maximum evapotranspiration and unlimited water availability (Han et al., 2010; Stisen et al., 2008). The triangular shape in the LST/NDVI domain is primarily controlled by the vegetation fractional cover, surface moisture conditions, net radiation and local climatic state (Nemani et al., 1993; Lambin and Ehrlich, 1996). Based on the above interpretation of the LST/NDVI triangle feature space, the NDTI varying from 0 at the driest pixels to 1 at the wettest pixels is expressed as follows:

$$NDTI = \frac{T_{\max} - T_s}{T_{\max} - T_{\min}}. \tag{2.1}$$

Where T_s is the observed surface temperature for a given pixel whose NDVI value is $NDVI_i$, $T_{\max}$ and $T_{\min}$ are the corresponding highest and lowest surface temperatures which have the same $NDVI_i$ value.

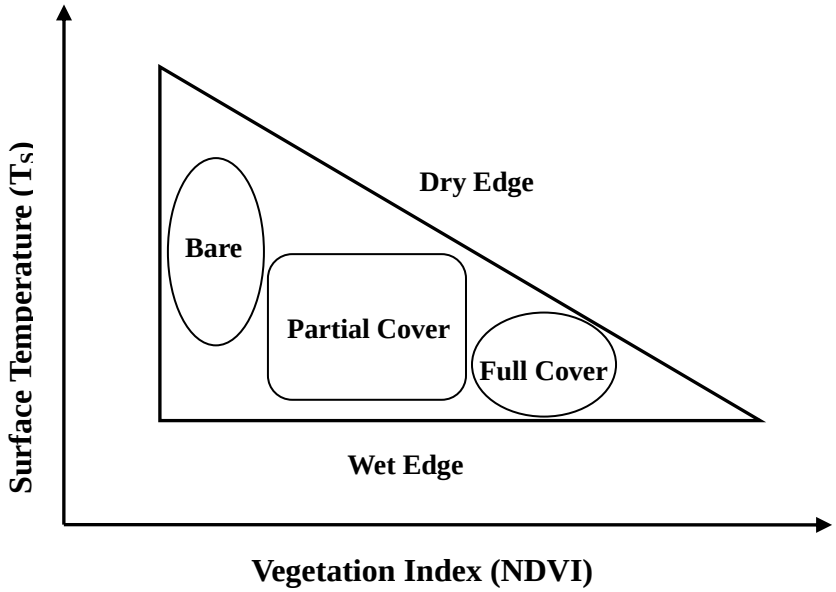

Figure 2.1: T_s and NDVI triangular feature space (after Lambin & Ehrlich, 1996, and Sandholt et al., 2002).

In order to retrieve LST from remote sensing data in thermal wavebands, many efforts have been devoted to the development of different methods and approaches, which mainly include the single-channel methods, split-window algorithms and multi-angle algorithms (Atitar and Sobrino, 2009; Jiménez-Muñoz and Sobrino, 2003; Sobrino et al., 2004b). All of them are based on the thermal radiance transfer from the ground to the remote sensor. The radiance measured at a satellite sensor is composed of emitted radiance from the ground, reflected atmospheric radiance by the surface and upwelling radiance from the atmosphere itself. Considering all these impacts, the radiance transfer equation can be written in the thermal infrared region as (Prata et al., 1995; Qin and Karnieli, 1999; Sobrino et al., 2004a):

$$L_i = t_i \varepsilon_i B_i(T_s) + t_i R_i + I_{\uparrow}. \tag{2.2}$$

Where L_i is the TOA radiance received by the sensor in channel i, t_i is the total transmittance of the atmosphere in channel i, ε_i is the surface emissivity, T_s is the land surface temperature, $B_i(T_s)$ is the radiance emitted by a blackbody at temperature T_s, R_i is the reflected atmospheric radiance by the surface, $I_{\uparrow}$ is the upwelling atmospheric radiance in channel i. It is noted that the above magnitudes also depend on the satellite viewing angle, also known as satellite nadir angle. The expression for $B_i(T_s)$ is defined by Planck's function as (Dozier, 1981):

$$B_i(T_s) = \frac{C_1}{\lambda^5 (e^{C_2/\lambda T_s} - 1)}. \tag{2.3}$$

Where C_1 and C_2 are the spectral constants with $C_1 = 1.19104 \times 10^8$ W $\mu m^4 m^{-2} sr^{-1}$ and $C_2 = 1.43877 \times 10^4$ μm K. $B_i(T_s)$ is given in W $m^{-2} sr^{-1} \mu m^{-1}$ if wavelength λ is given in μm.

The upwelling atmospheric radiance $I_{\uparrow}$ and the reflected atmospheric radiance R_i are usually given by (Coll et al., 1994; Franc and Cracknell, 1994; Sòria and Sobrino, 2007):

$$I_{\uparrow} = (1-t_i)B_i(T_a) \tag{2.4}$$

$$R_i = (1-t_i)(1-\varepsilon_i)B_i(T_a). \tag{2.5}$$

Where T_a represents the effective mean temperature of the atmosphere. The detailed derivation of I↑ and R_i was described by Sobrino et al. (1991) and Qin et al. (2001). On the basis of Eqs. (2.4) and (2.5), Eq. (2.2) can be rewritten as:

$$L_i = t_i\varepsilon_i B_i(T_s) + (1-t_i)[1+(1-\varepsilon_i)t_i]B_i(T_a). \tag{2.6}$$

To relate the TOA radiance to T_s from Eqs. (2.3) and (2.6) the most common way is to approximate the Planck function using a first-order Taylor expansion around a given temperature value ($\overline{T}$) (Price, 1983; Sobrino et al., 1996). Following this method, the Taylor series expansion of Planck's function can be written as:

$$B_i(T_s) = B_i(\overline{T}) + (T_s - \overline{T})\left(\frac{\partial B_i}{\partial T_s}\right)_{\overline{T}} = T_s\left(\frac{\partial B_i}{\partial T_s}\right)_{\overline{T}} + B_i(\overline{T}) - \overline{T}\left(\frac{\partial B_i}{\partial T_s}\right)_{\overline{T}}. \tag{2.7}$$

It should be noted here that the uncertainty associated within this expansion will increase when the temperature difference is up to 50 K. Combining Eq. (2.7) with Eq. (2.6), T_s is given as:

$$T_s = \frac{\dfrac{L_i - (1-t_i)[1+(1-\varepsilon_i)t_i]B_i(T_a)}{t_i\varepsilon_i} - B_i(\overline{T}) + \overline{T}\left(\dfrac{\partial B_i}{\partial T_s}\right)_{\overline{T}}}{\left(\dfrac{\partial B_i}{\partial T_s}\right)_{\overline{T}}}. \tag{2.8}$$

For the simplification of the mathematical expression, the path radiance P_i is introduced which is defined as $P=\dfrac{(1-t_i)[1+(1-\varepsilon_i)t_i]B_i(T_a)}{t_i\varepsilon_i}$.

According to the Eq. (2.8), T_s can be retrieved for a given wavelength of a satellite sensor. Substituting Eq. (2.8) into Eq. (2.1), the NDTI can be rewritten using the following equation:

$$NDTI = \frac{\dfrac{L_i^{\max} - (1-t_i^{\max})[1+(1-\varepsilon_i^{\max})t_i^{\max}]B_i(T_a^{\max})}{t_i^{\max}\varepsilon_i^{\max}} - \dfrac{L_i^{s} - (1-t_i^{s})[1+(1-\varepsilon_i^{s})t_i^{s}]B_i(T_a^{s})}{t_i^{s}\varepsilon_i^{s}}}{\dfrac{L_i^{\max} - (1-t_i^{\max})[1+(1-\varepsilon_i^{\max})t_i^{\max}]B_i(T_a^{\max})}{t_i^{\max}\varepsilon_i^{\max}} - \dfrac{L_i^{\min} - (1-t_i^{\min})[1+(1-\varepsilon_i^{\min})t_i^{\min}]B_i(T_a^{\min})}{t_i^{\min}\varepsilon_i^{\min}}}$$

$$= \frac{\frac{L_i^{\max}}{t_i^{\max}\varepsilon_i^{\max}} - \frac{L_i^s}{t_i^s\varepsilon_i^s} - P_i^{\max} + P_i^s}{\frac{L_i^{\max}}{t_i^{\max}\varepsilon_i^{\max}} - \frac{L_i^{\min}}{t_i^{\min}\varepsilon_i^{\min}} - P_i^{\max} + P_i^{\min}}. \quad (2.9)$$

Eq. (2.9) can then be simplified using only TOA radiances under some assumptions as discussed in the following. The impact of these assumptions on the accuracy of NDTI estimates will be given in section 2.3.

In a first order it is reasonable to assume that the surface emissivity is constant for a given NDVI value because a monotonous relation has been found between surface emissivity and NDVI (Sobrino et al., 2001; Valor and Caselles, 1996b; Van De Griend and Owe, 1993). Thus we obtain:

$$\varepsilon_i^s = \varepsilon_i^{\max} = \varepsilon_i^{\min}. \quad (2.10)$$

If the atmospheric transmittance and atmospheric temperature show very little spatial variation over the investigated area, it is possible to obtain the following equations:

$$t_i^s = t_i^{\max} = t_i^{\min} \quad (2.11a)$$

$$T_a^s = T_a^{\max} = T_a^{\min}. \quad (2.11b)$$

Based on Eqs. (2.10), (2.11a) and (2.11b), we further obtain:

$$P_i^s = P_i^{\max} = P_i^{\min}. \quad (2.12)$$

On the basis of the above reasons and assumptions, Eq. (2.9) can be simplified as:

$$NDTI = \frac{L_i^{\max} - L_i^s}{L_i^{\max} - L_i^{\min}}. \quad (2.13)$$

Which is the NDTI as a function of TOA radiances only.

It is however impossible in practice to determine whether the parameters like t_i and T_a are spatially homogeneous as these parameters are difficult to obtain directly in the real world. To assess the uncertainties in NDTI estimates a detailed sensitivity analysis is carried out in the following section in order to ascertain how variations in atmospheric and surface parameters (t_i, ε_i, and T_a) affect the NDTI.

2.3 Sensitivity Analysis

As the estimation of NDTI based on TOA radiances is assumed on spatial homogeneous fields of surface and atmospheric conditions, the sensitivity of the results on these assumptions is investigated in this section. A sensitivity analysis of the NDTI to key surface and atmospheric parameters (t_i, ε_i, and T_a) is carried out to

provide a better understanding of the limitations of the proposed method. The sensitivity of Eq. (2.9) to changes in surface emissivity, effective atmospheric temperature and total column water vapor is therefore explored for a wide range of conditions (Table 2.1). We estimate NDTI by using either the land surface temperature (LST) or TOA radiances and use the relative change in NDTI as a measure for the sensitivity of surface and atmospheric parameters.

The total atmospheric transmittance t_i affects the magnitude of the radiance transferred through the atmosphere. In the atmospheric window, the transmittance depends mainly on the atmospheric water vapor content (Prata, 1993). The atmospheric transmittance decreases when the atmospheric water vapor increases. Figure 2.2 shows the simulated atmospheric transmittance as a function of water vapor content for a standard mid-latitude atmosphere. Radiative transfer simulations were conducted using the MODTRAN 4 atmospheric radiative transfer model (Berk et al., 1998). The transmittance changes from 0.965 to 0.334 within the water vapor content range 0.15-6.5 g cm^{-2}, which is a reasonable range from very dry to moist conditions for cloud-free atmosphere.

Table 2.1: Ranges of surface and atmospheric conditions used for sensitivity analysis.

Condition	Minimum	Maximum	Interval
Total column water vapor	0.15 g cm^{-2}	6.5 g cm^{-2}	0.5 g cm^{-2}
Effective atmospheric temperature	250 K	310 K	10 K
Surface emissivity	0.90	0.99	0.01

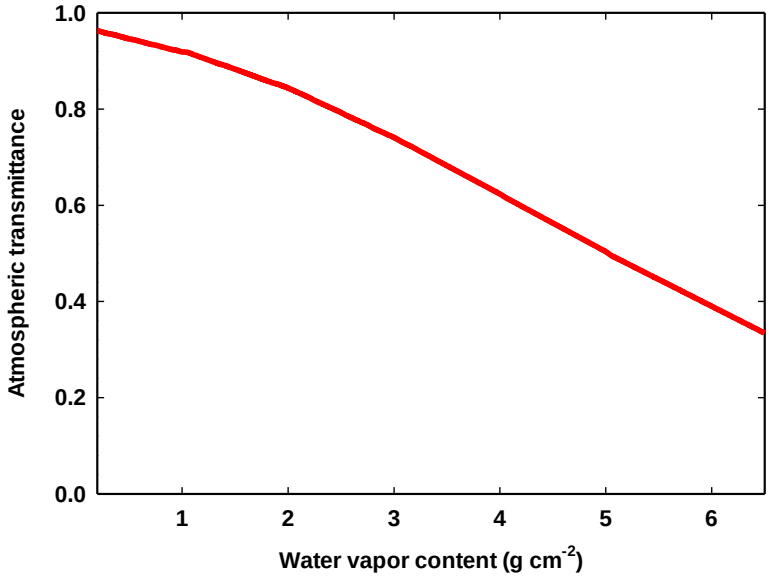

Figure 2.2: The simulated atmospheric transmittance as a function of water vapor content for mid-latitude summer standard atmosphere.

The surface emissivity is generally not homogeneous over natural surfaces and sensitive to spatial heterogeneity. In the spectral region from 8 μm to 14 μm, most of the Earth's surface exhibits emissivity values which range from approximately 0.90 to 0.99 (Kerr et al., 1992). Considering a possible effective atmospheric temperature range of the Earth, 250-310 K is selected to represent natural atmospheric conditions.

As atmospheric transmittance, surface emissivity and effective atmospheric temperature are spectrally dependent. In most cases the atmospheric window (10-12 μm) is the most transparent region in the thermal infrared spectrum, where aerosol absorption and scattering are negligible and generally ignored (Price, 1983) and most of the thermal sensors on board satellites work in this spectral domain. Monochromatic radiative transfer simulations are conducted at a wavelength of 11 μm to calculate the TOA radiance L_i for our study. In order to calculate NDTI, we assume that the LST ranges from 273K to 323K, considering the possible temperature difference in real situations. To investigate how variations in surface emissivity, effective atmospheric temperature and water vapor affect the NDTI, we compute the relative variation of NDTI as follows:

$$\Delta NDTI = \frac{\left| NDTI_{TOA}(x \pm \Delta x) - NDTI_{LST} \right|}{NDTI_{LST}} \times 100\%. \tag{2.14}$$

Where x is the variable of surface emissivity, effective atmospheric temperature or water vapor content, Δx is the corresponding variation amount of the variable x, $NDTI_{LST}$ and $NDTI_{TOA}$ are calculated using LST and TOA radiances respectively.

2.4 Study Area and Data Processing

2.4.1 Study area and materials

The study area is located in the Poyang Lake basin of China, which lies on the Southern bank of the middle and lower reaches of the Yangtze River. The Poyang Lake wetland is well-known as the first batch of the Ramsar convention list of wetlands of international importance. It has great hydrological, biological, ecological and economic significance. The basin belongs to a humid subtropical climate zone with an annual mean air temperature of 290.5 K and an annual average precipitation of 1680 mm (Guo et al., 2008). The surface elevation of the basin ranges roughly from 5 m to 2100 m above the sea level. Most parts of the basin are dominated by hilly or mountainous topography. In order to avoid the effect of mountainous terrain, a relatively flat area was chosen for the case study, with the latitude ranging from 27.6ºN to 28.6ºN and longitude from 114.6ºE to 116.8ºE. Figure 2.3 shows the land cover features over the study area, acquired from the Moderate resolution Imaging Spectroradiometer (MODIS) data on 2 May 2007. It is a heterogeneous land cover area characterized by agricultural field (54%), grassland (22%), bare soil surface (1%), forested areas (19%) , and inland water surface (4%). The diversity of land covers co-

uld reflect the spatial variability of surface emissivity. In order to examine the feasibility of the proposed approach, six clear sky day images in year 2007 were selected for the case study mainly according to the following criteria: the images are very clear and the MODIS LST products have very few void values. These 6 days are day of year (DOY) 30 (January 30), DOY80 (March 21), DOY122 (May 2), DOY208 (July 27), DOY279 (October 6), DOY332 (November 28), covering the whole seasons of the year.

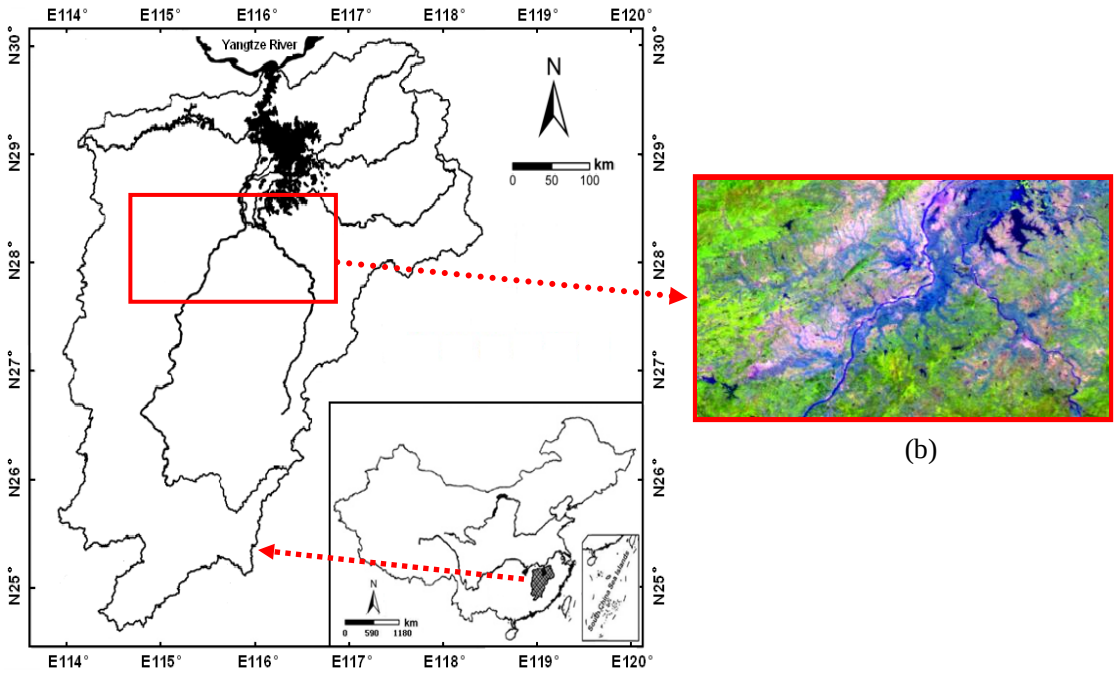

(a) (b)

Figure 2.3: Quick view of the study area. (a) Location of the study area in Poyang Lake basin; (b) False-color image of MODIS (red/green/blue: band 621) for the study area, dated May 2, 2007.

The MODIS is the primary instrument in the NASA Earth Observing System (EOS) for land, ocean and atmosphere research. The MODIS Collection 5 data products used in this study consist of MOD02_1KM, MOD03_L1A, MOD05_L2, MOD07_L2, MOD09_GA, and MOD11_L2. The MOD02_1KM dataset contains Level-1B calibrated and geolocated TOA radiances for 36 bands at 250-m, 500-m, and 1-km resolutions, respectively. The MOD03_L1A geolocation product comprises of geodetic coordinates, ground elevation, and satellite zenith and azimuth angles for each MODIS 1-km pixel. The MOD05_L2 consists of column water-vapor amounts over the area. The MOD07_L2 contains atmospheric profile parameters including atmospheric stability, temperature and moisture profiles, and atmospheric water vapor at 5-km resolution (King et al., 2003). The MOD09_GA comprises of surface spectral reflectance from atmospheric correction, which was used to calculate NDVI in our study. The MOD11_L2 data contains LST and band-averaged emissivity in band-31

(10.780–11.280 μm) and band-32 (11.770–12.270 μm) calculated using the generalized split-window algorithm (Wan and Dozier, 1996), which have spatial resolutions of 1-km. All the above MODIS data were acquired from the Earth Observing System Data Gateway (EDG) and re-projected to Universal Transverse Mercator (UTM) with a World Geodetic System (WGS)-84 as reference datum.

2.4.2 Data processing

The image data was first screened for contamination by clouds in the study area which was removed using a simple threshold method (Wu and Zhong, 1994). Theoretically the construction of the triangular space requires a large number of pixels over a flat area which is the reason why the pixels with much higher elevation (> 100 m) were excluded from the analysis to minimize the effect of elevation variation on the LST/NDVI triangular space.

In order to construct the LST/NDVI triangular feature space, NDVI values were calculated using the following formula:

$$NDVI = (\alpha_{nir} - \alpha_{red})/(\alpha_{nir} + \alpha_{red}). \tag{2.15}$$

Where α_{nir} and α_{red} are the surface reflectances in near infrared (NIR) band and red band from MOD09_GA product. It is noted that the 250-m red and NIR bands data were resampled to 1-km resolution to match the spatial resolution of LST product. Then, the NDTI value for each pixel was calculated on the basis of the triangular space using all valid image pixels in the test site as input. The highest temperature pixel and lowest temperature pixel for each NDVI interval was determined first. This procedure is very important, because the uncertainty in the determination of the dry and wet edges will transfer to the estimation of NDTI and further affect the comparison of the $NDTI_{LST}$ and $NDTI_{TOA}$. In this study, the algorithm proposed by Tang et al. (2010) for quantitatively determining the dry edge was used, namely:

$$T_{\max} = a + bNDVI. \tag{2.16}$$

Where $T_{\max}$ is the maximum surface temperature for a given NDVI and a and b respectively define the intercept and slope of the dry edge. The wet edge is assumed to be the line with the minimum temperature parallel to the NDVI axes. The next step is to interpolate between the extreme temperatures for a given NDVI value using Eq. (1). Based on the interpolation scheme, the NDTI value for the study area was calculated respectively from MODIS LST product and TOA radiance (band-31) using Eqs. (2.1) and (2.13).

In order to test the robustness of NDTI estimates, the spatial variability of water vapor content, surface emissivity and effective atmospheric temperature across the study area were investigated using the relevant MODIS data products.

2.5 Results and Discussion

2.5.1 Sensitivity analysis

1) Surface emissivity: Figure 2.4 illustrates the average relative variation and standard deviation (S.D.) of NDTI due to possible surface emissivity variation □x = [0.01, 0.03, 0.05, 0.07]. It can be seen that NDTI variation is only dependent on emissivity variation but not on the level of emissivity itself. As an example, for the emissivity variation 0.01, the relative variation of NDTI is always 1.93% for emissivity values between 0.90 and 0.99. Besides, the linear correlation between NDTI variation and emissivity variation is also very clear in all the cases. The NDTI variation increases steadily with the emissivity variation. A variation on emissivity of 0.03, 0.05 and 0.07 may lead to the change of 5.8%, 9.6% and 13.5% on NDTI. For most natural surfaces the possible variation of emissivity is usually less than 0.05 (Freitas et al., 2010; Humes et al., 1994), which leads to a maximum relative variation of 9.6% on NDTI. Generally, the variation of 10% is an acceptable level for NDTI estimation because most techniques based on NDTI for the estimation of heat fluxes have uncertainties in the 15–30% range (Kalma et al., 2008).

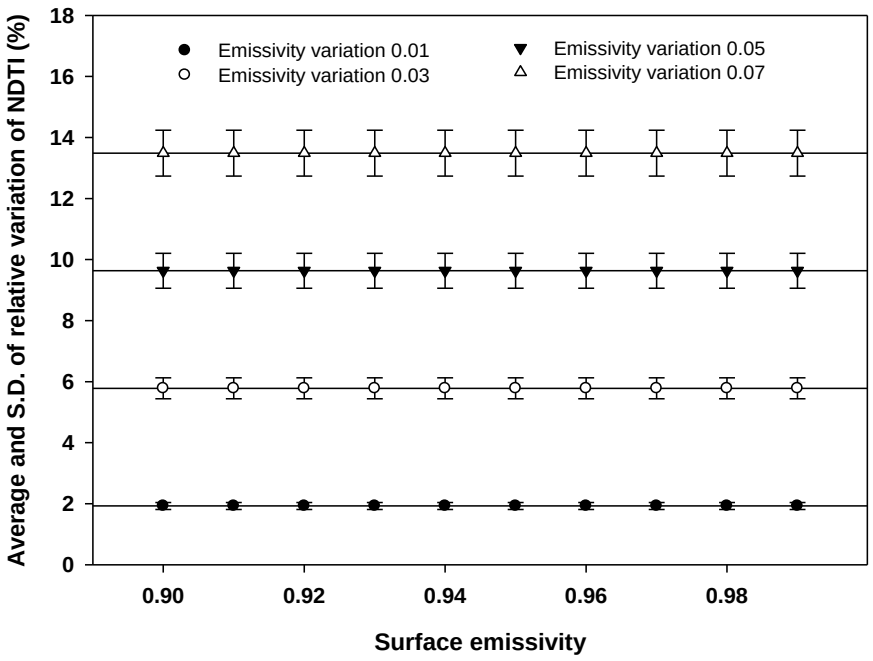

Figure 2.4: Average and S.D. value of the relative variation of NDTI due to change of surface emissivity.

2) Effective atmospheric temperature: As shown in Figure 2.5, the probable NDTI variation caused by effective atmospheric temperature variation is dependent on temperature level. For the atmospheric temperature variation 1 K, the NDTI variation

changes from 1.4% at temperature level 250 K to 2.6% at the level 310K. The maximum relative change of 5.2%, 10.5% and 15.6% on NDTI is obtained when the variation of atmospheric temperature is 2 K, 4 K and 6 K. In fact, the spatial variation of the atmospheric temperature is usually below 4 K at regional scale (Courault et al., 1998), and the maximum atmospheric temperature is less than 310 K. Under these conditions, the maximum relative variation of NDTI is 10.5%.

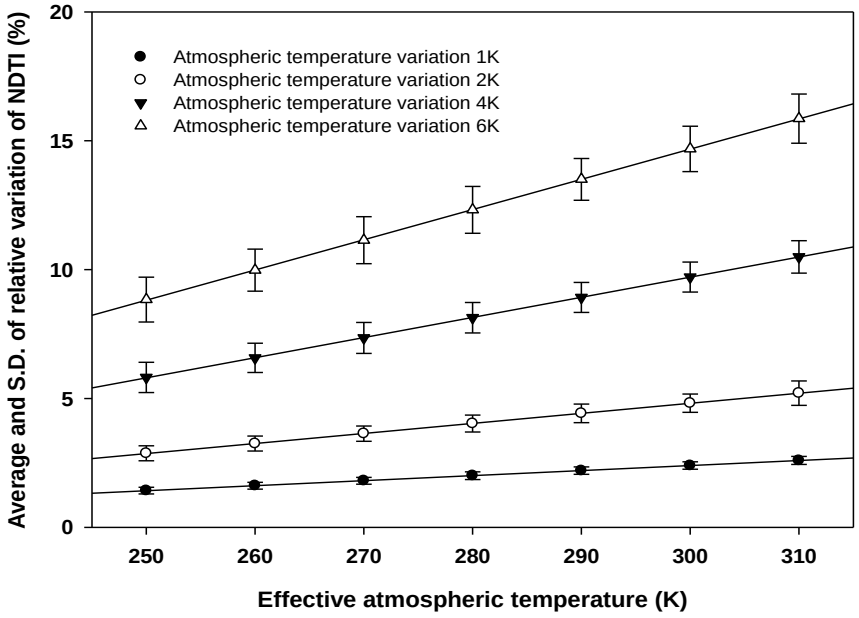

Figure 2.5: Average and S.D. value of the relative variation of NDTI due to change of effective atmospheric temperature.

3) Total column water vapor: The change of the NDTI due to the variation of water vapor content is shown in Figure 2.6. In contrast with the variations of surface emissivity and atmospheric temperature, the NDTI variation is more sensitive to the variation of water vapor content. As shown in Figure 2.6, the NDTI variation is 2.2%-10.4% for water vapor content variation equal to 0.2 g cm^{-2}. The NDTI variation may increase to 5.3%-25.4% for water vapor content variation equal to 0.5 g cm^{-2} and 12.4%-51.1% for water vapor content variation of 1 g cm^{-2}. However, the NDTI variation is less than 5% when the water vapor content variation is 0.05 g cm^{-2}. The analysis conducted with MODIS data has shown that the relative spatial variability of water vapor content at regional scale is usually below 10% at different seasons. Figure 2.6 shows that this variation leads to the maximum variation of 9.5% on NDTI, when the water vapor content is within the 0-3 g cm^{-2} range. The relative NDTI variation increases significantly when the water vapor content is higher than 3 g cm^{-2}. This implies that this method may not work well for moist condition with water vapor content higher than 3 g cm^{-2}.

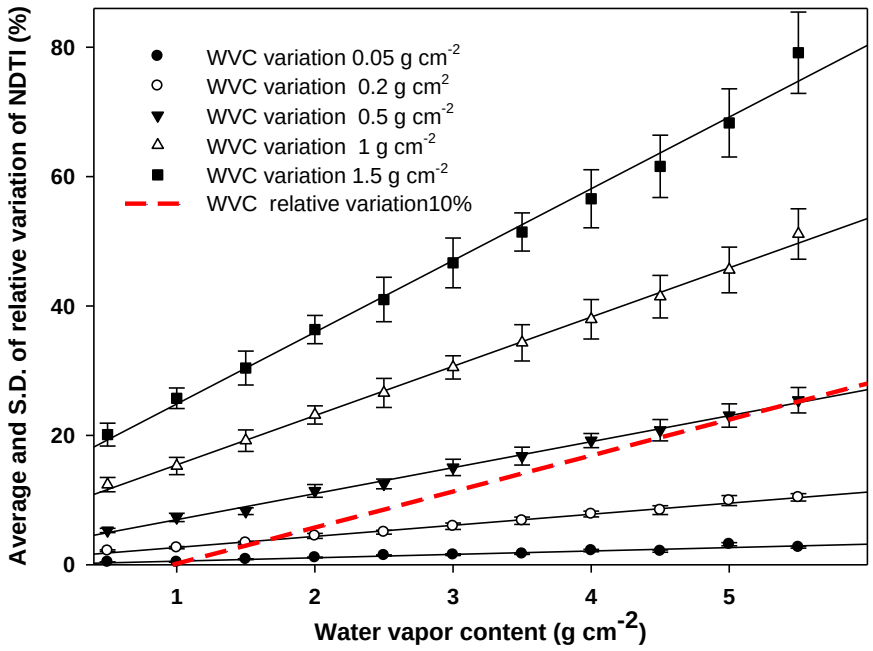

Figure 2.6: Average and S.D. value of the relative variation of NDTI due to change of WVC.

Based on these results, we conclude that uncertainties in NDTI estimates based on TOA radiances are expected to be less than 10% for typical spatial variations of surface emissivity, water vapor and effective atmospheric temperature at the regional scale. Largest uncertainties result from spatial variations in total column water vapor profile as would have been expected. Thus largest uncertainties are expected if large spatial contrast in water vapor coincides with humidity.

2.5.2 Triangular scatter plots

In order to calculate NDTI from LST and TOA radiances for the six case days, the dry and wet edges of the triangular space were estimated firstly. Figure 2.7 gives examples of LST/NDVI and TOA radiance/NDVI scatter plots for a sample day (DOY 122). The two scatter plots show a similar shape which should allow for the estimation of comparable NDTI values from both data sets. The corresponding dry and wet edges of the triangular space were determined as described in the previous section with high coefficient of determinations (R^2) of 0.931 for LST/NDVI scatter plots and 0.907 for TOA radiance/NDVI scatter plots. Similar robust results are obtained for the other five case days (Table 2.2). Thus the difference between $NDTI_{LST}$ and $NDTI_{TOA}$ caused by the subjective determination of the dry edge will be significantly decreased.

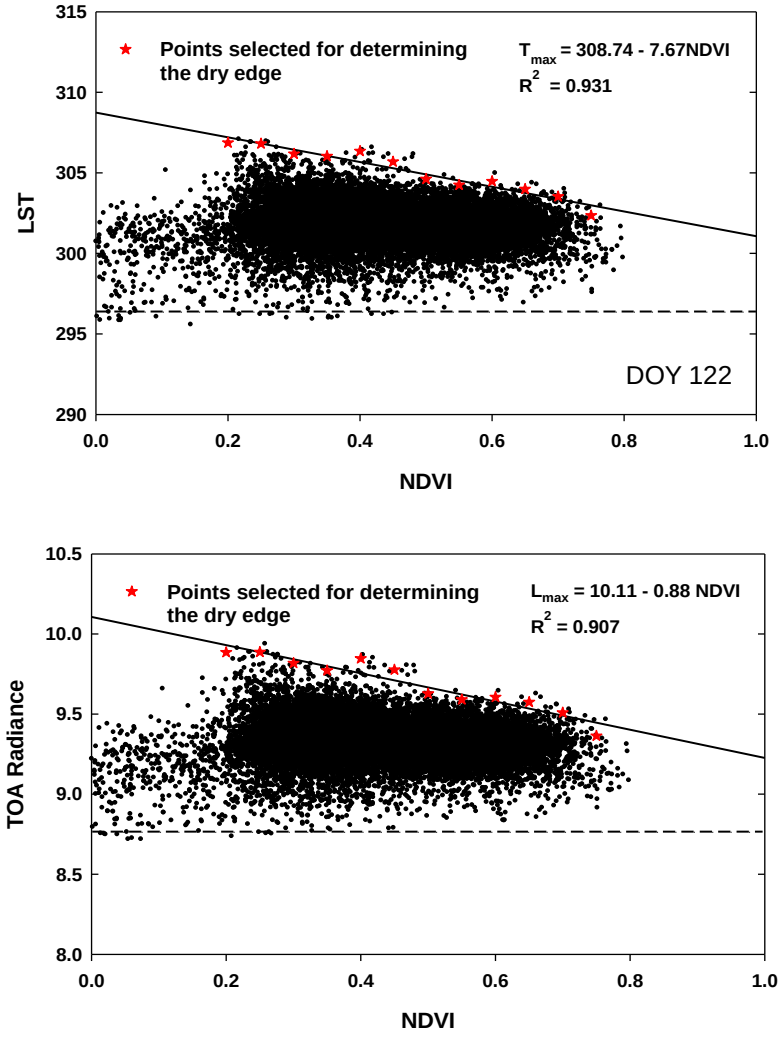

Figure 2.7: Examples of LST/NDVI and TOA Radiance/NDVI scatter plots for a sample day (DOY 122).

Table 2.2: Statistics of the dry edge values used for estimation of NDTI. (a and b represent the intercept and slope of the dry edge respectively).

Case Day	Scatter Plot	a	b	R^2
DOY30	NDVI-LST	293.86	-6.94	0.946
	NDVI-TOA Radiance	8.47	-0.89	0.926
DOY80	NDVI-LST	302.13	-11.12	0.897
	NDVI-TOA Radiance	9.47	-1.42	0.929
DOY122	NDVI-LST	308.74	-7.67	0.931
	NDVI-TOA Radiance	10.11	-0.88	0.907
DOY208	NDVI-LST	314.71	-8.18	0.984
	NDVI-TOA Radiance	10.67	-1.25	0.961
DOY279	NDVI-LST	313.55	-11.38	0.932

	NDVI-TOA Radiance	10.56	-1.25	0.917
DOY332	NDVI-LST	294.15	-5.03	0.961
	NDVI-TOA Radiance	8.56	-0.67	0.945

2.5.3 Comparison between $NDTI_{LST}$ and $NDTI_{TOA}$

Table 2.3 summarizes the observed variability of surface and atmospheric variables. The minimum, maximum, mean and S.D. over the study area for each of the six case days are given for surface emissivity, atmospheric temperature and water vapor content. One can see that the standard deviations of both the surface emissivity and the atmospheric temperature are small for all the case studies (less than 0.01 for surface emissivity, and 1 K for atmospheric temperature), which indicates the minor spatial variability of these two parameters. The typical spatial variability of water vapor content is in the order of 10% for most cases. However, the mean values of water vapor content are higher than 3.9 g cm^{-2} for DOY 208 and DOY 279, implying that the atmosphere is relatively humid. Under these conditions, the calculation of NDTI using TOA radiances might result in higher uncertainties as it is more sensitive to the variation of water vapor.

Table 2.3: The spatial variability of surface emissivity, atmospheric temperature and water vapor content in terms of minimum, maximum, mean and standard deviation (S.D.) over the study area.

Case Day	Emissivity				Atmospheric Temperature (K)				Water Vapor (g cm^{-2})			
	Min	Max	Mean	S.D.	Min	Max	Mean	S.D.	Min	Max	Mean	S.D.
DOY30	0.966	0.992	0.982	0.0022	281.37	286.24	284.74	0.905	0.411	1.371	0.840	0.082
DOY80	0.968	0.992	0.982	0.0020	287.36	291.97	290.71	0.728	0.789	1.837	1.359	0.170
DOY122	0.952	0.992	0.982	0.0022	296.75	301.34	299.99	0.718	1.651	3.795	2.417	0.148
DOY208	0.946	0.992	0.982	0.0024	302.87	307.95	305.97	0.647	3.480	16.053	5.853	0.444
DOY279	0.958	0.992	0.982	0.0025	301.06	305.69	303.73	0.679	1.589	6.976	3.914	0.388
DOY332	0.956	0.992	0.982	0.0021	283.65	288.64	286.68	0.767	0.138	1.695	0.530	0.098

In order to validate the feasibility of estimating NDTI using TOA radiances instead of LST, we compare the $NDTI_{LST}$ value and the $NDTI_{TOA}$ value for every pixel over the study area. Figure 2.8 shows the scatter plots between $NDTI_{LST}$ and $NDTI_{TOA}$ for all days. Table 2.4 summarizes the statistics of $NDTI_{LST}$ and $NDTI_{TOA}$. NDTI values calculated from LST and TOA radiances have maximum difference of ±0.032 in mean while S.D. values are similar for both. Besides, the root mean square deviation (RMSD), bias and R^2 derived from $NDTI_{LST}$ and $NDTI_{TOA}$ are also displayed in Table 2.4. The RMSD values vary from 0.033 to 0.098 and the biases from -0.028 to 0.032. These RMSD values correspond to 8.8-11% of the $NDTI_{LST}$

mean except DOY 208 and DOY 279, which indicates that the NDTI estimates are comparable. Furthermore, the high R^2 values, ranging from 0.904 to 0.939 except DOY 208 and DOY 279, indicate good agreements between the NDTI estimated from MODIS LST products and TOA radiances. It is noted that DOY 208 and DOY 279 present relatively low R^2 values (0.549 and 0.793) and high RMSD values (20% and 19% of the mean $NDTI_{LST}$). According to the theoretical derivation and sensitivity analysis, the reason for this may be related to the inhomogeneity of the atmosphere in our study area. Given the variations of atmospheric temperature and surface emissivity are quite small and similar over the study area (Table 2.3), the difference between $NDTI_{LST}$ and $NDTI_{TOA}$ might be mainly caused by the relative high water vapor content over the study area. As described in the sensitivity analysis, the variation of 10% on water vapor may lead to the change of NDTI higher than 16% when the water vapor content is higher than 4 g cm^{-2} which is a limitation of the proposed method.

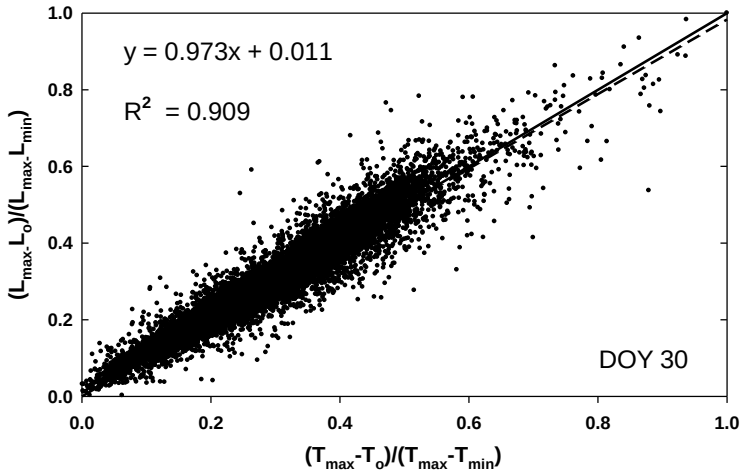

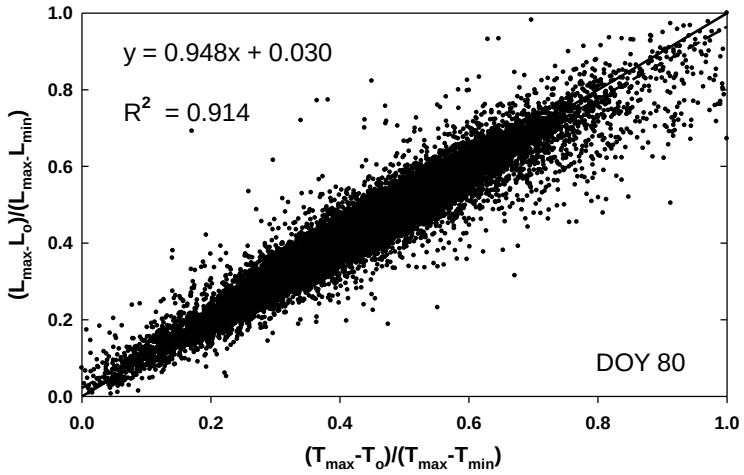

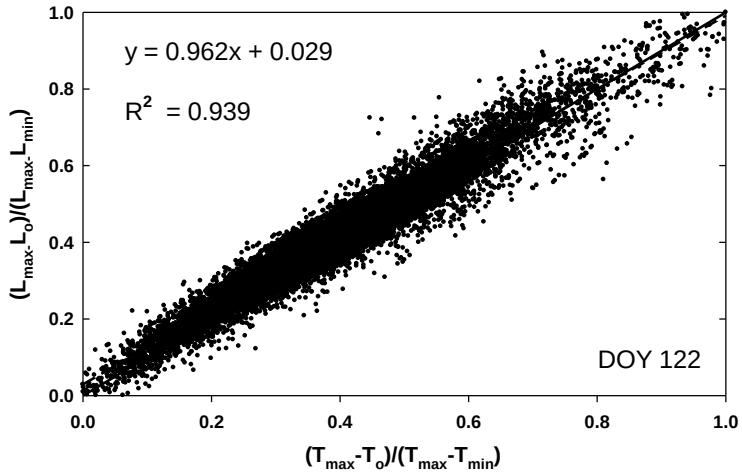
y = 0.962x + 0.029
R2 = 0.939
DOY 122
(Lmax-Lo)/(Lmax-Lmin)
(Tmax-To)/(Tmax-Tmin)
0.0
0.2
0.4
0.6
0.8
1.0

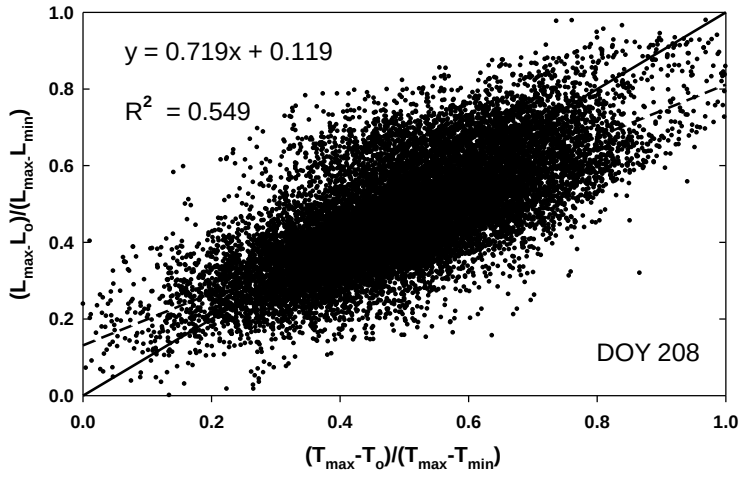
y = 0.719x + 0.119
R2 = 0.549
DOY 208
(Lmax-Lo)/(Lmax-Lmin)
(Tmax-To)/(Tmax-Tmin)
0.0
0.2
0.4
0.6
0.8
1.0

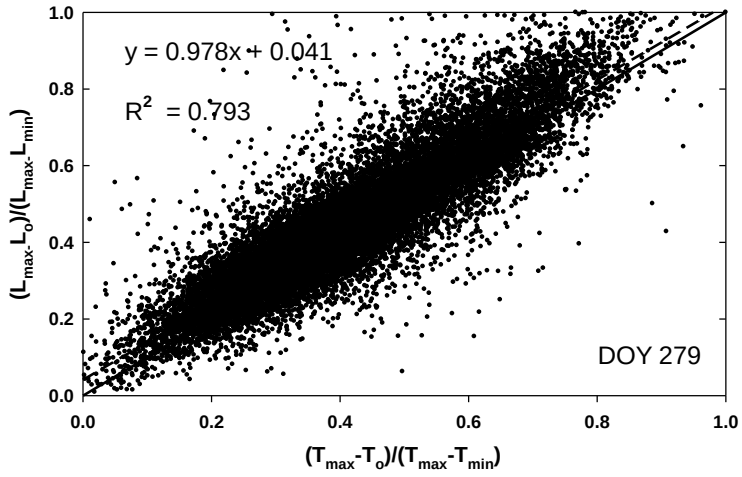
y = 0.978x + 0.041
R2 = 0.793
DOY 279
(Lmax-Lo)/(Lmax-Lmin)
(Tmax-To)/(Tmax-Tmin)
0.0
0.2
0.4
0.6
0.8
1.0

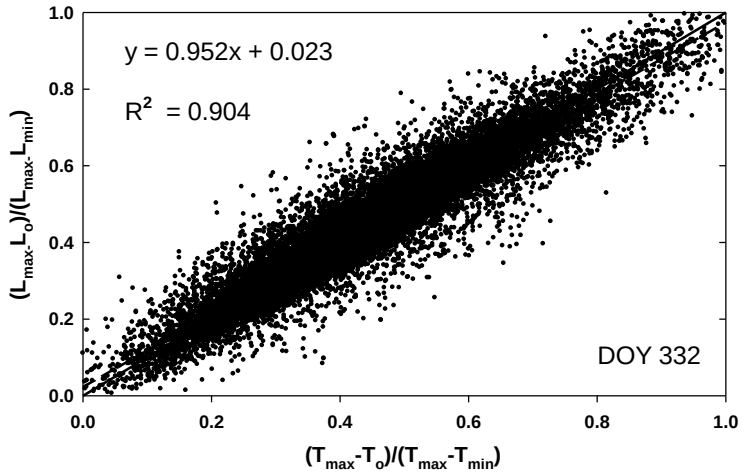

Figure 2.8: Comparison of the NDTI values calculated from LST and TOA radiance (band-31) for the study area. The solid line corresponds to the 1:1 relation and the dashed line to the regression equation.

Table 2.4: Statistical comparison of the NDTI calculated from LST and TOA radiance (band-31) for six case days.

Case Day	$(T_{max}-T_o)/(T_{max}-T_{min})$		$(L_{max}-L_o)/(L_{max}-L_{min})$		RMSD	Bias	R^2
	Mean	S.D.	Mean	S.D.			
DOY30	0.296	0.110	0.299	0.112	0.033	0.003	0.909
DOY80	0.453	0.145	0.449	0.143	0.042	-0.004	0.914
DOY122	0.398	0.136	0.412	0.136	0.035	0.014	0.939
DOY208	0.497	0.149	0.469	0.141	0.098	-0.028	0.549
DOY279	0.415	0.155	0.447	0.170	0.077	0.032	0.793
DOY332	0.450	0.165	0.451	0.166	0.051	0.001	0.904

However, in general, the results of the sensitivity analysis and case studies suggest that the use of TOA radiances instead of LST appears to be a reasonable and accurate alternative to $NDTI_{LST}$ estimates, if the water vapor spatial variability of the study area does not exceed 10%.

2.6 Conclusions

In this study, we have explored the feasibility of using TOA radiances instead of LST to calculate NDTI which is widely used as a pre-cursor for the estimation of surface latent heat fluxes. The method is derived theoretically on the basis of the radiance transfer equation and Planck's law. The results suggest that the method is applicable under the condition that the atmospheric parameters (transmittance and atmospheric temperature) and the surface emissivity are stable spatially. A sensitivity analysis is

carried out to ascertain how variations in surface emissivity, atmospheric temperature and water vapor content affect the NDTI. The uncertainties in NDTI estimates based on TOA radiances are expected to be less than 10%, if the spatial variabilities of atmospheric parameters (water vapor, effective atmospheric temperature) and surface emissivity are below 10%, 4 K and 0.05, respectively. Compared with the variations of surface emissivity and atmospheric temperature, the variation of water vapor would significantly influence the method under moist conditions. Thus, the method should be used with care for humid conditions with water vapor higher than 3 g cm^{-2}.

The proposed method was tested over a heterogeneous area of the Poyang Lake basin for six cases varying from January to November. The results are promising and confirm the applicability of the proposed method when the spatial variations of surface emissivity, atmospheric temperature and water vapor content across the study area are below 0.01, 1 K and 0.2 g cm^{-2} separately. At the same time, the results also show that the variation of water vapor content under humid condition dramatically influence the performance of the method, which is in accordance with the sensitivity analysis.

It should be emphasized that the proposed method is only applicable in regional areas, because the atmospheric conditions are not constant anymore over continental scales. If the atmospheric conditions are constant over the image, the derived equation is a rather simple method. In order to evaluate the proposed method, more practices and validation should be carried out in other different regions using different kinds of satellite data. In addition, future work needs also to be carried out to explore the feasibility of using TOA radiances for the estimation of NDTI over larger continental areas.

Acknowledgements

The authors would like to thank the anonymous reviewers for their valuable comments and suggestions, which have greatly improved this manuscript. This work was partly supported by a Key Program of The Knowledge Innovation Program of CAS (KZCX2–YW–337) and a 100–talent Project of The Chinese Academy of Sciences (CAS) and a National Natural Science Foundation of China (40901162). MODIS data were obtained from the Warehouse Inventory Search Tool at https://wist.echo.nasa.gov/~wist/api/imswelcome/. We thank Mr. D. Zhao for his assistance in data preprocessing. Mr. Peng is financially supported by a joint MPG/CAS doctoral promotion program for his stay in MPI-M, Hamburg. Dr. Loew was supported through the Cluster of Excellence ‘CliSAP’ (EXC177) which is gratefully acknowledged.

Chapter 3

Evaluation of Remote Sensing Based Evaporative Fraction from MODIS TOA radiances using Tower Eddy Flux Network Observations[3]

Abstract

The LST/NDVI (Land Surface Temperature/Vegetation Index) feature space has been widely used to estimate ET (Evapotranspiration) or EF (Evaporative Fraction, defined as the ratio of latent heat flux to surface available energy) in recent decades. Traditionally, it is essential to pre-process satellite TOA (top of atmosphere) radiances to obtain LST and NDVI before estimating EF. However, pre-processing TOA radiances is a cumbersome task including corrections for atmospheric, adjacency and directional effects. Based on the contextual relationship between LST and NDVI, some studies proposed the direct use of TOA radiances instead of satellite products to estimate EF, and found that use of TOA radiances is applicable in some regional studies. The purpose of the present study is to test the robustness of the TOA radiances based EF estimation scheme over different climatic and surface conditions. Flux measurements from 16 FLUXNET (a global network of eddy covariance towers) sites were used to validate the MODIS (Moderate Resolution Imaging Spectro radiometer) TOA radiances estimated EF. It is found that the EF estimates perform well across a wide variety of climate and biome types – grasslands, crops, cropland/natural vegetation mosaic, closed shrublands, mixed forest, deciduous broadleaf forest, and savannas. The overall BIAS (mean bias error), MAD (mean absolute difference), RMSD (root mean square difference) and R (correlation coefficient) values for all the sites 0.018, 0.147, 0.178 and 0.590, respectively, which are comparable with published results in the literature. We conclude that the direct use of measured TOA radiances to estimate EF is feasible and applicable, and would facilitate the relevant applications where minimum pre-processing is important.

[3] Peng, J., Loew, A.: Evaluation of Remote Sensing Based Evaporative Fraction from MODIS TOA radiances using Tower Eddy Flux Network Observations, *In preparation.*

3.1 Introduction

Mapping of the land surface heat fluxes and modeling the mass and energy interactions between land and atmosphere are significant for understanding regional and global water and energy cycles (Jung et al., 2010; Sellers et al., 1997). The complicated physical mechanisms such as turbulent transport, the feedback in the soil-plant-atmosphere continuum and the heterogeneity of land surface all combine to make estimation of energy balance components a challenge (Lettau, 1969; Rodriguez-Iturbe, 2000). Nevertheless, much work has been done in quantifying the surface turbulent fluxes and partitioning among energy balance components (Farahani et al., 2007; Kalma et al., 2008; Wang and Dickinson, 2012). As one fundamental parameter of surface heat fluxes, the EF (Evaporative fraction: defined as the ratio of latent heat flux to available energy) represents the surface control on latent heat and sensible heat fluxes portioning (Caparrini et al., 2003; Bateni et al., 2013). Considering the spatial and temporal variability of the EF characteristic, satellite remote sensing is recognized as a promising technique to provide reasonable EF estimates over large areas and continents (Wang et al., 2006). The approaches proposed in the literature use either empirical or physically based schemes (Gómez et al., 2005; Caparrini et al., 2004; Nishida et al., 2003).

One popular method among them is using the relationship between LST (Land Surface Temperature) and NDVI (Normalized Difference Vegetation Index) (Jiang and Islam, 2001). If the satellite derived LST and NDVI over heterogeneous areas are plotted, the shape of the pixel envelope resembles a physically meaningful triangular or trapezoidal feature space. The physical properties encapsulated in the LST/NDVI space are simple: The LST has low sensitivity over vegetated areas, but increased sensitivity over bare soil regions. The wet edge presents high EF because it has high thermal inertia and strong evaporative cooling. In contrary, the lowest EF occurs at dry edge due to its weakest evaporative cooling (Nemani and Running, 1989; Price, 1990a). The LST/NDVI method uses the spatial variations of LST and NDVI to infer EF without parameterizing surface and aerodynamic resistances that are required by one or two-source energy balance models. On the basis of semiempirical error analysis, Jiang et al. (2004) found that the upper bounds of absolute error and relative error in LST/NDVI estimated EF are less than 0.25 and 33.3%, respectively. Due to its simplicity and relatively high accuracy, this type of approach has already been widely accepted and used (Batra et al., 2006; Stisen et al., 2008; Long and Singh, 2012b). Two comprehensive and systematic reviews about this method have been provided by Carlson et al. (2007) and Petropoulos et al. (2009).

The notable advantage of this method is that it needs only satellite data to retrieve EF with minimum requirements of model inputs and ancillary data (Tang et al., 2011b). However, when satellite data are used to represent traditionally ground-based measurement, such as LST, correcting satellite data based on radiative transfer theory are necessary. Because the information received by the satellite sensors is TOA (Top

of Atmosphere) radiances that are affected by viewing angles and atmospheric variables (Li et al., 2013). This actually poses great challenges for the remote sensing community to develop different correction procedures to eliminate the atmospheric attenuation effects (Vermote et al., 1997). Although much effort has been devoted to establish sophisticated and streamlined data correction procedures, these procedures are troublesome and need independent observation data to satisfy the mathematical and physical constraints. These limitations practically increase the operational difficulty. Under this background, several studies focus on the EF estimation from the TOA radiances rather than satellite products, and found that use of TOA radiances is adequate to estimate EF (Venturini et al., 2004; Peng et al., 2013c). The feasibility of estimating EF using TOA radiances stems from the contextual relationship between LST and NDVI. For applications that depend on contextual information from remote sensing, absolute radiometric calibration to remote sensing data is thought to be unnecessary (Jiang and Islam, 2003; Long and Singh, 2012a). A recent study by Peng et al. (2013a) investigated the general possibility of estimating NDTI (Normalized Difference Temperature Index, a key parameter for EF estimation) from TOA radiances through a physical understanding of Planck radiation law and radiative transfer equation, and performed a detailed sensitivity analysis of NDTI on surface and atmosphere variability. They concluded that the TOA radiances based estimates have similar level of accuracy as obtained using atmospherically corrected data products. However, as indicated by Peng et al. (2013c), more validation work of TOA radiances retrieved EF against ground-based measurements over different climatic and surface conditions still needs to be carried out.

The main objective of this study is to evaluate the applicability and robustness of the TOA radiances based EF estimation scheme through comparison with measurements from 16 FLUXNET (a global network of eddy covariance towers) sites. These sites represent a wide range of climates and biome types – grasslands, crops, cropland/natural vegetation mosaic, closed shrublands, mixed forest, deciduous broadleaf forest, and savannas.

3.2 Materials and methodology

3.2.1 Methodology

According to the definition of EF, the instantaneous EF (dimensionless) calculated from instantaneous flux tower measurements can be written as:

$$EF(t) = \frac{LE(t)}{R_n(t) - G(t)} = \frac{LE(t)}{LE(t) + H(t)} \quad (3.1)$$

Where R_n is the surface net radiation (W m^{-2}), G is the ground heat flux (W m^{-2}), LE is latent heat flux (W m^{-2}) and H the sensible heat flux (W m^{-2}). Meanwhile, the daytime EF is determined using the following equation:

$$EF_{daytime} = \frac{\int_{t_1}^{t_2} LE(t)\,dt}{\int_{t_1}^{t_2} [H(t) + LE(t)]\,dt} \quad (3.2)$$

Where the time difference $t_2 - t_1$ refers to the time from 8:00 LT to 17:00 LT in the present study. The daytime rather than daily was selected as study period, because the eddy covariance technique is more reliable during daytime (Wilson et al., 2003). The daytime EF can also be estimated by averaging EF from different time periods. The two approaches would have similar results if EF is stable during daytime. In practice, the latter approach is more sensitive to the errors in LE and H measurements when they have low absolute values during early morning and late afternoon.

On the basis of the LST/NDVI feature space, the parameterization of EF using TOA radiances is given as follows:

$$EF = \phi \frac{\Delta}{\Delta + \gamma} \quad (3.3)$$

Where ϕ combines the effects of Budyko–Thornthwaite–Mather wetness parameter and Priestley Taylor coefficient, which accounts for aerodynamic and canopy resistances (Choi et al., 2009). Δ is the slope of saturated vapor pressure at the air temperature (kPa K^{-1}) and γ is the psychrometric constant (kPa K^{-1}) (Crago and Brutsaert, 1992).

Details about the calculation of ϕ and Δ can be found in the work of Jiang et al. (2001). In this study, ϕ is calculated using TOA radiances:

$$\phi = \phi_{\max} \frac{L_{\max} - L_s}{L_{\max} - L_{\min}} \quad (3.4)$$

Where ϕ_{max} is the maximum ϕ without surface water stress and often set to 1.26. L_s is the observed TOA radiance for a given pixel whose NDVI value is $NDVI_i$, L_{max} and L_{min} are the corresponding highest and smallest TOA radiance which have the same $NDVI_i$ value.

3.2.2 Flux tower observations

The publicly available FLUXNET observations were used to validate TOA radiances estimated EF. Through a suit of instruments, the flux towers can measure half-hourly averaged fluxes (net radiation, soil heat flux, latent heat flux and sensible heat flux) and meteorological data (e.g., air temperature, precipitation). The relevant FLUXNET methodologies and summaries could be found in the research of Aubinet et al. (1999) and Baldocchi et al. (2001). In this study, 16 FLUXNET sites were selected mainly according to the following criteria: (1) the land cover for the 1 km^2 area centered on the flux tower is homogeneous; (2) the land cover for a 10000 km^2 area encompassing the flux tower is heterogeneous with a range of fractional vegetation cover, and the terrain of the area is also flat. More information about these sites is given in Table 3.1.

Table 3.1: Details about the FULXNET sites used in this study.

Site	Location	Biome type	Latitude	Longtitude	Elevation (m)	Years	Data Size	Reference
USARM	United States	Grasslands	36.6058	-97.4888	314	2003--2006	105	Fischer et al. (2007)
CASF2	Canada	Grasslands	54.2539	-105.8775	520	2003-2005	81	Amiro et al. (2006)
DEGri	Germany	Grasslands	50.9495	13.5125	385	2004-2009	175	Gilmanov et al. (2007)
CHOe1	Switzerland	Grasslands	47.2856	7.7321	450	2002-2003	54	Ammann et al. (2007)
USNe2	United States	Croplands	41.1649	-96.4701	362	2001--2005	112	Verma et al. (2005)
USNe3	United States	Croplands	41.1797	-96.4396	363	2001--2005	115	Verma et al. (2005)
USBkg	United States	Croplands	44.3453	-96.8362	510	2004--2006	130	Gilmanov et al. (2005)
USGoo	United States	Cropland/Natural vegetation mosaic	34.2547	-89.8735	87	2002--2006	252	Bolstad et al. (2004)
CASF3	Canada	Closed shrublands	54.0916	-106.0053	540	2003-2005	81	Amiro et al. (2006)
USWCr	United States	Deciduous broadleaf forest	45.8059	-90.0799	520	2000--2006	297	Cook et al. (2004)
DEHai	Germany	Deciduous broadleaf forest	51.0793	10.452	430	2003-2007	142	Reichstein et al. (2005)
ITRo1	Italy	Deciduous broadleaf forest	42.4081	11.93	235	2000-2006	251	Rey et al. (2002)
USMMS	United States	Mixed forest	39.3231	-86.4131	275	2000--2005	189	Curtis et al. (2002)
ITNon	Italy	Mixed forest	44.6898	11.0887	25	2001-2003	106	Reichstein et al. (2003)
DEMeh	Germany	Mixed forest	51.2753	10.6555	286	2003--2006	110	Wang et al. (2011)
BWMa1	Botswana	Savannas	-19.917	23.5603	950	2000--2001	211	Veenendaal et al. (2004)

These sites are located across Europe, North America and Africa and cover a broad range of land cover types (Table 3.1). According to the IGBP (International Geosphere-Biosphere Programme) classification scheme, the sites are classified into seven main groups: grasslands, crops, cropland/natural vegetation mosaic, closed shrublands, mixed forest, deciduous broadleaf forest, and savannas. Further details about these sites are provided by the corresponding publications and references therein.

Eddy covariance technique has already been found to underestimate latent and sensible heat flux by extensive studies (Foken et al., 2011; Twine et al., 2000; Wilson et al., 2002). Therefore, the eddy covariance measured heat fluxes need to be adjusted to force energy balance closure. One commonly used solution is the Bowen ratio method, which repartitions the available energy into latent and sensible heat flux according to the Bowen ratio (Twine et al., 2000). Since this method is relatively simple and accurate and has been successfully used by many applications (Anderson et al., 2005; Barr et al., 2012; Nagler et al., 2005), we also applied the method in the present study to correct the eddy covariance measured latent and sensible heat fluxes.

3.2.3 Remote sensing data

MODIS (Moderate Resolution Imaging Spectro radiometer) is the primary satellite sensor in the NASA Earth Observing System (EOS) for land, ocean and atmosphere research. Specifically, the Terra-MODIS Collection 5 data products used in this study mainly include MOD021KM, MOD03, MOD09GA and MOD35_L2. The MOD021KM and MOD03 datasets are used to provide geolocated and calibrated thermal band TOA radiance. And the MOD09GA product contains surface reflectance that is used to calculate NDVI in this study. As the LST/NDVI method requires the study area to have relatively constant atmospheric condition and flat topography, different square domains covering each flux tower site are used as study areas. The size of each domain is about 60000 km^2, representing a wide range of fractional vegetation cover and soil wetness. On the basis of MOD35_L2 cloud mask product, the clear sky condition was indentified when larger than 85% of the study domain being clear. The number of clear sky days (clear sky at MODIS overpass time) for each flux site is also shown in Table 3.1.

3.2.4 Algorithm evaluation

A number of quantitative indices, including BIAS (mean bias error), MAD (mean absolute difference), RMSD (root mean square difference), RE (relative error) and R (correlation coefficient) are selected in this study to evaluate the model performance. Furthermore, the results were also compared with published studies.

3.3 Results and discussion

3.3.1 Energy imbalance of flux tower measurements

The energy closure of the flux tower measurements was investigated for the selected clear sky case days. Figure 3.1 shows the comparisons of observed daytime average available energy R_n – G against measured turbulent fluxes LE + H for all the FLUXNET sites except CASF2 and CASF3, because these two sites both have no G measurements. The closure ratio CR=(LE + H)/(R_n – G) varies from 0.57 to 0.98 with residual energy E=R_n – LE – H – G ranging from -136.53 to -8.83 W/m^2 at all the sites. Overall, the S (slope) and R from the linear least squares regression for observed LE + H and R_n – G are 0.70 and 0.79, respectively. It can also be seen that the measured LE + H fluxes are generally less than R_n – G for all these sites with the averaged closure ratio CR_m of 0.78 and mean residual energy E_m of 78.14 W/m^2. Similar results were reported by Wilson et al. (2002) and Foken (2008). However, the causes of the lack of energy balance closure are still under discussion and might be related to systematic bias in instrumentation, neglected energy sinks, landscape heterogeneity and mismatch in source areas.

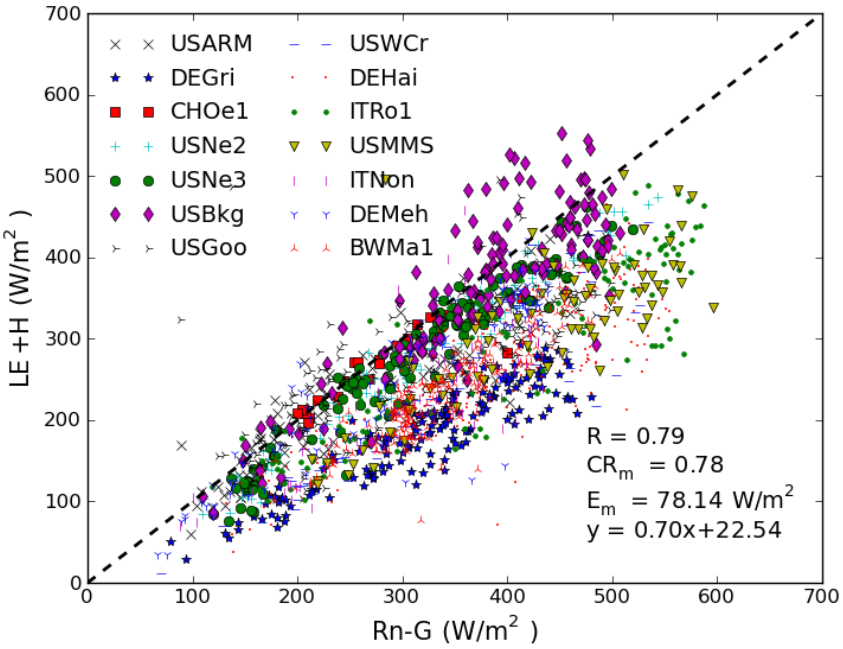

Figure 3.1: Comparison of the observed available energy (R_n – G) against the sum of latent heat and sensible fluxes (LE + H) from all the FLUXNET sites. CRm, Em and dashed line represent the averaged closure ratio, mean residual energy and perfect agreement, respectively.

3.3.2 Can near noon instantaneous EF represent daytime EF?

The EF has been found to be stable during daylight hours in many studies (Peng et al., 2013b; Caparrini et al., 2004; Crago, 1996), making it possible to extrapolate instantaneous EF values to daytime scale. In this study, the instantaneous EF at MODIS overpass time was used to represent daytime EF value. To examine the feasibility of this assumption, the FLUXNET measurements were used to respectively estimate instantaneous and daytime EF as described in section 3.2.1. Figure 3.2 shows the comparison between the instantaneous EF at the time of MODIS overpass and the daytime EF for all the FLUXNET sites in our study. Table 3.2 presents the BIAS, MAD, RMSD, RE and R values for every FLUXNET site. It can be seen that these statistical indices values range from -0.035 to -0.011 for BIAS, from 0.023 to 0.050 for MAD, from 0.031 to 0.084 for RMSD, from -7.19% to -2.82% for RE and from 0.931 to 0.996 for R. On the whole, a good agreement and negligible bias between the instantaneous and daytime EF is obtained with BIAS = 0.019, MAD = 0.031, RMSD = 0.042 and RE (Relative Error) = 4.42% for all the sites. Besides, it can be observed that R = 0.986 (Table 3.2). These statistics results indicate the reliability of using EF constant assumption to estimate daytime EF without incurring substantial errors.

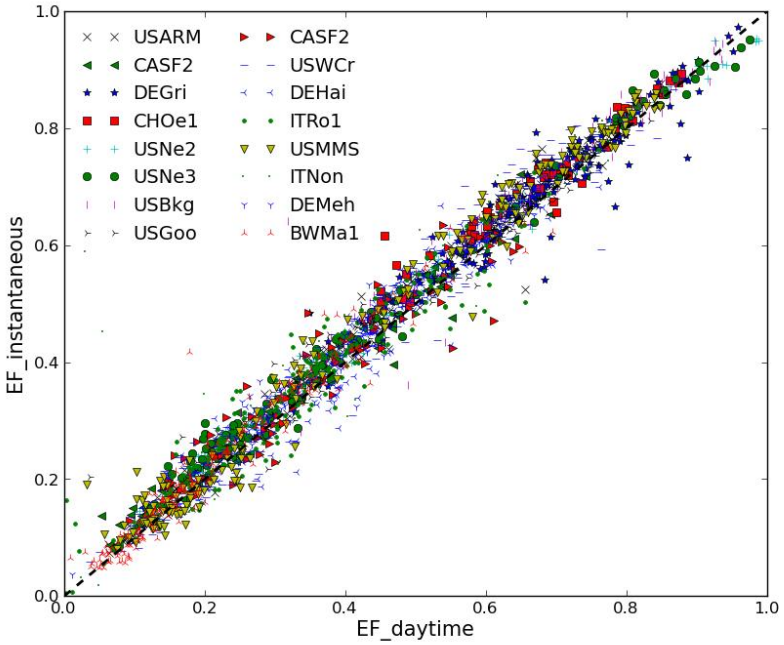

Figure 3.2: Comparisons of MODIS overpass time EF and daytime average EF for all the sites.

Table 3.2: Statistical results for the comparisons between instantaneous EF at MODIS overpass time and daytime average EF.

Site	BIAS	MAD	RMSD	Relative error(%)	R
USARM	-0.019	0.029	0.036	-5.33	0.990
CASF2	-0.016	0.025	0.032	-4.28	0.989
DEGri	-0.019	0.032	0.041	-2.82	0.961
CHOe1	-0.033	0.036	0.045	-4.63	0.973
USNe2	-0.020	0.027	0.032	-4.33	0.996
USNe3	-0.024	0.030	0.035	-5.47	0.995
USBkg	-0.027	0.034	0.048	-4.01	0.978
USGoo	-0.018	0.023	0.031	-3.25	0.991
CASF3	-0.011	0.033	0.046	-2.89	0.952
USWCr	-0.017	0.032	0.042	-3.78	0.988
DEHai	-0.013	0.033	0.041	-3.14	0.964
ITRo1	-0.017	0.032	0.042	-4.85	0.968
USMMS	-0.021	0.032	0.042	-4.71	0.991
ITNon	-0.035	0.050	0.084	-7.19	0.931
DEMeh	-0.021	0.029	0.036	-4.47	0.985
BWMa1	-0.016	0.025	0.035	-6.33	0.980
All sites	-0.020	0.031	0.042	-4.47	0.977

3.3.3 Evaluation of EF from MODIS TOA radiances

The MODIS TOA radiances estimated EF is evaluated with FLUXNET measured EF. The comparison results are illustrated by Figure 3.3. Different colors of the points indicate the slopes for the dry edges of the LST/NDVI scatter plots. The variations of the slopes imply the variety of hydrological conditions during the study period, and could capture the variability of gradient in virtual surface dryness and wetness pattern. In general, the derived EF agrees reasonably well with tower-measured EF with data points distributed around the dashed 1:1 line without a significant discrepancy. The grasslands, croplands, cropland/natural vegetation mosaic and mixed forest show good accuracy, whereas the savannas have slightly poorer performance.

Table 3.3 gives a comprehensive summary of the statistical metrics for each FLUXNET site. It can be observed that the BIAS values range from -0.08 to 0.12. The RMSD values vary from 0.103 to 0.224, and the R values appear to be low to high ranging from -0.280 to 0.846. The overall BIAS, MAD, RMSD and R values for all the sites are 0.018, 0.147, 0.178 and 0.590, respectively. This suggests the feasibility of estimating EF with MODIS TOA radiances alone. If we excluded the results of

savannas, the BIAS, MAD and RMSD are further reduced to 0.006, 0.138, and 0.168 with a better R of 0.648. The LST/NDVI feature space has already extensively been used to estimate EF. The performance of this method has also been reported in the literature. It would be interesting to compare our results from TOA radiances with those results based on products. Table 3.4 summarizes the statistics of the differences between satellite products derived EF and observed EF from previous published studies. It can be seen that the statistical results found in this study are comparable to those reported previously. It further suggests that using TOA radiances can provide reasonable estimation accuracy for EF, while requiring less input data and preprocessing like in classical LST/NDVI feature space approaches.

In terms of error assessment, most discrepancies between estimated and measured EF are less than 0.2, presented in Figure 3.3. As precipitation could introduce a large error of EF estimation through enhancing soil moisture and leaf interception, we used plus symbols to indicate the days contaminated by precipitation which occurred before satellite overpass. Besides, Wang and Dickinson (2012) found that the LST/NDVI method is most suitable for a growing season in middle latitude areas. In other words, the range of vegetation index should be large enough, and the soil moisture rather than air temperature or available energy is the key control of EF. It means the sample days that are not during growing season will have more uncertainties, which is in accordance with our results. We marked the days not belonging to the growing season using x marker in Figure 3.3. Other sources of uncertainty of our results could be related to the scale discrepancy between the FLUXNET footprint measurements and satellite pixel estimates, as well as the linear parameterization of ϕ (without inclusion of wind speed and surface humidity) within the LST/NDVI feature space. Considering the simplicity and acceptable accuracy level of the LST/NDVI method, we conclude that the use of TOA radiances appears to be adequate for the estimation of EF, and would facilitate direct use of remote sensing data for the situations (e.g., multi-sensor studies, data assimilation) where minimum pre-processing is important.

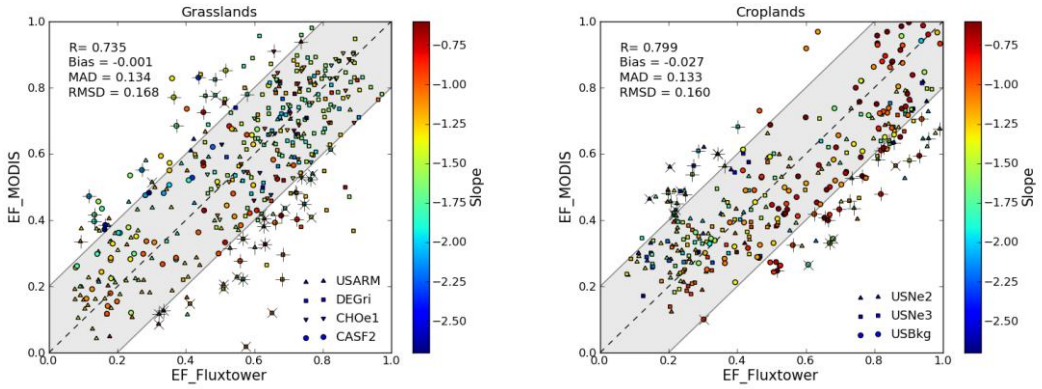

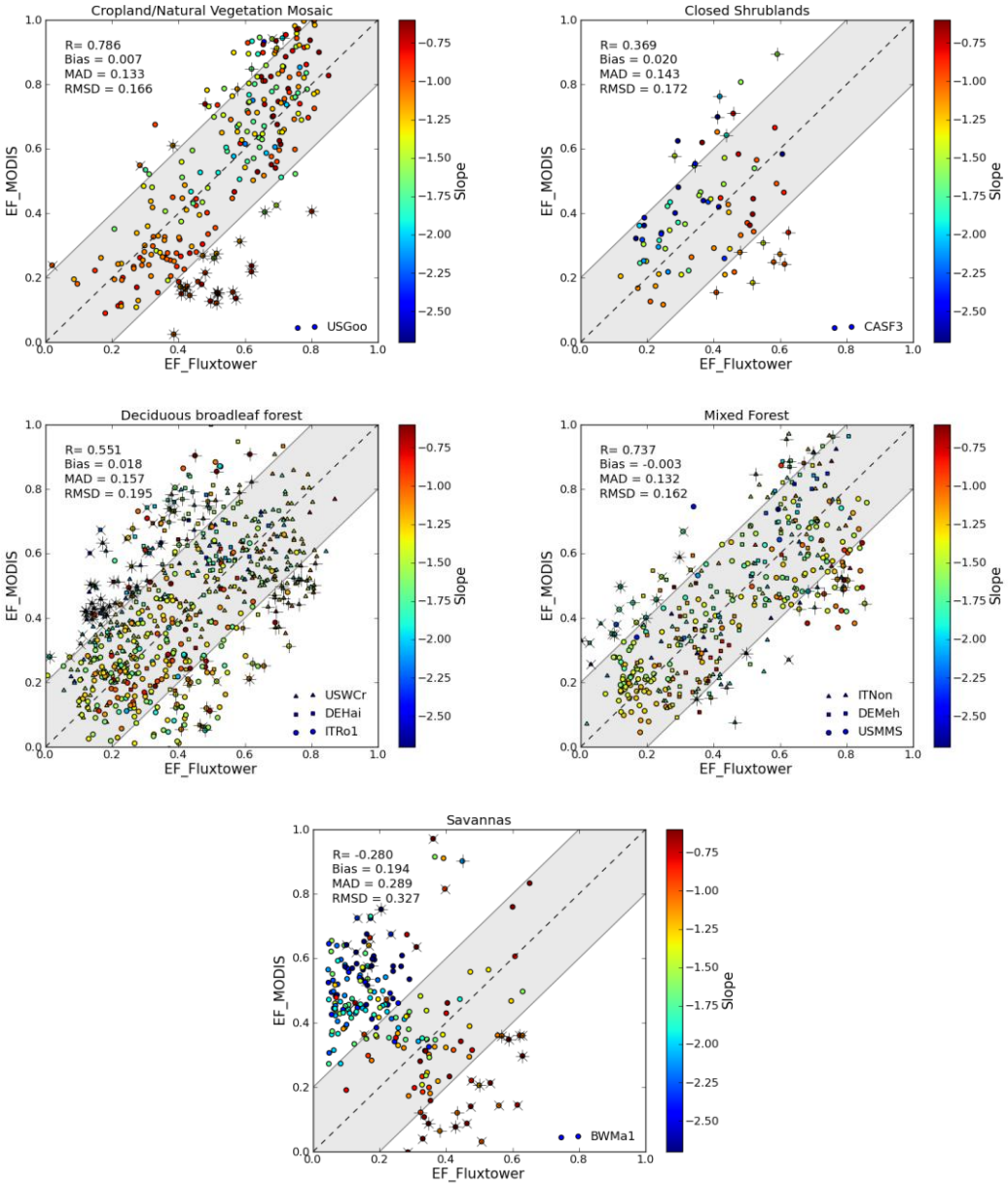

Figure 3.3: Comparisons of estimated and observed EF at FLUXNET sites for different biome types. Dashed line is the 1:1 line. Grey area represents that the discrepancies between estimated and observed EF are less than 0.2. The points with plus markers are the samples contaminated by precipitation. The x marker indicates those samples outside the growing season. Different colors indicate the slopes for the dry edges of the LST/NDVI scatter plots.

Table 3.3: Statistics on differences between estimated and observed EF for each FLUXNET site.

Site	Biome type	BIAS	MAD	RMSD	R
USARM	Grasslands	0.004	0.129	0.153	0.741
CASF2	Grasslands	0.077	0.160	0.190	0.524
DEGri	Grasslands	-0.035	0.141	0.182	0.382
CHOe1	Grasslands	-0.013	0.080	0.103	0.714
USNe2	Croplands	0.011	0.150	0.177	0.787
USNe3	Croplands	-0.003	0.115	0.140	0.846
USBkg	Croplands	-0.080	0.133	0.160	0.790
USGoo	Cropland/Natural Vegetation Mosaic	0.007	0.133	0.166	0.786
CASF3	Closed Shrublands	0.020	0.143	0.172	0.369
USWCr	Deciduous broadleaf forest	0.028	0.142	0.172	0.702
DEHai	Deciduous broadleaf forest	0.120	0.184	0.224	0.400
ITRo1	Deciduous broadleaf forest	-0.052	0.161	0.202	0.365
USMMS	Mixed forest	-0.024	0.132	0.167	0.780
ITNon	Mixed Forest	-0.002	0.145	0.173	0.725
DEMeh	Mixed Forest	0.033	0.118	0.142	0.807
BWMa1	Savannas	0.194	0.289	0.327	-0.280
All sites		0.018	0.147	0.178	0.590

Table 3.4: Accuracy assessment of the LST/NDVI feature space method used to derive EF in the literature.

Reference	Sensor used	BIAS (Mean value)	RMSD (Mean value)	R (Mean value)
Nishida et al. (2003)	MODIS	-0.130--0.100 (0.010)	0.110--0.280 (0.170)	0.100--0.900 (0.710)
Venturini et al. (2004)	MODIS, AVHRR	-0.069--0.088 (0.009)	0.081--0.188 (0.130)	0.442--0.768 (0.580)
Wang et al. (2006)	MODIS	-0.182--0.131 (-0.018)	0.077--0.244 (0.157)	-0.634--0.89 (0.437)
Stisen et al. (2008)	MSG SEVIRI	-0.040--0.120 (0.060)	0.130--0.190 (0.160)	0.350--0.640 (0.510)
Jiang et al. (2009)	AVHRR	-0.038--0.154 (0.049)	0.119--0.242 (0.158)	-0.868--0.037 (-0.414)
Tang et al. (2011a)	MODIS	0.039--0.067 (0.057)	0.100--0.125 (0.112)	0.338--0.648 (0.496)

3.4 Conclusions

The motivation of this study was to investigate the applicability and robustness of the TOA radiances based EF estimation scheme using global FLUXNET observations. From direct comparison with measured EF at different FLUXNET sites, the estimated EF from TOA radiances perform well across a wide variety of climate and biome types. The accuracy level is also comparable with published results in the literature, and different land covers have similar performances except savannas. Diagnostic anal-

ysis suggests that the large error in the TOA radiances based EF estimates are related to the precipitation before satellite overpass and the linear parameterization of ϕ. If the sample days are not in the growing season, the uncertainties and errors will occur more easily. Besides, using FLUXNET measurements, the instantaneous EF is also found to be applicable for representing daytime EF, without incurring substantial errors. Overall, the present study, together with the work by Peng et al. (2013a; 2013c) demonstrated that the direct use of measured TOA radiances to estimate EF is feasible and applicable. The notable advantage of this approach is that no atmospheric corrections are required. This would facilitate data assimilation and multi-sensor studies due to its minimal pre-processing requirements. The problem of using polar-orbiting satellites data such as MODIS is the temporal gaps due to cloud cover. One possible solution is utilizing the geostationary satellites data with high temporal resolution. Future work will examine the full capacities of the TOA radiances approach for geostationary satellites data.

Acknowledgements

The authors would like to thank the FLUXNET community for making the data public available (http://www.fluxdata.org/) as well as the principal investigators and collaborators of these sites. The MODIS datasets used in this study were obtained from the Level 1 and Atmosphere Archive and Distribution System (LAADS, http://ladsweb.nascom.nasa.gov/). We thank Friedrich Richter for his assistance with downloading MODIS data. The work was partly supported by the Cluster of Excellence CliSAP (EXC177), University of Hamburg, funded through the German Science Foundation (DFG) and by the CAS-MPG Doctoral Promotion Programme (DPP).

Chapter 4

How representative are instantaneous evaporative fraction measurements of daytime fluxes?[4]

Abstract

Sun synchronous optical and thermal remote sensing is a promising technique to provide instantaneous ET (Evapotranspiration) estimates during satellite overpass. The common approach to extrapolate the instantaneous estimates to values for daily or longer periods relies on the assumption that the EF (Evaporative Fraction, defined as the ratio of latent heat flux to surface available energy) remains nearly constant during daytime. However, there is still no consensus on the validity of the self preservation of the EF. We use FLUXNET (a global network of eddy covariance stations) measurements to examine this self preservation, and the conditions under which it can hold. It is found that the instantaneous EF could represent daytime EF under clear sky conditions especially between 11:00 h LT (local time) and 14:00 h LT for all stations. However, the results show that the EF is more variable during cloudy sky conditions so that an increase in cloud cover results in an increase in the variability of the EF during daytime.

[4] Peng, J., Borsche, M., Liu, Y., and Loew, A.: How representative are instantaneous evaporative fraction measurements of daytime fluxes?, *Hydrology and Earth System Sciences*, 17(10):3913-3919, 2013.

4.1 Introduction

Estimates of land surface ET (Evapotranspiration) are crucial for better understanding climate and hydrological interactions (Jung et al., 2010; Oki and Kanae, 2006). Over the last few decades, numerous physical and empirical remote sensing-based models that vary in complexity have been proposed to estimate ET. Most of them provide instantaneous ET estimates at the time of satellite overpass. For a review, see e.g. Kalma et al. (2008) and Wang and Dickinson (2012). In order to acquire ET values over daily or longer time periods, there is a need to extrapolate instantaneous to daily values (Chávez et al., 2008). The most widely used method is the assumption of daytime self preservation of EF (Evaporative Fraction) (Sugita and Brutsaert, 1991; Brutsaert and Sugita, 1992; Crago and Brutsaert, 1996). The EF is normally a diagnostic of surface energy balance and defined as the fraction of available energy partitioned toward latent heat flux. Theoretically, the EF is supposed to isolate vegetation and soil control from other factors in the determination of surface energy balance components. Furthermore, it can remove the daily sinusoidal like variations of the latent heat flux and sensible heat flux at the land surface, and it remains almost constant during daytime under clear sky conditions (Gentine et al., 2007; Gentine et al., 2011; Li et al., 2008) (Figure 4.1). Shuttleworth et al. (1989), Nichols and Cuenca (1993) and Crago and Brutsaert (1996) used in situ measurements of surface energy balance components and showed that the EF is nearly constant during daytime under clear sky days. Model studies by Lhomme and Elguero (1999) and Gentine et al. (2007) found that daytime self preservation of the EF is only satisfied under limited environmental conditions. Hoedjes et al. (2008) found that the EF remains fairly constant under dry conditions and presents a pronounced concave up shape under wet conditions. However, most of the above studies are generally based on measurements from relatively short time periods and across a small range of environmental and climatological conditions. Since the daytime constant EF assumption is the basis for extrapolating instantaneous ET estimates to daily values, whether it holds or not is a fundamental issue to the satellite-based temporal extrapolation applications. The objective of this paper is to further examine how representative instantaneous EF measurements are for daytime values. To address this question, long term time series of data from a global network of EC (Eddy Covariance) stations (FLUXNET) are analyzed across a wide range of ecosystems and climates.

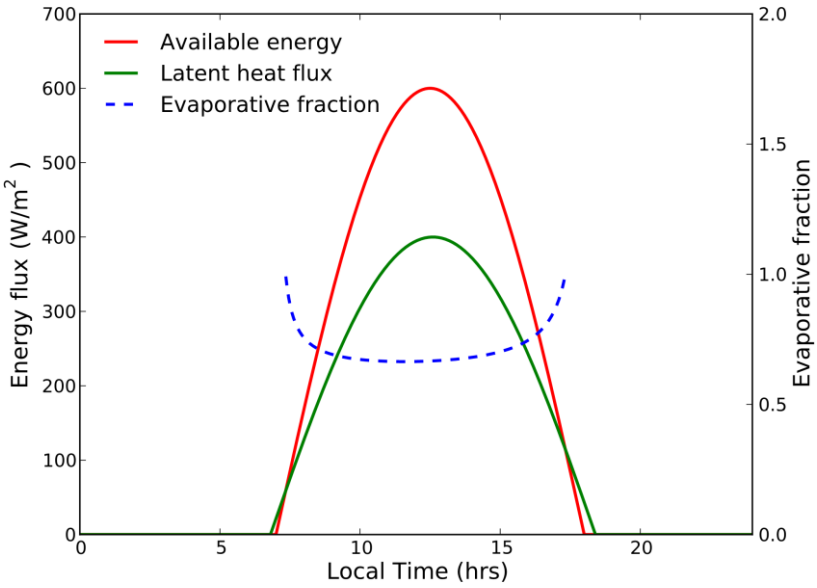

Figure 4.1: Conceptual framework for the diurnal variations of surface energy components and EF. Solid red line represents surface available energy, solid green line represents latent heat flux, and dashed blue line represents EF.

4.2 Data and Methods

The FLUXNET methodology and review papers can be found in the work of Aubinet et al. (1999), Baldocchi et al. (2001) and Baldocchi (2008). There are a total of seventy-two FLUXNET sites over a variety of vegetation types and geographic locations used in the present study (Table 4.1; Figure 4.2). For each site, in situ measurements (non gap-filled) of net radiation, ground heat flux, latent heat flux and sensible heat flux are used to test the EF self preservation hypothesis. These measurements are half-hourly measured and quality controlled. More information about the selected sites is given in Table 4.1. Energy balance closure is an important criterion for evaluating the quality of measured heat fluxes from EC systems. However, flux towers typically do not exhibit energy closure because of systematic bias in instrumentation, mismatch in source areas, neglected energy sinks, and landscape heterogeneity (Foken et al., 2011; Twine et al., 2000; Wilson et al., 2002). In this study, the Bowen ratio correction method recommended by Twine et al. (2000) is used to adjust EC measured heat fluxes to constrain energy balance closure.

Table 4.1: Summary of the FLUXNET sites used in this study. More site information can be found at http://www.fluxdata.org/

Site	Biome type	Elevation (m)	Years
CASF3	Closed Shrublands	540	2003--2005
USLos	Closed Shrublands	480	2001--2005

CAMer	Croplands	70	1998--2005
USGoo	Croplands	87	2002--2006
NLLut	Croplands	TBD	2006--2006
USBkg	Croplands	510	2004--2006
USBo1	Croplands	219	1996--2007
USNe1	Croplands	361	2001--2005
USNe2	Croplands	362	2001--2005
USNe3	Croplands	363	2001--2005
DEHai	Deciduous broadleaf forest	430	2000--2007
FRHes	Deciduous broadleaf forest	300	1997--2008
ITRo1	Deciduous broadleaf forest	235	2000--2006
ITRo2	Deciduous broadleaf forest	224	2002--2006
USBar	Deciduous broadleaf forest	272	2004--2005
USHa1	Deciduous broadleaf forest	340	1991--2006
USMMS	Deciduous broadleaf forest	275	1999--2005
USUMB	Deciduous broadleaf forest	234	1999--2003
USWCr	Deciduous broadleaf forest	520	1999--2006
AUTum	Evergreen broadleaf forest	1200	2001--2006
FRPue	Evergreen broadleaf forest	270	2000--2008
PTEsp	Evergreen broadleaf forest	95	2002--2008
ZMMon	Evergreen broadleaf forest	1053	2000--2009
CAMan	Evergreen needleleaf forest	259	1994--2003
CANS1	Evergreen needleleaf forest	260	2002--2005
CANS2	Evergreen needleleaf forest	257	2001--2005
CANS3	Evergreen needleleaf forest	258	2001--2005
CANS4	Evergreen needleleaf forest	260	2002--2003
CANS5	Evergreen needleleaf forest	254	2001--2005
CASF1	Evergreen needleleaf forest	536	2003--2005
CZBK1	Evergreen needleleaf forest	908	2000--2008
DETha	Evergreen needleleaf forest	380	1996--2003
DEWet	Evergreen needleleaf forest	785	2002--2008
FIHyy	Evergreen needleleaf forest	181	1996--2008
FISod	Evergreen needleleaf forest	180	2000--2008
FRLBr	Evergreen needleleaf forest	61	1996--2003
ILYat	Evergreen needleleaf forest	650	2001--2003
ITRen	Evergreen needleleaf forest	1730	1999--2008
ITSRo	Evergreen needleleaf forest	4	1999--2008
NLLoo	Evergreen needleleaf forest	25	1996--2008
RUFyo	Evergreen needleleaf forest	265	1998--2008
SESk2	Evergreen needleleaf forest	55	2004--2005
UKGri	Evergreen needleleaf forest	340	1997--2006
USBlo	Evergreen needleleaf forest	1315	1997--2006
ATNeu	Grasslands	970	2002--2007

CASF2	Grasslands	520	2003--2005
CHOe1	Grasslands	450	2002--2003
DEGri	Grasslands	385	2004--2009
HUBug	Grasslands	140	2002--2008
NLCa1	Grasslands	0.7	2003--2008
USARM	Grasslands	314	2003--2006
USAud	Grasslands	1469	2002--2006
USFPe	Grasslands	634	2000--2006
BEBra	Mixed forests	16	1997--2008
BEVie	Mixed forests	450	1996--2008
CHLae	Mixed forests	689	2004--2008
DEMeh	Mixed forests	286	2003--2006
DKSor	Mixed forests	40	1996--2008
ITLav	Mixed forests	1353	2000--2002
ITNon	Mixed forests	25	2001--2003
UKESa	Mixed forests	97	2003--2005
USHo1	Mixed forests	60	1996--2004
USHo2	Mixed forests	91	1999--2004
USSyv	Mixed forests	540	2002--2006
CANS6	Open shrublands	260	2001--2005
CANS7	Open shrublands	297	2002--2005
ITPia	Open shrublands	18	2002--2003
BWMa1	Savannas	950	1999--2001
AUFog	Woody savannas	27	2006--2007
AUHow	Woody savannas	41	2001--2006
USTon	Woody savannas	177	2001--2006
USVar	Woody savannas	129	2001--2006

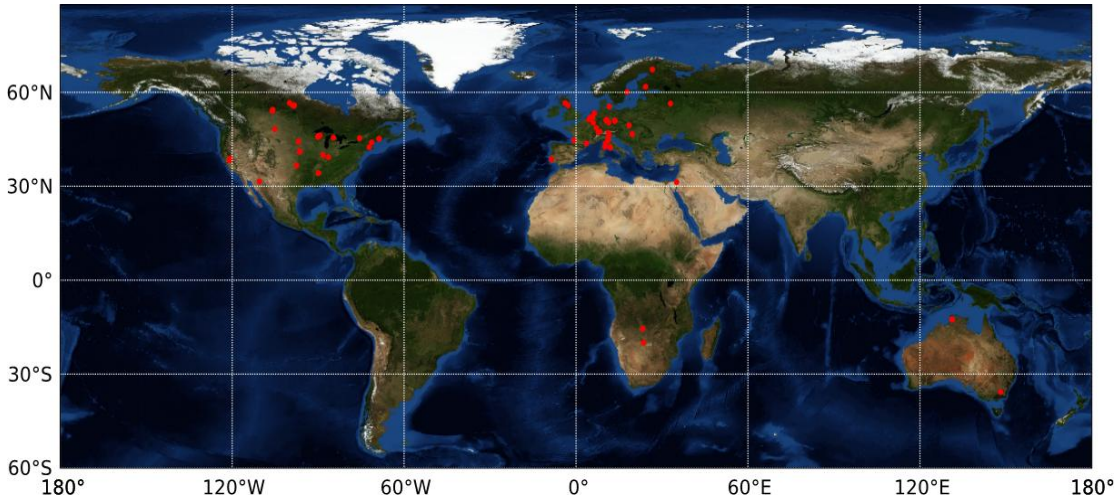

Figure 4.2: The seventy-two FLUXNET sites locations (solid red circle).

The instantaneous EF (dimensionless) is then calculated from the corrected instantaneous flux values as follows:

$$EF(t) = \frac{LE(t)}{R_n(t) - G(t)} = \frac{LE(t)}{LE(t) + H(t)} . \tag{4.1}$$

Where R_n is the surface net radiation (W m^{-2}), G is the ground heat flux (W m^{-2}), LE is the latent heat flux (W m^{-2}) and H the sensible heat flux (W m^{-2}). In addition, the daytime EF is determined by the following equation:

$$\begin{aligned} EF_{daytime} &= \frac{\int_{t_1}^{t_2} LE(t)\,dt}{\int_{t_1}^{t_2} [R_n(t) - G(t)]\,dt} \\ &= \frac{\int_{t_1}^{t_2} LE(t)\,dt}{\int_{t_1}^{t_2} [H(t) + LE(t)]\,dt} . \end{aligned} \tag{4.2}$$

Where the time difference $t_2 - t_1$ refers to the time from 8:00 h LT (local time) to 17:00 h LT in the present study. In order to evaluate the relationship between instantaneous EF and daytime EF, the statistics metrics of R^2 (coefficient of determination) and RMSD (Root mean square difference) and RE (relative error) are chosen in this study.

Considering the effects of clouds on the stability of EF, previous studies have no consensus opinions. For example, Hall et al. (1992) suggested that cloudiness induced variations in net radiation should not affect EF significantly, whereas Crago and Brutsaert (1996) attributed variations of EF to cloudiness. In this study, the effects of different clouds cover on EF are analyzed. The clearness index K_T (the ratio of the global solar radiation measured at the surface to the total solar radiation at the top of the atmosphere) (Liu and Jordan, 1960; Okogbue et al., 2009) is used to perform the sky conditions classification. In order to examine the effects of cloudiness on the EF self preservation, K_T values of $0 \le K_T \le 0.15$, $0.15 < K_T \le 0.65$, $0.65 < K_T \le 1$ are used to define cloudy, partly cloudy and clear-sky conditions, respectively.

4.3 Results and discussion

In order to find the relationships between instantaneous EF and daytime EF under clear sky conditions, statistical results between the EF at different time periods and daytime EF are illustrated in Figure 4.3a. These results are analyzed based on all seventy-two FLUXNET sites to reach more general conclusions. Figure 4.3a shows the box plots of R^2, RMSD and RE respectively for the relationships between instantaneous EF and daytime EF. In general, the EF at different time periods of the daytime agrees well with daytime EF except for the 8:00 h LT to 9:00 h LT and 16:00 h LT to 17:00 h LT periods. The relatively low R^2 and high RMSD and RE values for these time periods indicate the large variations in EF in the early morning and late

afternoon. This agrees with Rowntree (1991) and Nichols and Cuenca (1993), who found that the EF at low level of radiation loading was higher than through the midday period. From 11:00 h LT to 14:00 h LT, the minimum R^2 value is higher than 0.75, the maximum RMSD is less than 0.087, and RE is in the range from -10.15% to 3.79%. These statistics indicate that EF during these time periods is close to the daytime EF. The midday (12:00 h LT to 13:00 h LT) EF is closest to daytime EF with $R^2 = 0.920 \pm 0.053$, RMSD = 0.050±0.013, RE = -4.47%±2.48%. A similar result was found by other authors (e.g. Farah et al., 2004). The possible reason for such a result is that energy fluxes change at a slower rate compared to early morning and late afternoon. Since the analysis is based on long term FLUXNET measurements under a wide range of surface, environmental and climate condition, we conclude that the instantaneous EF can generally represent daytime EF under clear-sky conditions especially from 11:00 h LT to 14:00 h LT. This EF self preservation can also be explained from a physical perspective. The EF during daytime mainly depends on land surface properties such as vegetation amount, soil moisture and surface resistance to heat and momentum transfer. Most of them tend to vary slowly during daytime compared to other fast changing variables (e.g. surface temperature, radiation). In summary, the above results confirm that the self preservation of EF can be used to calculate daytime ET from instantaneous estimates based on sun synchronous satellite observations during clear sky conditions. Because the midday EF is closest to daytime EF, the midday overpass satellites (e.g. MODIS and AVHRR) are expected to provide better results than platforms which have an overpass time in the morning or late afternoon (e.g. Landsat). However, the self preservation of the EF should be used with caution. The negative RE values (-4.47%±2.48%) suggest that the midday EF tends to slightly underestimate daytime EF, due to the concave shape of the diurnal variation of the EF (Brutsaert and Sugita, 1992; Crago, 1996; Sugita and Brutsaert, 1991).

As the FLUXNET sites cover a wide range of climates and biome types (croplands, deciduous broadleaf forests, evergreen needleleaf forests, grasslands, mixed forest, woody savannas, savannas, open shrublands, closed shrublands, and evergreen broadleaf forests), we investigate the influences of biome types on the self preservation of the EF. Table 4.2 gives a comprehensive summary of the statistical metrics for the comparisons between midday EF and daytime EF for different biome types. It can be observed that the self preservation of the EF over different biome type has similar performance with R^2 higher than 0.894, RMSD lower than 0.054, and RE less than 10.15%. The detailed comparison results between instantaneous EF at different time periods and daytime EF over different biome types are provided in Supplementary material Figure A.1. Therefore, little evidence is found from the above results based on FLUXNET data that the biome type affects the self preservation of the EF.

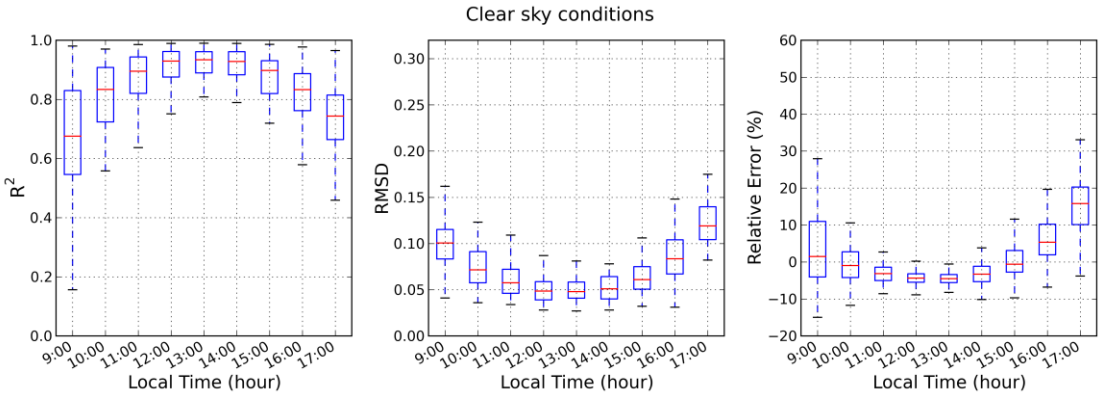

(a)

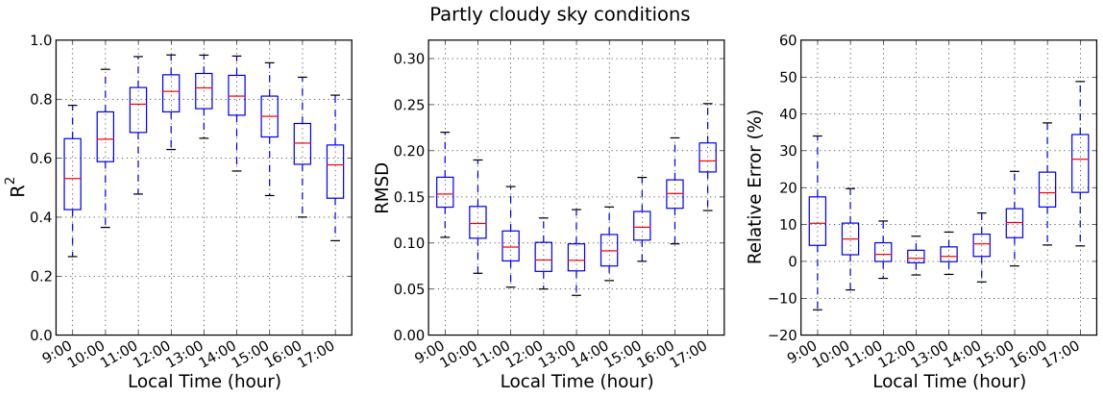

(b)

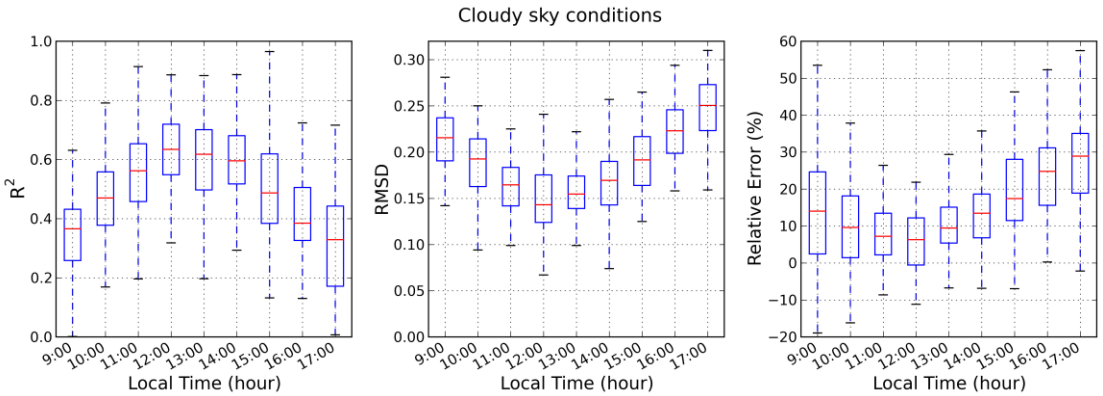

(c)

Figure 4.3: Box plots of statistical results for the comparison between instantaneous EF in different time of daytime and daytime EF for all the FLUXNET sites (number = 72) under different sky conditions: (a) clear sky conditions; (b) partly cloudy sky conditions; and (c) cloudy sky conditions. Each box lies between the 0.25 and the 0.75 quartile, the median value is drawn as a horizontal red line, and the whiskers indicate the range of the data within the maximum and the minimum values.

Table 4.2: Statistical results for the comparisons between midday EF and daytime EF over different biome types.

Biome type	R^2	RMSD	Relative error (%)	Sample size
Croplands	0.954±0.026	0.051±0.008	-2.81±1.50	8
Deciduous broadleaf forests	0.956±0.034	0.043±0.008	-4.48±1.64	9
Evergreen needleleaf forests	0.904±0.053	0.051±0.014	-5.40±1.35	21
Grasslands	0.901±0.062	0.053±0.015	-2.01±3.62	9
Mixed forests	0.902±0.052	0.054±0.013	-4.70±2.03	11
Woody savannas	0.946±0.028	0.041±0.010	-4.05±0.93	4
Savannas	0.966±0.000	0.042±0.000	-11.15±0.00	1
Open shrublands	0.915±0.063	0.049±0.019	-7.12±1.60	3
Closed shrublands	0.968±0.016	0.035±0.002	-2.06±0.67	2
Evergreen broadleaf forests	0.894±0.031	0.053±0.011	-5.63±1.53	4
All types	0.920±0.053	0.050±0.013	-4.47±2.48	72

Figures 4.3b and 4.3c display the performance of the EF constant assumption under different cloud cover conditions. It can be seen that the stability of the EF is related to cloudiness. The EF is more variable under partly cloudy conditions compared to clear sky conditions. An increase in cloud cover results in an increase in the variability of the EF during daytime. For total cloud cover the R^2 values between instantaneous EF in different time periods and daytime EF obviously decrease as compared to clear skies. Poorer RMSD and RE are also obtained at the same time. This is because cloudiness causes significant fluctuations in available energy and the rate of surface heating, which further leads to variability in both instantaneous EF and daytime EF. Thus, the EF tends to be more variable during cloudy sky conditions. It is necessary to consider the effects of cloudiness, when the EF self preservation assumption is used to upscale instantaneous estimates to continuous longer time periods (Brutsaert and Sugita, 1992; Van Niel et al., 2012). The above results provide additional information on the uncertainty resulting from cloudy sky conditions for the EF daytime estimates.

4.4 Conclusions

The commonly used method to extrapolate remote sensing based instantaneous EF to daily values is to assume constant EF during daytime (so-called daytime self preservation). However, evidence for this constant EF approach is based on limited duration field measurements. Taking advantage of a global network of long term ground-based measurements from FLUXNET, the daytime EF constant hypothesis is examined here. It is found that the EF during daytime from 11:00 h LT to 14:00 h LT agrees well with daytime EF under clear sky conditions (R^2>0.75, RMSD<0.087, -10.15%<RE <3.79%), and the midday (12:00 h LT to 13:00 h LT) EF is closest to

daytime EF with R^2 = 0.920±0.053, RMSD = 0.050±0.013, RE = -4.47%±2.48%. However, the EF is more variable during cloudy conditions when compared to clear sky conditions, and an increase in cloud cover results in an increase in the variability of the EF during daytime. Thus the EF constant hypothesis is strictly true only for clear sky conditions. Nonetheless, the above results provide a basis for remote sensing-based estimation of the EF based on sun synchronous satellite observations. The midday overpass satellites (e.g. MODIS and AVHRR) are expected to give better results than other overpass time platforms. The important conclusion from the present study is that the EF constant assumption is valid over a wide range of ecosystems and climates.

Acknowledgements

Many thanks are given to the FLUXNET community for making the data publicly available (http://www.fluxdata.org/) as well as to the principal investigators and collaborators of each FLUXNET site. The authors would also like to thank Editor Bob Su, Reviewer Tom Van Niel and three anonymous reviewers for their valuable comments and suggestions that have greatly improved the manuscript. This work was partly supported by the Cluster of Excellence CliSAP (EXC177), University of Hamburg, funded through the German Science Foundation (DFG) and by the CAS-MPG Doctoral Promotion Programme (DPP).

Chapter 5

Estimation of Evapotranspiration from MODIS TOA radiances in the Poyang Lake basin, China[5]

Abstract

Routine and rapid estimation of ET (Evapotranspiration) at regional scale is of great significance for agricultural, hydrological and climatic studies. A simplified single-source energy balance parameterization scheme, known as the LST/NDVI (Land Surface Temperature/Vegetation Index) triangle method, has been applied successfully to estimate regional clear sky ET in many studies. Based on the triangle method, we proposed a new method in this study to estimate daily ET directly using the TOA (Top of Atmosphere) radiances without performing atmospheric correction and other complicated processes. Firstly, the EF (Evaporative Fraction, defined as the ratio of latent heat flux to surface available energy) was estimated by interpolation in the LST/NDVI triangular–shaped scatter space, which was constructed using the MODIS (Moderate Resolution Imaging Spectro radiometer) TOA radiances over a heterogeneous area of the Poyang Lake Basin in China. Then the net radiation over the same study area was derived based entirely on MODIS TOA radiances as well. Finally, daily ET maps were estimated from these EF and net radiation maps by using a sinusoidal temporal interpolation model. The estimated EF, net radiation and ET have been validated against field observations collected for the period October 2007-July 2008. The results indicate comparable accuracy to results of other current widely used satellite-based methods. In addition, intercomparisons between the proposed method-based estimates and MODIS products-based estimates were also carried out over the validation site. The results suggest that the proposed method could reach similar level of accuracy as the MODIS products-based triangle method. Overall, the proposed algorithm requires fewer assumptions and can avoid complex atmospheric corrections associated with the satellite derived products. It should facilitate direct use of satellite data for determining ET and relevant applications. Nonetheless, more validation work needs to be carried out over various climatic regions and under different surface conditions in the future.

[5] Peng, J., Liu, Y., Zhao, X., and Loew, A.: Estimation of evapotranspiration from MODIS TOA radiances in the Poyang Lake basin, China, *Hydrology and Earth System Sciences*, 17(4):1431-1444, 2013.

5.1 Introduction

ET (Evapotranspiration), including plant transpiration and direct evaporation from soil and water surface, is an important variable in water and energy balances on the Earth's surface. Accurate estimation of the temporal and spatial distribution of ET is of great significance for better understanding the mechanism of climate change and plays a crucial role in the agricultural, hydrological and meteorology studies (Jung et al., 2010). The major factors that control the rate of ET are the availability of water, the amount of available energy, the wind speed and the humidity gradient in the air above the evaporating surface (Monteith, 1981). To account for all such factors, various micrometeorological techniques (e.g., Bowen ratio, eddy covariance and lysimeter systems) have been designed to measure ET on various spatial scales from hundreds to thousands of meters (Farahani et al., 2007). Although ET is quantifiable at the small scale using ground-based techniques, larger-scale estimates require alternative measurements and estimation approaches. They need a variety of land surface and atmospheric variables, such as temperature, albedo, and vegetation indices. Such quantities, however, are difficult to obtain over large-scale heterogeneous areas and have to be extrapolated/interpolated to various temporal and spatial scales with limited accuracy. Therefore, it is important and necessary to develop other methods for estimating regional ET.

Satellite remote sensing is a promising technique for mapping temporally and spatially continuous patterns of regional ET with a reasonable degree of accuracy. It can provide unprecedented spatial distribution of critical land surface and atmospheric variables, such as land surface temperature, albedo, and vegetation indices, which are logistically and economically impossible to obtain from conventional observation networks. Over the last few decades, a number of physical and empirical remote sensing based models that vary in complexity have been proposed to estimate ET. For a review, see e.g. Kalma et al. (2008). These methods usually need ancillary surface and atmospheric data like wind speed, aerodynamic resistance, and surface roughness, which cannot readily be measured through remote sensing techniques. Therefore, it is still challenging to routinely map regional and even global ET distribution using satellite remote sensing without ground measurements or reanalyzed meteorological data.

In order to overcome this problem, some attempts have been made to develop new parameterizations for ET estimation that depend entirely on remote sensing. One widely used approach among them is the LST/NDVI (land surface temperature/vegetation index) triangle method, which was proposed by Jiang and Islam (1999). This method is based on the P–T (Priestley–Taylor) equation (Priestley and Taylor, 1972), which can be considered as a simplified version of the more general Penman equation (Penman, 1948). The most difficult part in this approach is the determination of the P–T parameter, which accounts for aerodynamic and canopy resistances. The essence of the LST/NDVI triangle method is to estimate the P–T

parameter on the basis of the triangular shape of the LST/NDVI feature space, which is formed by the scatter of LST against NDVI over a wide range of soil moisture content and fractional vegetation cover. The emergence of the triangular shape is caused primarily by different sensitivity of LST to soil moisture variations over bare soil and vegetated areas. Recent and detailed reviews of the triangle method have been provided in terms of the theoretical basis, biophysical properties and limitations by Carlson (2007) and Petropoulos et al. (2009).

A number of researchers have also demonstrated the applicability of this method for the estimation of regional ET and soil moisture from various satellite sensors, such as NOAA-AVHRR, TERRA/AQUA-MODIS, MSG-SEVIRI and FY-2C (Tang et al., 2011b; Sandholt et al., 2002; Han et al., 2010). The notable advantages of this method lie in its simplicity, easiness to parameterize ET, and relatively high accuracy. The assessment of ET derived by the triangle method (Stisen et al., 2008; Long et al., 2012; Jiang et al., 2004; Jiang and Islam, 2003; Batra et al., 2006), shows that the root mean square difference (RMSD) and relative error (RE) are generally within 60 W m^{-2} and 30% at the hourly and daily timescales.

In general, the uncertainty associated with the estimation of ET could be attributed to many sources, one of which is the accuracy of the input satellite data products, such as LST, NDVI and albedo. However, these satellite derived variables are associated with a series of errors due to residual atmospheric effects, spatial and temporal resolution, viewing angles, etc. Since the triangle method is dependent on these variables, the uncertainties associated with the estimations of these variables will be accumulated and impact the accuracy of ET. Besides, the derivations of these variables rely on a series of steps in the processing chain, typically including angular modeling, atmospheric and radiative transfer correction. This poses a challenge to the remote sensing community in their effort to incorporate these processing procedures. In practice, these procedures are often complicated and increase the operational difficulty.

The objective of the present study is to develop an alternative scheme to estimate daily ET directly using the TOA (Top of Atmosphere) radiances without performing atmospheric correction and other processes. This idea stems from our earlier study that links TOA radiances with EF (evaporative fraction, defined as the ratio of latent heat flux to surface available energy) based on physical understanding of radiative transfer theory and Planck's law (Peng et al., 2013a; Peng and Liu, 2011). Several earlier studies have also focused on the estimation of net surface shortwave and longwave radiation from measurements at the TOA (Wang and Liang, 2009; Tang et al., 2006), which significantly simplified the procedure and introduced relative few sources of error. The method proposed here is based on the triangle method, utilizing the EF and net radiation schemes mentioned above to derive an instantaneous ET from the MODIS (Moderate Resolution Imaging Spectro radiometer) TOA radiances over a heterogeneous area of the Poyang Lake Basin in China. A temporal interpolation scheme was subsequently implemented to produce a daily ET from our instantaneous estimates. To evaluate the performance of this new method, the

estimates from the MODIS products were also derived based on the triangle method. Then the both estimates were compared to a time series of ground-based measurements from Nanchang Ecological Experiment Station in the Poyang Lake Basin of China.

The paper is organized as follows: Section 5.2 presents the methodology and issues related to the retrieval of daily ET. Section 5.3 describes the data used in this study. Section 5.4 presents the results of implementing the proposed method over the study area for selected case days. Validations of the estimates against field observations are also discussed in this section. The conclusion is presented in Section 5.5.

5.2 Methodology for ET retrieval

5.2.1 Triangle method

On the basis of spatial contextual information between land surface temperature and vegetation index, various methods have been proposed to retrieve soil water content, monitor drought conditions and analyze land use and land cover change (Wan et al., 2004; Sun and Kafatos, 2007; Lambin and Ehrlich, 1996; Carlson et al., 1995). The triangle method for ET by Jiang and Islam (1999) belongs to this category. It is named after the triangular or trapezoidal shape when plotting LST against NDVI (Figure 5.1). The two boundaries of the LST/NDVI feature space constitute limiting conditions for the surface fluxes. The dry edge corresponding to higher temperatures represents minimum ET with unavailability of soil moisture for different vegetation indices. Here the surface temperature reaches a physical maximum where no evaporative cooling occurs. The wet edge corresponding to lower temperatures represents potential ET with unlimited soil water availability for different vegetation indices.

The implicit assumption of the triangle method is that ET primarily depends on soil moisture and vegetation cover. This assumption requires a heterogeneous area with a full range of possible soil moisture and vegetation fraction values, and at the same time relatively uniform atmospheric forcing (Margulis et al., 2005; Tang et al., 2011a). For a detailed description and discussion of the LST/NDVI triangle feature space for ET estimation, the reader is referred to the work of Jiang and Islam (2001). On the basis of an extension of the P–T equation and the existence of a physically meaningful relationship between evaporative fraction and remotely sensed spatial variables (e.g., NDVI, LST and soil moisture), the parameterization of ET proposed by Jiang and Islam (1999) is expressed with the following equation:

$$ET = \phi\left(\frac{\Delta}{\Delta+\gamma}\right)(R_n - G). \tag{5.1}$$

Where ET is evapotranspiration (W m^{-2}), R_n is the surface net radiation (W m^{-2}), G is the soil heat flux (W m^{-2}), Δ is the slope of saturated vapor pressure at the air tempera-

ture (kPa K^{-1}) and γ is the psychrometric constant (kPa K^{-1}). Φ is a substitute for the P–T coefficient, which accounts for aerodynamic and canopy resistances. In the standard application of the P–T method, Φ is approximately 1.26 for wet surface equilibrium conditions (Eichinger et al., 1996). In practice, Φ, which is determined by wind speed, air temperature and surface moisture, should not be assigned to a constant value (Komatsu, 2003; Davies and Allen, 1973). It is important to note that in the absence of significant advection and convection, Φ in equation (1) can take a wider range of 0 (no ET) to (Δ+γ)/Δ (maximum ET). This scheme is more applicable for a wide range of surface evaporative conditions where R_n-G is the driving force for ET.

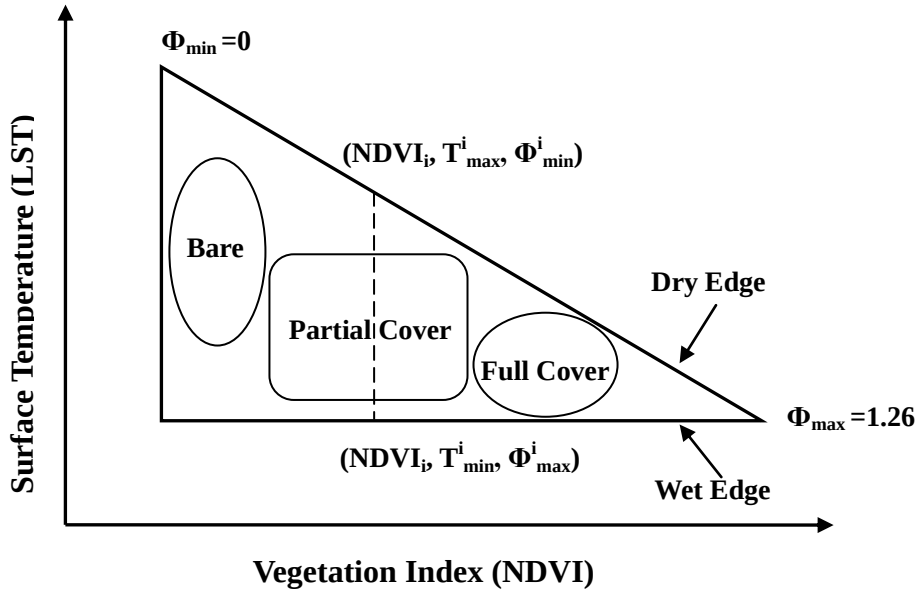

Figure 5.1: Conceptual diagram of the LST/NDVI scatter plot to estimate evaporative fraction using wet and dry surfaces assumption. The dry (upper solid line) and wet (lower solid line) edges represent the maximum ET and minimum ET, respectively (after Tang et al., 2010; Lambin and Ehrlich (1996) and Sandholt et al. (2002)).

In order to obtain the value of Φ, a three-step linear interpolation scheme based on the LST/NDVI triangle is used in the following manner (see Figure 5.1): (1) determine the dry and wet edges in the triangular space; (2) the global minimum and maximum Φ are respectively set to $\Phi_{min} = 0$ for the driest bare soil pixel and $\Phi_{max} = 1.26$ for the densely vegetated pixel with largest NDVI and lowest LST, then Φ^i_{min} is linearly interpolated for each NDVI interval ($NDVI_i$) between Φ_{min} and Φ_{max}, and Φ^i_{max} for each $NDVI_i$ is obtained from the lowest LST pixel with that NDVI interval (Φ^i_{max} is generally set to $\Phi^i_{max} = \Phi_{max} = 1.26$); (3) Φ^i value within each NDVI interval is interpolated between the lowest LST pixel (T^i_{min}, Φ^i_{max}), and highest LST pixel (T^i_{max}, Φ^i_{min}). Consequently, the Φ value for each pixel can be calculated using a normalized form of LST, and the mathematical expression is given as follows (Jiang and Islam, 2001):

$$\Phi = \frac{T^i_{\max} - T^i}{T^i_{\max} - T^i_{\min}} (\Phi^i_{\max} - \Phi^i_{\min}) + \Phi^i_{\min}. \quad (5.2)$$

The key procedure associated with the implementation of the above scheme is the accurate determination of the dry and wet edges. The wet edge (a horizontal line representing potential ET) is generally identified from the lowest surface temperature over different vegetation indices (Jiang and Islam, 2001). However, the dry edge (oblique line representing minimum ET) determination is a little subjective, which could incur uncertainty in the calculation of Φ. Tang et al. (2010) proposed an automatically iterative process to determine the dry edge more objectively. This procedure is applied here to get the linear-relation:

$$T^i_{\max} = a + bNDVI_i, \quad (5.3)$$

where a and b respectively define the intercept and slope of the dry edge.

According to equation (5.1) and the definition of EF, EF can be directly estimated as:

$$EF = \Phi(\frac{\Delta}{\Delta+\gamma}). \quad (5.4)$$

The slope of saturated vapor pressure Δ at the air temperature T_a is given as:

$$\Delta = \frac{26297.76}{(T_a - 29.65)^2} \exp(\frac{17.67(T_a - 273.15)}{T_a - 29.65}). \quad (5.5)$$

The sensitivity of Δ/(Δ+γ) on the variation of T_a is quite small with a reported 1%–2% change per 1 K change in T_a (Jiang and Islam, 2001; Garatuza-Payan et al., 2001). Therefore, the T_a used in this equation can be obtained by using mean surface temperature or mean inland water surface temperature as a surrogate without incurring much error (Jiang and Islam, 2001; Tang et al., 2010). In this work, the MODIS MOD07 air temperature product will be used to provide spatially distributed T_a, which is derived through a statistical relationship between observed TOA radiances and corresponding atmospheric profiles (Menzel et al., 2002).

The major advantages of the triangle method are that：(1) it holds true for a wide range of surface conditions; (2) it is relatively insensitive to uncertainties associated with atmospheric corrections and land surface heterogeneity; (3) all of the four quantities (Φ, R_n, G, and Δ) involved in equation (5.1) can be derived independently using remotely sensed data alone; (4) EF and R_n are estimated independently from each other, which provides the possibility to evaluate the performance of EF and R_n estimations respectively. The main limitation of the triangle method is that a large number of pixels over a flat area with a wide range of soil wetness and fractional vegetation cover are required to make sure that the dry and wet limits exist in the triangular space.

5.2.2 Estimation of ET from MODIS products

Instead of getting T_s and NDVI from in-situ measurements, the parameters estimated from satellite data are used. In the following, MODIS products are used to derive ET ($ET_{Products}$). In order to apply the triangle method to MODIS products, the EF and R_n will be estimated respectively. Several steps need to be carried out for EF calculation. As stated in Section 5.2.1, the LST/NDVI triangular space should be constructed firstly. The NDVI is calculated using the MOD09GA surface reflectance products after atmospheric correction, and LST is from the MODIS surface temperature product retrieved from MOD11_L2. Then, the wet and dry edges of the triangular space are determined using the algorithm described in Section 5.2.1. Finally, the EF value for each pixel in the study area is calculated from the triangular space.

R_n, the sum of R_{sn} (shortwave net radiation) and R_{ln} (longwave net radiation), has to be estimated from satellite data. Here we employed the algorithm proposed by Bisht et al. (2005) for estimating R_n entirely from MODIS products. The method can be expressed as:

$$R_n = R_{sn} + R_{ln} = (1-\alpha)\frac{S_0 \cos^2\theta}{d} + \sigma\varepsilon_a T_a^4 - \sigma\varepsilon_s T_s^4 \tag{5.6}$$

with

$$d = 1.085\cos\theta + e_0(2.7+\cos\theta)\times 10^{-3} + 0.1,$$

$$\varepsilon_a = \left[1-(1+\xi)\exp\left\{-(1.2+3\xi)^{1/2}\right\}\right],$$

$$\text{and } \xi = 46.5 e_0 / T_a. \tag{5.7}$$

Where α is the land surface albedo calculated from MOD43, S_0 is the solar constant at the atmospheric top (1367 W m^{-2}), θ is the solar zenith angle extracted from MOD03, σ is the Steffan – Boltzmann constant (5.67× 10^{-8} Wm^{-2} K^{-4}), T_a is the air temperature retrieved from MOD07, ε_s and T_s are the surface temperature and surface emissivity both extracted from MOD11_L2, e_0 is the vapor pressure calculated from MOD07 dew point temperature by using the Clausius-Clapeyron equation:

$$e_0 = 6.11\exp\left[\frac{L_V}{R_V}\left(\frac{1}{T_0}-\frac{1}{T_d}\right)\right]. \tag{5.8}$$

Where L_v is the latent heat of vaporization (2.5×10^6 J kg^{-1}), R_v is the gas constant for water vapor (461 J kg^{-1} K^{-1}), T_d is the dew point temperature and T_0 = 273 K.

5.2.3 Estimation of ET from MODIS TOA Radiances

In order to avoid certain difficulties associated with the processing chain for derivation MODIS products, we directly used MODIS TOA radiances to estimate ET. The algorithm for estimating EF from MODIS TOA radiances is the same to the

MODIS TOA products-based EF except for the input data source. About EF, Peng and Liu (2011) demonstrate the feasibility of using TOA radiances to estimate EF with the triangle method. Firstly, the TOA reflectance is used for calculating the TOA Normalized Difference Vegetation Index ($NDVI_{TOA}$). It can be computed from the Level 1 MOD021KM and MOD03 datasets by converting the scaled integers (SI) to reflectance value with the following equation as given by (Toller et al., 2006):

$$TOA\_refectance = reflectance\_scale*(SI-reflectance\_offset)/\cos(\theta). \quad (5.9)$$

Where the SI, reflectance_scale and reflectance_offset values are extracted from the MOD021KM head file, and θ, the solar zenith angle, is extracted from the MOD03 dataset. Then $NDVI_{TOA}$ is calculated using the TOA reflectance values as follows:

$$NDVI_{TOA} = (\rho_{NIR} - \rho_{RED})/(\rho_{NIR} + \rho_{RED}). \quad (5.10)$$

Where ρ_{Nir} and ρ_{Red} are the TOA reflectances in the near infrared (NIR) and the red band from the MOD021KM dataset. The TOA radiance of the MODIS thermal infrared band 31 (L_{31}) is used instead of the MODIS LST product. It is extracted using the following scaling equation:

$$TOA\_radiance = radiance\_scale*(SI - radiance\_offset). \quad (5.11)$$

With the SI, radiance_scale and radiance_offset values coming from the MOD021KM head file. Then, EF value for each pixel in the study area can be calculated using TOA reflectances and radiances as input.

The parameterization scheme for estimating R_n based on MODIS TOA radiances is different from the one applied to TOA MODIS products in Section 5.2.2. In this study, a parameterization of R_{sn} fully based on MODIS TOA radiances proposed by Tang et al. (2006) is used:

$$R_{sn} = \frac{E_0 \cos\theta_S}{D^2}(\alpha' - \beta' r), \quad (5.12)$$

$$r = b_0 + \sum_{i=1}^{7} b_i \rho_i. \quad (5.13)$$

Here E_0 is the solar irradiance at TOA, D is the earth–sun distance in astronomical unit. θ_s is the solar zenith angle extracted from MOD03, r is the broadband albedo at TOA, α' and β' are parameters dependent on solar zenith angle and atmospheric precipitable water extracted from MOD05 over land surface, ρ_i is the TOA reflectance in the MODIS band i (i =1–7) as provided in MOD021KM. b_0–b_7 are coefficients depending on the view zenith angle and the solar zenith angle, which are both retrieved from MOD03.

Similarly, Wang et al. (2009) and Wang and Liang (2009) a method to directly estimate the R_{ln} with merely MODIS TOA radiances as inputs:

$$R_{ln} = L_{Tair}(a_0 + a_1 L_{27} + a_2 L_{29} + a_3 L_{33} + a_4 L_{34} + b_1 \frac{L_{32}}{L_{31}} + b_2 \frac{L_{33}}{L_{32}} + b_3 \frac{L_{28}}{L_{31}} + c_1 H) + d_0 + d_1 L_{31} + d_2 L_{32} + d_3 L_{29}. \quad (5.14)$$

Here L_i are the TOA radiances measured by the MODIS thermal infrared channel extracted from MOD021KM and the number in the subscript indicates the thermal channel of the MODIS sensor. L_{Tair} represents surface air temperature (equal to L_{31} during night time and equal to L_{32} during day time). a_i (i=0-4), b_i (i=1-3), c1 and d_i (i=0-3) are regression coefficients depending on the viewing zenith angle extracted from MOD03. H is the surface elevation retrieved from MOD03. For detailed information about the above parameterizations of R_n, readers are recommended to refer to relative papers.

5.2.4 Estimation of daily ET

The main objective of this work is to estimate ET on a daily scale, as daily ET is more applicable than instantaneous ET in hydrological and water resources management studies. However, the triangle method introduced above provides only instantaneous ET at the time of satellite overpass. In this work, we use the following scheme for extrapolating instantaneous ET values to a daily time step:

Firstly, the near noon instantaneous EF is used to represent the daily average EF value. This is based on observations (Caparrini et al., 2004; Crago, 1996) that for both homogeneous and heterogeneous land surfaces EF remains fairly constant for daylight hours, particularly between 10:00 LT and 16:00 LT. Several studies have also concluded, that using local near noon EF instead of all-day EF for daily ET estimation incurs very small error (Farah et al., 2004; Hall et al., 1992; Hoedjes et al., 2008; Jia et al., 2009).

Secondly, daily R_n is estimated through a sinusoidal model (Bisht et al., 2005) that has been applied successfully in several studies (Bhattacharya et al., 2010; Bisht and Bras, 2010; Kim and Hogue, 2008). The sinusoidal model is given as:

$$R_n^{daily} = \frac{\int_{t_{rise}}^{t_{set}} R_n(t)dt}{\int_{t_{rise}}^{t_{set}} dt} = \frac{2R_n^{overpass}}{\pi \sin\left[\left(\frac{t_{overpass} - t_{rise}}{t_{set} - t_{rise}}\right)\pi\right]}, \quad (5.15)$$

where $R_n^{overpass}$ is the instantaneous R_n estimated at satellite overpass time, t_{rise}, t_{set}, $t_{overpass}$ denote local sunrise time, sunset time and satellite overpass time, respectively. Thus daily ET can be approximated as follows:

$$ET^{daily} = \left(R_n^{daily} - G^{daily}\right) EF^{daily}. \quad (5.16)$$

It should be noted here that soil heat flux G^{daily} is ignored in this study, as it is usually

assumed negligible over the diurnal cycle (Galleguillos et al., 2011; Jiang et al., 2009; Sánchez et al., 2008; Tang et al., 2011a). The above equation can thus be rewritten as:

$$ET^{daily} = R_n^{daily} \cdot EF^{daily}. \quad (5.17)$$

5.2.5 Assessment strategy

A two-step assessment strategy is applied to investigate the performance of the triangle method in the estimates of ET using TOA radiances (ET_{TOA}). Firstly, the daily ET_{TOA} is compared against in situ measurements. Since the estimation of EF in this study is obviously independent of R_n estimation, the EF_{TOA}, R_{n_TOA} and ET_{TOA} will be validated against in situ measurements, respectively. Then the intercomparisons between MODIS TOA radiances-based estimates and MODIS products-based estimates are carried out over the validation site. A flowchart is shown in Figure 5.2 to illustrate the above strategy. A number of statistical indices, including mean bias error (BIAS), mean absolute difference (MAE), root mean square difference (RMSD), relative error (RE) and coefficient of the determination (R^2) are chosen to evaluate the model performance in this study.

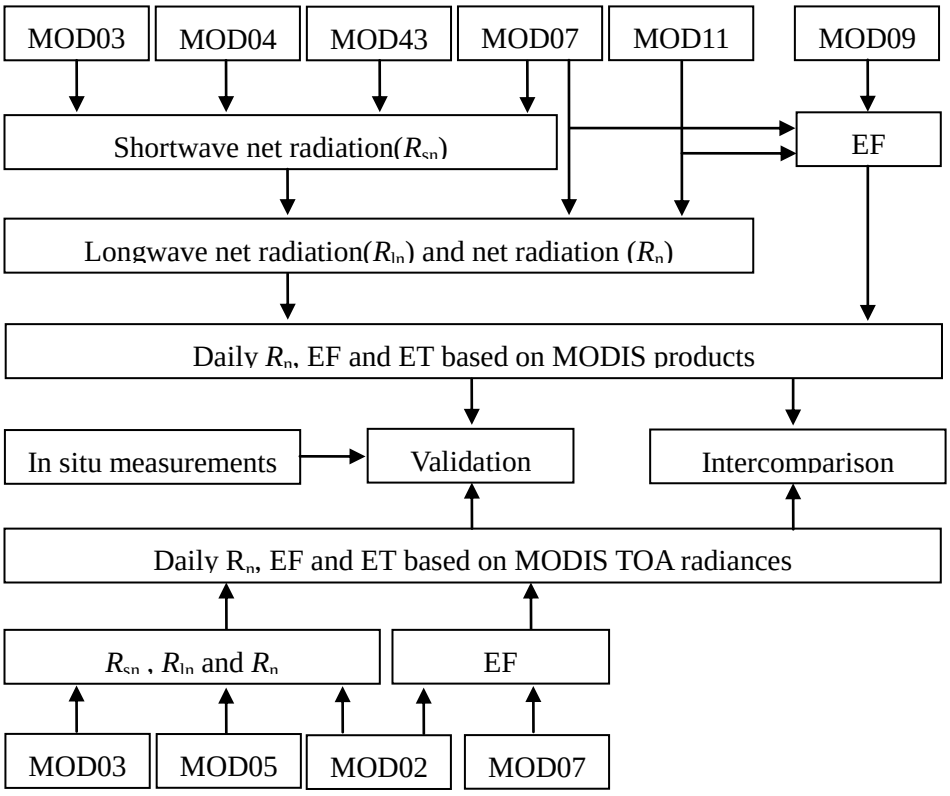

Figure 5.2: Flowchart for the estimation of daily ET respectively from various MODIS products and the MODIS TOA radiances using the triangle method, and the validation of the satellite retrievals with in situ measurements.

5.3 Study area and data collection

5.3.1 Study area

The study area in this work is located within the Poyang Lake basin of China, which lies on the Southern bank of the middle and lower reaches of the Yangtze River. The domain is defined by latitude and longitude ranges 27.62 – 28.78º N and 114.51 – 116.95º E, respectively. The surface elevation of most areas is approximately10 – 200 m above the sea level. A mountainous region with average elevation of 1000 m above sea level lies in the northwestern part of the study region. Under the influence of the monsoon systems, the study area belongs to a humid subtropical climate zone. The annual mean air temperature and annual average precipitation based on observations during years 1951–2001 were nearly 17.6° C and 1615 mm, respectively. The annual rainfall over the study area occurs mainly during the humid summer months, with very little during spring and autumn, and much less during the cold, dry winters (Liu *et al.*, 2010). Figure 5.3 shows the yearly land cover classification map in 2005 over the study area, provided by the Data sharing Network of Earth System Sciences, Chinese Academy of Sciences. It is a heterogeneous land cover area characterized by cropland (35%), forest (45%), grassland (3%), urban areas (2%), and inland water surface (5%). Data used for validating the estimated R_n, EF and ET are collected from Nanchang Ecological Experiment Station (indicated in Figure 5.3), which is located in the Nanchang County, Jiangxi Province. It is geographically situated at 28.6º N, 115.92º E at an elevation of 47 m above sea level. Land cover across the Nanchang station is grassland.

5.3.2 Satellite data

MODIS sensors were launched on board the National Aerodynamics and Space Administration (NASA) Earth Observing System (EOS) Terra and Aqua satellites on December 1999 and May 2002, respectively. With 36 discrete spectral bands ranging from visible, near-infrared, to thermal infrared and high spatial resolution at 250, 500, and 1000 m, the MODIS sensor can provide data covering the entire surface of the Earth every 1 to 2 days. To date, the MODIS science team has developed 44 products for a variety of disciplines, including land, atmosphere, ocean and calibration. The Terra-MODIS Collection 5 data products used in this study consist of MOD021KM, MOD03, MOD04, MOD05_L2, MOD07_L2, MOD09GA, MOD11_L2, MOD35_L2 and MOD43B3 (Table 5.1). A brief description of the data products used is given below. In order to validate and compare the estimation of ET, clear sky day images were selected on the basis of visual inspection of the MODIS true color image and the MOD35_L2 cloud mask product. We characterized 85% of the study area being clear as a clear sky condition, because it is difficult to avoid cloudy pixels over the whole domain. Finally, a total of 16 clear sky daytime MODIS data products ranging from

fall to summer between 2007 and 2008 over our study area were used to estimate ET. The period from October 2007 to July 2008 was selected also because all the required satellite data and in situ measurements are both available during this period. Seven of the selected days are from 2007 (DOY: 277, 279, 283, 290, 300, 327, 332) in 2007, and nine days are from 2008 (DOY: 003, 005, 061, 062, 084, 134, 138, 206, 209). During this study period, environmental conditions at the Nanchang station change considerably between dry and wet (see Figure 5.6). Table 5.2 gives the description of selected days, satellite overpass time over the study region, and image quality for each day.

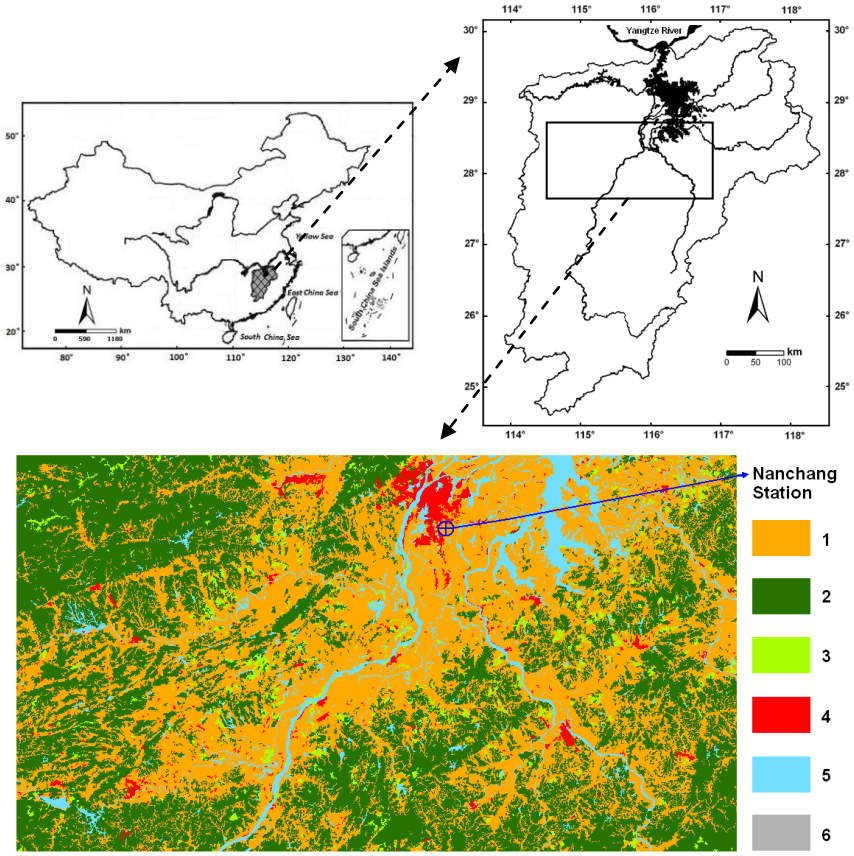

Figure 5.3: Geographical location of the study area (up) and land cover map of the study area (down). Poyang lake basin is located in southeast of China and a relatively flat region within the basin is selected as our study area. The yearly land cover classification map in 2005 was provided by the "Data sharing Network of Earth System Science, Chinese Academy of Sciences". 1 = cropland, 2 = forest, 3 = grassland, 4 = urban areas, 5 = water, 6 = bare soil. The location of the Nanchang Ecological Experimental station is also shown in the land cover map.

Table 5.1: MODIS data products used in this study and their characteristics as obtained from LAADS (Level 1 and Atmosphere Archive and Distribution System).

MODIS data	Category	Version	Spatial resolution	Parameters used
MOD021KM	Level 1B	5	1 km	TOA radiance and reflectances
MOD03	Level 1A	5	1 km	Geodetic coordinates, ground elevation, Solar zenith and azimuth angles, satellite zenith and azimuth angles
MOD04	Level 2	5	10 km	Aerosol optical depth
MOD05	Level 2	5	1 km	Column water vapor amounts
MOD07	Level 2	5	5 km	Air temperature and dew point temperature
MOD09GA	Level 2	5	1 km	Surface reflectance after atmospheric correction
MOD11	Level 2	5	1 km	Surface emissivity and temperature
MOD35	Level 2	5	1 km	Cloud mask
MOD43	Level 3	5	1 km	Black- and white sky albedos

Table 5.2: Day of year, date, overpass time and image quality for the study days.

Day of the year (DOY)	Date	Overpass time (Local time)	Image quality (Cloud free pixels %)
2007277	4 October 2007	11:05	96.74
2007279	6 October 2007	10:55	96.00
2007283	10 October 2007	10:30	93.62
2007290	17 October 2007	10:35	92.73
2007300	27 October 2007	11:10	99.19
2007327	23 November 2007	10:55	97.64
2007332	28 November 2007	11:10	98.99
2008003	3 January 2008	10:45	96.09
2008005	5 January 2008	10:35	94.80
2008061	1 March 2008	11:25	98.24
2008062	2 March 2008	10:30	95.23
2008084	24 March 2008	11:30	95.90
2008134	13 May 2008	11:20	92.37
2008138	17 May 2008	10:55	91.91
2008206	24 July 2008	10:30	88.50
2008209	27 July 2008	11:00	97.11

MODIS TOA radiances

TOA radiances for 36 bands were obtained from the MODIS Level 1B MOD021KM file, which is calibrated Earth View data at 1 km resolution from the MODIS Characterization and Support Team (MCST). The Level 1A MOD03 file consists of geolocation field data calculated for each 1 km MODIS Instantaneous Field of View (IFOV), including geodetic coordinates, ground elevation, and satellite zenith and azimuth angles for each 1km pixel.

MODIS products

The MOD04_L2 aerosol product provides aerosol optical depth (AOD) on a 10 × 10 km pixel array (Remer et al., 2005). The MOD05_L2 product is the near-infrared total precipitable water data consisting of column water vapor amounts over clear land areas and above clouds over both land and ocean (King et al., 2003). The MOD07_L2 atmospheric profile product has a spatial resolution of 5 × 5 km at 20 vertical atmospheric pressure levels, of which air and dew-point temperature were extracted from the vertical pressure level of 1000 hPa (Bisht et al., 2005). The MOD09GA comprises of surface spectral reflectances from atmospheric correction, which are computed from MODIS Level 1B land bands 1-7 (Vermote and Kotchenova, 2008). The MOD11_L2 data contains LST and band-averaged emissivity in band-31 (10.780–11.280 μm) and band-32 (11.770–12.270 μm) calculated using the generalized split-window algorithm (Wan and Dozier, 1996) at a spatial resolution of 1km. The MOD35_L2 is a cloud mask product which assigns a clear-sky confidence level (clear, probably clear, uncertain, cloudy) to each IFOV (Frey et al., 2008). The MOD43B3 product provides clear-sky observations at 1 km spatial resolution for both Bidirectional Reflectance Distribution Function (BRDF) and albedo (Schaaf et al., 2002). Using the MODIS Reprojection Tool (MRT) and MODIS Reprojection Tool Swath (MRTSwath), all the MODIS data used in this work were transformed from HDF-EOS swath format to a Universal Transverse Mercator (UTM) projected GeoTIFF image and resampled for 1km pixel size. It should be mentioned that all the above products are MODIS Level 2 data except land surface albedo, which is a global MODIS Level 3 data.

5.3.3 Ground measurements

A weighing lysimeter (1 m^2 in area and 1 m in height) at the Nanchang Ecological Experiment Station has been set up to measure ET at daily scale since August, 2007 (Liu et al., 2010). The precision of the ET measurements is estimated to be 0.01 mm per day (Liu et al., 2010). The land cover across the Nanchang station is grassland, which relies on natural rainfall to grow and survive. Ground-measured surface net radiation, air temperature and rainfall were provided by the meteorology station, which locates only 30 meters away from the lysimeter. The EF for the lysimeter is cal-

culated as the ratio of the daily ET and daily net radiation.

5.4 Results and discussion

5.4.1 Triangular scatter plots

In order to calculate ET from MODIS products and MODIS TOA radiances for the case days, the dry and wet edges of the triangular space need to be determined firstly. This procedure is very important, because the uncertainty in the determination of the dry and wet edges will transfer to the estimation of EF and further affect the accuracy of estimated ET. Figure 5.4 gives examples of LST/$NDVI_{Products}$ and TOA radiance/$NDVI_{TOA}$ scatter plots for five different representative months over the seasons (October 2007, January 2008, March 2008, May 2008 and July 2008). As expected, January was characterized by low NDVI and low LST. From March to July, the NDVI and LST increased as the vegetation cover is increasing rapidly. In October both NDVI and LST decreased. The variations over different seasons show that both NDVI and LST rise first and then decline, reflecting the state of the soil moisture over the study area. When the soil moisture is low over the study area, the bare land surface is drying rapidly, and ET is small and absorption of the solar energy is mainly consumed for surface temperature. The absorption of the solar energy is mainly used for ET when the soil moisture is high.

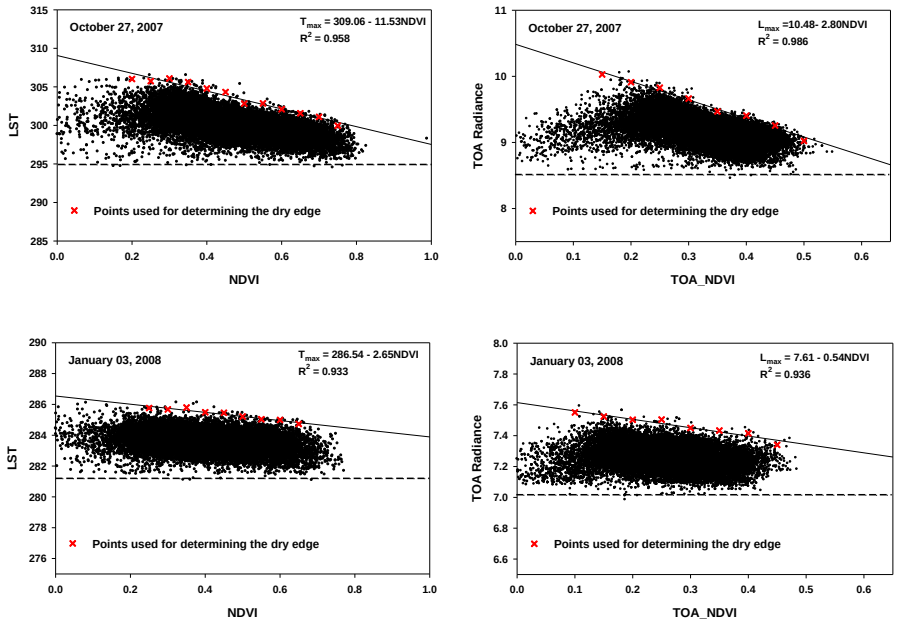

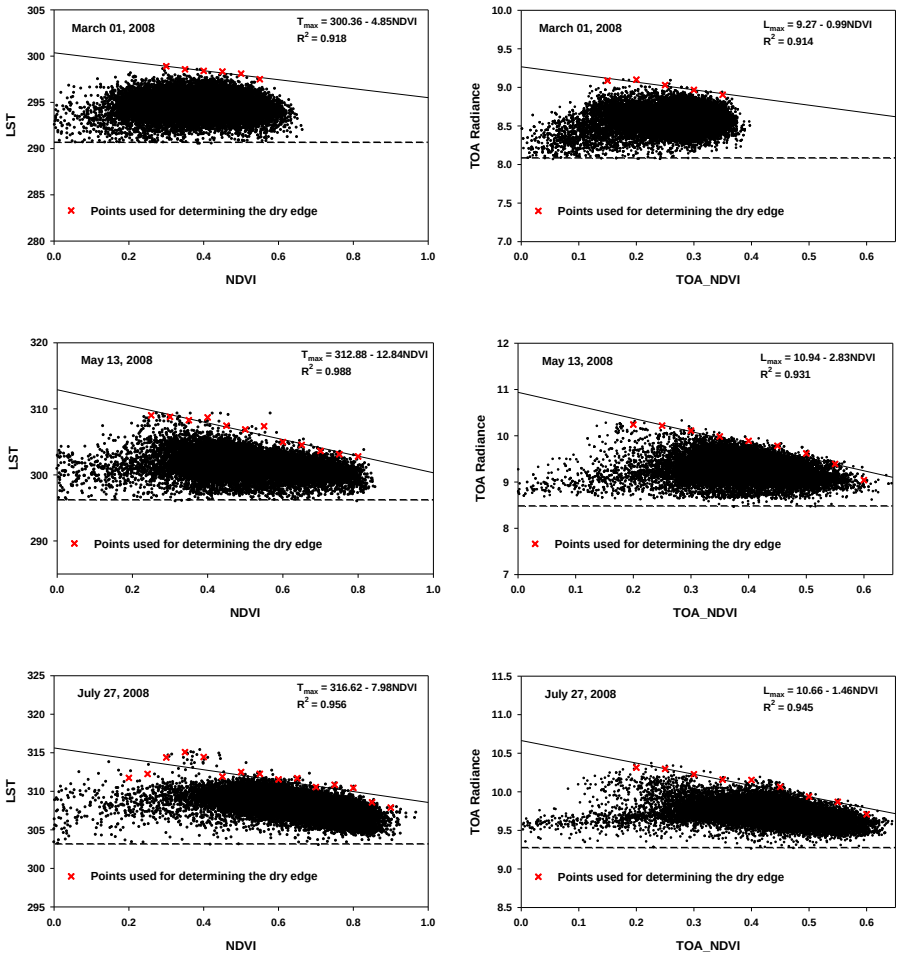

Figure 5.4: Illustrative examples of LST/NDVI scatter plots constructed respectively from MODIS products and TOA radiances for five representative days over the study area during the study period.

It can also be seen in Figure 5.4 that the shapes of the TOA radiance/$NDVI_{TOA}$ spatial variations are similar to those of the LST/$NDVI_{Products}$ spatial variations, which makes it possible to estimate comparable EF values from both data sets. The corresponding dry and wet edges of the triangular space were determined as described in the previous section. As shown in Figure 5.4, they define the maximum and minimum envelopes of temperatures in the scatter plots. Table 5.3 illustrates the intercepts, slopes and the R^2 values for the dry edges of the LST/$NDVI_{Products}$ and TOA radiance/$NDVI_{TOA}$ scatter plots observed for the case days. One can see that the dry edge intercept in the LST/$NDVI_{Products}$ triangle varies from 286.54 K to 316.62 K, and from 7.61 W/m^2/μm/sr to 10.94 W/m^2/μm/sr in the TOA radiance/$NDVI_{TOA}$ triangle. The dry edge slope also exhibited temporal variation ranging from -12.84 K to -2.65 K for LST/$NDVI_{Products}$ scatter plot, and from -2.83 -0. W/m^2/μm/sr to 54 W/m^2/μm/sr for TOA radiance/$NDVI_{TOA}$ scatter plot throughout the study period. These variations of the parameters (slope and intercept) imply that a variety of hydrological conditions were present in the study period, and could capture the variability and direction of gradient in virtual surface dryness and wetness pattern.

Furthermore, the high R^2 values, ranging from 0.921 to 0.988 for LST/$NDVI_{Products}$ triangular space and 0.88 to 0.998 for TOA radiance/$NDVI_{TOA}$ triangular space, indicate the reliability of the algorithm for determining the dry edge. Thus the uncertainty in the estimation of EF caused by the subjective determination of the dry edge will be significantly decreased.

Table 5.3: Statistics of the dry edge values used for estimation of EF (a and b represent the intercept and slope of the dry edge respectively).

DOY	Scatter Plot	a	b	R^2
2007277	NDVI-LST	313.04	-5.92	0.985
	NDVI-TOA Radiance	10.60	-1.54	0.936
2007279	NDVI-LST	311.26	-7.39	0.931
	NDVI-TOA Radiance	10.73	-2.11	0.88
2007283	NDVI-LST	304.39	-9.01	0.921
	NDVI-TOA Radiance	9.22	-1.42	0.968
2007290	NDVI-LST	304.02	-8.61	0.934
	NDVI-TOA Radiance	9.85	-2.58	0.965
2007300	NDVI-LST	309.06	-11.53	0.958
	NDVI-TOA Radiance	10.48	-2.80	0.986
2007327	NDVI-LST	297.91	-4.92	0.957
	NDVI-TOA Radiance	9.07	-1.16	0.907
2007332	NDVI-LST	295.05	-7.48	0.974
	NDVI-TOA Radiance	8.72	-1.71	0.975
2008003	NDVI-LST	286.54	-2.65	0.933
	NDVI-TOA Radiance	7.61	-0.54	0.936
2008005	NDVI-TOA Radiance	7.98	-0.85	0.978
2008061	NDVI-TOA Radiance	9.27	-0.99	0.914
2008062	NDVI-TOA Radiance	9.15	-1.86	0.998
2008084	NDVI-TOA Radiance	9.15	-0.68	0.974
2008134	NDVI-LST	312.88	-12.84	0.988
	NDVI-TOA Radiance	10.94	-2.83	0.931
2008138	NDVI-LST	314.46	-6.03	0.938
	NDVI-TOA Radiance	10.70	-1.03	0.896
2008206	NDVI-TOA Radiance	9.47	-0.56	0.910
2008209	NDVI-LST	316.62	-7.98	0.956
	NDVI-TOA Radiance	10.66	-1.46	0.945

5.4.2 Evaporative fraction, daily net radiation and ET estimated from TOA Radiances

In order to evaluate the accuracy of the estimated daily ET based on MODIS TOA

radiances, ground measurements from Nanchang Ecological Experiment Station are used as an independent data source for validation. Since EF and daily R_n are the key parameters in the estimation of ET and are calculated independently, their estimates from TOA radiances are evaluated before ET validation. In spite of the different spatial scales representative of satellite data and in situ data, R_n are believed to have very low spatial variability and validation of estimated R_n with ground-based measurements have been made in a variety of studies (Jin et al., 2011; Kim and Liang, 2010; Vinukollu et al., 2011). Daily R_n in this study is derived not by a complicated physics-based model but through a simple sinusoidal model following the work of Bisht et al. (2005). Figure 5.5 shows the scatterplot of the derived daily R_n versus the observed R_n at Nanchang station for the sixteen case days in our study. Overall, good agreement between the estimated and measured R_n is obtained with BIAS = 13.11 W m^{-2}, RMSD = 20.47 W m^{-2} and RE = 21.87% (Table 5.4). Furthermore, it can be observed that R^2 = 0.931. These statistics suggest the reliability of deriving R_n with MODIS TOA radiances alone and the applicability of the sinusoidal model for estimating daily R_n.

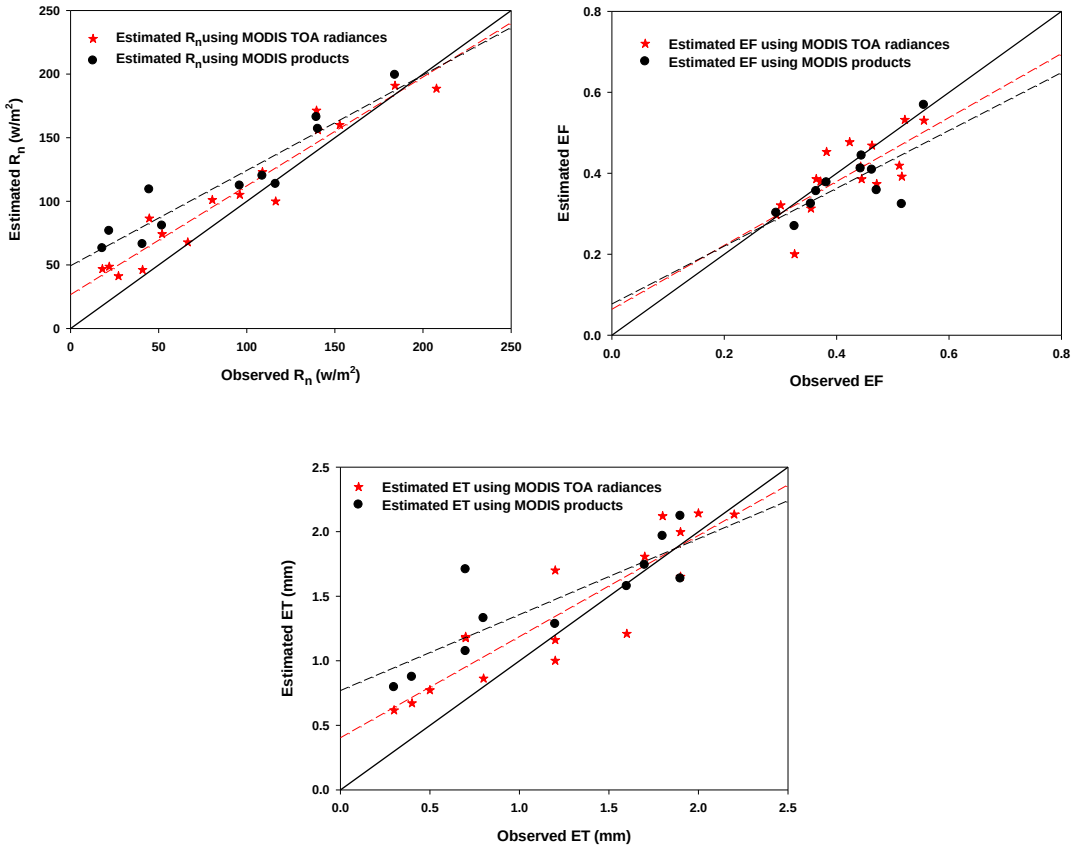

Figure 5.5: Comparison of daily net radiation, evaporative fraction and ET estimated respectively from MODIS products and TOA Radiances with field observations (data from Nanchang experimental station).

Table 5.4: Statistical results for the estimated R_n, EF and ET using MODIS TOA radiances and MODIS products in comparison with observations at Nanchang station.

Parameter	BIAS	MAD	RMSD	Unit	Relative error (%)	R^2	Number of days
R_n (TOA)	13.11	17.55	20.47	W m^{-2}	21.87	0.931	16
R_n (TOA)	16.88	19.87	22.69	W m^{-2}	25.92	0.919	11
R_n (Products)	27.38	27.89	33.38	W m^{-2}	38.13	0.892	11
EF (TOA)	-0.025	0.049	0.064		15.09	0.559	16
EF (TOA)	-0.036	0.055	0.069		16.48	0.553	11
EF (Products)	-0.043	0.047	0.073		17.30	0.512	11
ET (TOA)	0.132	0.250	0.292	mm	23.28	0.818	16
ET (TOA)	0.133	0.256	0.300	mm	25.26	0.800	11
ET (Products)	0.283	0.335	0.433	mm	36.64	0.716	11

The next step is the evaluation of the EF estimate. It is worth nothing that the comparison of estimated EF with ground-measured data is essentially the true validation of the triangle method for ET estimate, as EF is a fairly conservative quantity over the course of a single day and is calculated entirely based on the LST/NDVI triangular feature space. Comparison between the MODIS TOA radiances-derived EF and in situ-measured EF is shown in Figure 5.5. Statistics are also presented in Table 5.4. One can see from Figure 5.5 that the derived EF agrees well with measured EF with a BIAS of -0.025, RMSD of 0.064, RE of 15.09%, and R^2 of 0.559. The differences between the derived and measured EF may be attributed to the influence of topography (altitude and terrain orientation) (Carlson, 2007), the size of the domain, and the determination of the theoretical warm and wet edges (Long et al. 2012). Nevertheless, the results presented here are considered reasonable and satisfactory, given the simplicity of the method and the limited input requirements.

Similar evaluations of predictions of EF based on satellite products have been reported by other studies. Wang et at. (2006) estimated EF using MODIS products with a BIAS of -0.002, RMSD of 0.106 and R^2 of 0.605 based on ground observations collected at the Southern Great Plains of the United States. Stisen et al. (2008) obtained BIAS, RMSD and R^2 of 0.04, 0.13 and 0.63 respectively from the use of MSG-SEVIRI data products to derive EF in the Senegal River basin of West Africa. Another study validated over the North China Plain, using Fengyun-2C data products, reported BIAS, RMSD and R^2 of -0.017, 0.14 and 0.55 respectively (Shu et al., 2011). Some other methods may achieve higher accuracies, but they often need additional information from field observations, or the calibration against in situ measurements.

The final step is to examine the performance of the purely MODIS TOA

radiances-based daily ET. The daily ET estimate is compared with ground-based daily ET. Results for the comparison are shown in Figure 5.5 and statistics are provided in Table 5.4. The BIAS of 0.132 mm, RMSD of 0.292 mm, RE of 23.28% and R^2 of 0.818 are achieved compared to measured values. This suggests that the proposed MODIS TOA radiances-based method performs well for estimating daily ET during clear sky days and the assumptions associated with the method are reasonable for the derivation of daily ET. As compared to EF validations, the results of daily ET show a slight improvement in terms of R^2. The reason for this is obviously caused by the inclusion of daily R_n in obtaining daily ET. Similar tendency was reported by Batra et al. (2006) and Jiang et al. (2009). The sources of errors in the estimation of daily ET originate from the uncertainties in both the estimated daily R_n and daily EF. However, it is difficult to further quantify the detailed error contribution from R_n and EF based on these limited analyses. In general, the RE of 23.28% in daily ET estimate is within the range of accuracies reported in the literature, between 15% and 30% (Glenn et al., 2010; Kalma et al., 2008; Verstraeten et al., 2008). The results presented above with BIAS = 0.132 mm and RMSD = 0.292 mm are comparable to other triangle method based ET estimation results elsewhere. Nishida et al. (2003) has validated MODIS-derived ET against AmeriFlux stations and achieved BIAS = 0.197 mm , RMSD = 1.587 mm, and R^2 = 0.86. In the Southern Great Plains of USA, different studies on ET estimation using NOAA-AVHRR and MODIS data obtained BIAS between -1.021 and 0.423 mm, RMSE between 1.285 and 3.004 mm, R^2 between 0.47 and 0.89 (Batra et al., 2006;Jiang and Islam, 1999, 2001, 2003). Jiang et al. (2009) reported BIAS = -0.151 mm, RMSD = 1.100 mm, and correlation coefficient of 0.595 respectively from the comparison of NOAA-AVHRR data to multi-year ground observations over the South Florida region.

Figure 5.6 shows that the seasonal variation in estimated ET generally follows the rainfall and air temperature patterns. The high ET values appeared in wet periods with high air temperature, while the relatively low ET values occurred during dry seasons. The validation data set with a temporal variation between dry and wet conditions further gives confidence that the MODIS TOA radiances-based estimates can provide reasonable results at other locations under different surface and meteorological conditions. As an example, the spatial distribution map of ET estimated from TOA radiances over the study area on January 3, 2008, is shown in Figure 5.7. Comparing Figure 5.7 and land cover map in Figure 5.3, one can see that areas covered by forests and water-bodies in general have higher ET than other areas because of sufficient recharging of water resources from surface water or groundwater, while lowest ET appeared in cropland due to no crops grown in the winter season. These distribution characteristics are in agreement with the spatial pattern of NDVI (Figure 5.7), which is a measure of vegetation cover and crop growth condition.

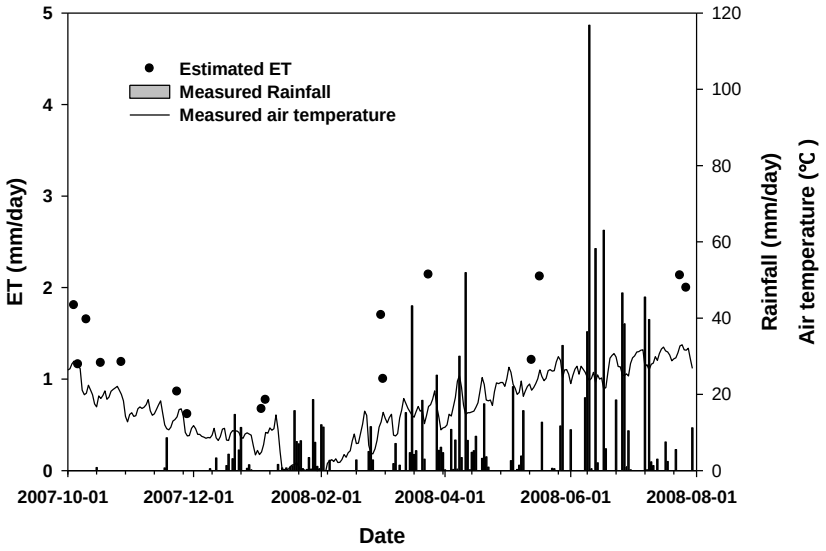

Figure 5.6: Seasonal variation of estimated ET for Nanchang experimental station during the study period.

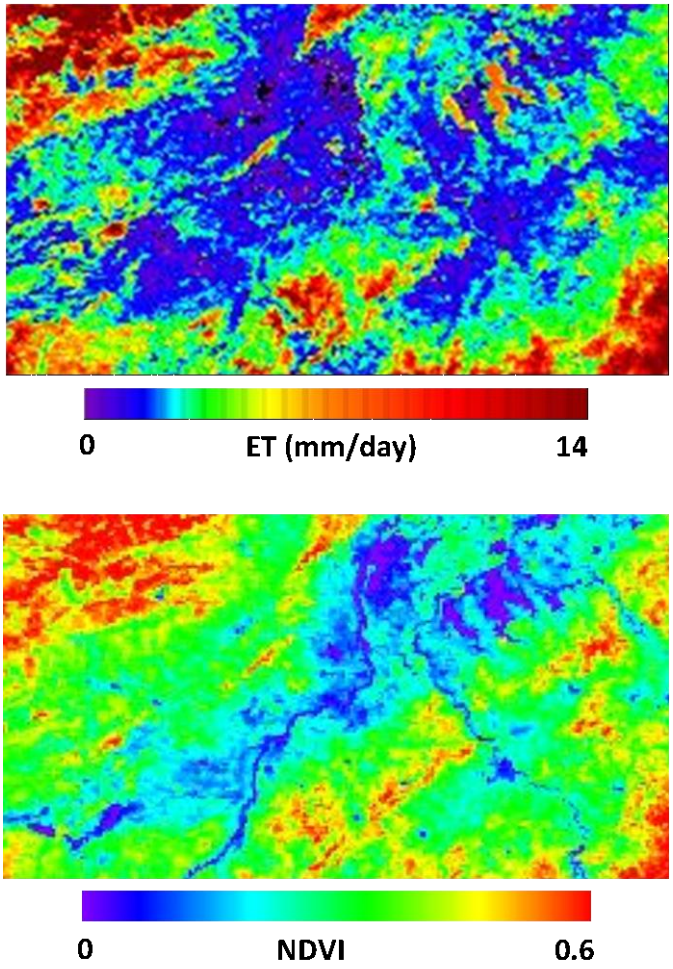

Figure 5.7: Spatial distribution of daily ET (up) and NDVI (down) maps at 1 km resolution for January 3, 2008 over the study area.

5.4.3 Inter comparison of MODIS products and TOA Radiances based EF, daily net radiation and ET

The first step of our assessment strategy focused on the validation of the MODIS TOA radiances-based estimates against ground observations. It is also very interesting to analyze how MODIS TOA radiances-based estimations compare to retrievals based on MODIS products. Thus, the intercomparisons between these two estimates are carried out over the validation site in the second step. It should be noted here that 11 case days rather than all 16 case days were selected for the intercomparisons, as the MODIS LST products have no values over the validation site for five days. Actually, these five days are quite clear over the study area as depicted in Section 5.2. The void values in the LST products may be caused by mis-classification of MODIS cloud mask product. It further addresses the advantage of using TOA radiances directly to estimate R_n, EF and ET. The validation exercise provided similar results for the TOA radiances-based and products-based estimates of the daily R_n, EF and ET when assessing from a visual inspection, as displayed in Figure 5.5. Corresponding statistics were summarized in Table 5.4. For TOA radiances-based estimates, the RE for daily R_n, EF and ET were less than 30%. The magnitude of this error is within the range for remote sensing based parameterization schemes. As stated previously, the general uncertainty in the estimation of heat fluxes is in the 15-30% range. The accuracy of R_n and EF are also in the same order of magnitude (Bisht et al., 2005; Jiang et al., 2004; Stisen et al., 2008). Validation results for products-based estimates were worse, with RE for daily R_n and ET both slightly higher than 30%. Overall, the TOA radiances-based estimates performed better than the products-based estimates, because the BIAS and RMSD for daily R_n, EF and ET are lower than the former, and the R^2 values higher than the former. The above results further suggest that the TOA radiances-based method is operationally feasible and can provide reasonable estimation accuracy for daily ET.

The discrepancies between the estimates and the measurements might be related to the differences in spatial scales between the satellite area integrated value and the field point measurement, and the heterogeneity of the land surface within the satellite footprint (Kustas et al., 2004; McCabe and Wood, 2006; Vinukollu et al., 2011). As depicted in Section 5.1, the lysimeter (1 m^2) is located in homogeneous land cover, while the satellite has a footprint of 1 km. This incompatibility in spatial scale will evidently introduce uncertainty in the comparative analysis.

An improved option to further investigate the importance of scale issues is using flux tower data for additional comparisons, as the tower fluxes represent a footprint of roughly 1–3 km (Cleugh et al., 2007; Running et al., 1999), which we plan for the fut-

ure. The validation of the proposed method against flux tower footprint measurements over various climatic regions and analysis of the uncertainties associated with the comparison will be the focus of our subsequent research.

5.5 Conclusions

Recently, various attempts have been made to estimate regional ET by using remote sensing derived products. However the derivations of these variables are composed of a series of processing steps. Errors associated with each step may be accumulated and finally impact the accuracy of these variables. Further, these uncertainties will be transferred to the estimation of ET. In this study, we proposed a method to estimate daily ET directly using TOA radiances, which attempted to overcome the limitations related to using satellite derived variables. It eliminated the complex processing chain of deriving these variables and provided a useful alternative for determining ET from satellite dada. The proposed method was derived through the following procedures. Firstly, the instantaneous EF and R_n were calculated from MODIS TOA radiances, respectively. Then, daily ET were estimated based on these EF and R_n estimates by using a sinusoidal temporal interpolation model.

The proposed method was tested in the Poyang Lake basin for sixteen case days varying from October 2007 to July 2008. The field observations collected for the same period were used to validate the estimated EF, R_n and ET. The results are promising and appear to provide comparable or better estimates than currently available satellite-based methods, given the common uncertainties in R_n, EF and ET. In addition, the intercomparisons between the proposed method-based estimates and MODIS products-based estimates were also carried out over the validation site. The results suggested that the proposed method achieved similar accuracy as the MODIS products-based triangle method, which further confirmed the feasibility of the proposed method for ET estimation. Consequently, we believe that the use of TOA radiances appears to be adequate for the estimation of daily ET in conjunction with the triangle method over large areas under the assumption of uniform atmospheric forcings.

The uncertainty in our MODIS TOA radiances-based estimates may be attributed to the incompatibility in spatial scale between satellite footprint and ground-based point measurement. This requires us to further explore more feasible comparison metrics for the validation of the remote sensing estimates using field observations. In addition, to make the proposed method more general and operational for the estimation of daily ET, more validation work needs to be carried out with more integration of satellite data and ground-based measurements over various climatic regions and under different surface conditions in the future.

Acknowledgements

This work was partly supported by the Cluster of Excellence CliSAP (EXC177), University of Hamburg, funded through the German Science Foundation (DFG) and by the CAS-MPG Doctoral Promotion Programme (DPP). The MODIS Level 1 and Level 2 datasets are downloaded from the Level 1 and Atmosphere Archive and Distribution System (LAADS, http://ladsweb.nascom.nasa.gov/). The MODIS Level 3 datasets are obtained in the Warehouse Inventory Search Tool (WIST, https://wist.echo.nasa.gov/~wist/api/imswelcome/). The authors would like to thank Prof. Zhang Qi for providing the lysimeter data and the China Meteorological Administration for supporting the climatic data. The authors would like to thank Editor Niko Verhoest, and Reviewer Carlos Jiménez and an anonymous reviewer for their valuable comments and suggestions.

Chapter 6

Conclusions and Outlook

6.1 Conclusions

The main motivation of this thesis is to develop a method to estimate ET directly using satellite TOA radiances without performing atmospheric correction and other complicated processes. Therefore, on the basis of the LST/NDVI feature space, a daytime ET parameterization scheme based entirely on TOA radiances is proposed and validated over regional scales. The answers to the research questions posted in the Introduction section can be summarized in the following:

What are the uncertainties in estimating NDTI from TOA radiances?
The feasibility of using TOA radiances instead of LST to calculate NDTI is explored in Chapter 2. The method is derived theoretically on the basis of the radiance transfer equation and Planck's law. The results suggest that the method is applicable under the condition that the atmospheric parameters (transmittance and atmospheric temperature) and the surface emissivity are spatially stable. A sensitivity analysis is carried out to ascertain how variations in surface emissivity, atmospheric temperature and water vapor content affected the NDTI. The uncertainties in NDTI estimates based on TOA radiances are expected to be less than 10%, if the spatial variabilities of atmospheric parameters (water vapor, effective atmospheric temperature) and surface emissivity are below 10%, 4 K and 0.05, respectively. Compared with the variations of surface emissivity and atmospheric temperature, the variation of water vapor would significantly influence the method under moist conditions. Thus, the method should be used with care for humid conditions with water vapor higher than 3 g cm^{-2}. The proposed method is tested over a heterogeneous area of the Poyang Lake basin. The results are promising and confirm the applicability of the proposed method when the spatial variations of surface emissivity, atmospheric temperature and water vapor content across the study area are below 0.01, 1 K and 0.2 g cm^{-2} separately. At the same time, the results also show that the variation of water vapor content under humid condition dramatically influences the performance of the method, which is in accordance with the sensitivity analysis.

How accurate is the EF estimation scheme based on TOA radiances?
The robustness of the EF estimation scheme based on TOA radiances is tested over different climatic and surface conditions. Flux measurements from 16 sites are used to

validate the EF estimated from MODIS TOA radiances. It is found that the EF estimates perform well across a wide variety of climate and biome types – grasslands, crops, cropland/natural vegetation mosaic, closed shrublands, mixed forest, deciduous broadleaf forest, and savannas. The overall BIAS, MAD, RMSD and R values for all the sites are 0.018, 0.147, 0.178 and 0.590, respectively. These results are comparable with published results in the literature. Diagnostic analysis suggests that the large errors in the TOA radiances based EF estimates are related to the precipitation before satellite overpass and the linear parameterization of ϕ. For sample days outside the growing season, larger uncertainties and errors occur.

How representative are instantaneous evaporative fraction measurements for daytime fluxes?

As stated in Chapter 4, there is no consensus in the scientific community on whether the instantaneous EF could represent daytime EF under clear-sky conditions. This study investigates this topic using long term ground-based measurements from FLUXNET. It is found that the EF during daytime from 11:00 h LT to 14:00 h LT agrees well with daytime EF under clear sky conditions (R^2>0.75, RMSD<0.087, -10.15%<RE <3.79%), and the midday (12:00 h LT to 13:00 h LT) EF is closest to daytime EF with R^2 = 0.920±0.053, RMSD = 0.050±0.013, RE = -4.47%±2.48%. However, the EF is more variable during cloudy conditions when compared to clear sky conditions, and an increase in cloud cover results in an increase in the variability of the EF during daytime. Thus the EF constant hypothesis is strictly true only for clear sky conditions. Nonetheless, the above results provide a basis for remote sensing-based estimation of the EF based on sun synchronous satellite observations. The midday overpass satellites (e.g. MODIS and AVHRR) are expected to give better results than other overpass time platforms. The important conclusion from the present study is that the EF constant assumption is valid over a wide range of ecosystems and climates.

Is it possible to estimate daily ET from TOA radiances?

The daytime ET estimation scheme based on TOA radiances is tested at a regional scale. Firstly, the EF is estimated using the MODIS TOA radiances over a heterogeneous area of the Poyang Lake Basin in China. Then the net radiation over the same study area is derived from MODIS TOA radiances only. Finally, daily ET maps are estimated from these EF maps and net radiation maps by using a sinusoidal temporal interpolation model. The estimated EF, net radiation and ET have been validated against field observations collected for the period October 2007-July 2008. The validation results indicate that the proposed method could provide daily EF, net radiation and ET with comparable accuracy to those of current widely used satellite-based methods. Besides, the intercomparisons between the proposed method-based estimates and MODIS products-based estimates are also carried out over the validation site. For TOA radiances-based estimates, the RE for daily R_n, EF and ET are less than 30%. The magnitude of this error is within the range for remote

sensing based parameterization schemes. The general uncertainty in the estimation of heat fluxes is in the 15-30% range. The accuracy of R_n and EF are also in the same order of magnitude. Validation results for products-based estimates are worse, with RE for daily R_n and ET both slightly higher than 30%. Besides, it is also found that the seasonal variation in estimated ET generally follows the rainfall and air temperature patterns. High ET values tend to appear in wet periods with high air temperature, while the relatively low ET values occur predominantly during dry seasons.

To the best of our knowledge, we are the first

1. to investigate the uncertainties in estimating NDTI from TOA radiances;
2. to evaluate the EF estimates based on TOA radiances using global FLUXNET observations;
3. to systematically examine the self preservation of the EF using long term FLUXNET data across a wide range of ecosystems and climates;
4. to estimate daily ET using TOA radiances.

Overall, the main results of this thesis demonstrate that the direct use of satellite TOA radiances to estimate ET is feasible and applicable. The accuracy is comparable with those satellite products based estimates. The notable advantage of the present method is that fewer assumptions are required and no complex atmospheric corrections are needed. It should facilitate direct use of satellite data for determining ET and relevant applications as well.

6.2 Outlook

Although the present study has made some progress in estimating ET using TOA radiances, there is still some interesting work that could be carried out in the future.

- The ET parameterization scheme proposed in this thesis is only applicable for daily scale. It is still a challenge to estimate weekly/monthly/yearly ET over different spatial scales. Due to the influence of clouds, the polar orbiting satellites data (e.g., MODIS) only has intermittent coverage so that estimates of ET are only limited to clear sky conditions. The possibility of solving this problem is to develop gap filling theory and integrate data from different satellite/sensor systems, such as data from passive microwave sensors which are not affected by clouds, and geostationary sensors which have high temporal resolution.

- The reliability and accuracy of the ET estimates are evaluated using in situ measurements in this thesis. This is feasible and applicable at pixel scale, but the validations over regional/global scales and long time periods are still to be

considered. One possible solution is to validate the remote sensing derived ET over basin scale by constructing the water balance equation from ground-based measurements. Besides, inter comparisons of ET estimates from different satellite based methods and land surface models are also interesting.

Bibliography

Amiro, B. D., Barr, A. G., Black, T. A., Iwashita, H., Kljun, N., McCaughey, J. H., Morgenstern, K., Murayama, S., Nesic, Z., Orchansky, A. L., and Saigusa, N.: Carbon, energy and water fluxes at mature and disturbed forest sites, Saskatchewan, Canada, *Agricultural and Forest Meteorology*, 136(3–4):237-251, 2006.

Ammann, C., Flechard, C. R., Leifeld, J., Neftel, A., and Fuhrer, J.: The carbon budget of newly established temperate grassland depends on management intensity, *Agriculture, Ecosystems & Environment*, 121(1–2):5-20, 2007.

Anderson, M. C., Norman, J. M., Kustas, W. P., Li, F., Prueger, J. H., and Mecikalski, J. R.: Effects of Vegetation Clumping on Two–Source Model Estimates of Surface Energy Fluxes from an Agricultural Landscape during SMACEX, *Journal of Hydrometeorology*, 6(6):892-909, 2005.

Atitar, M., and Sobrino, J. A.: A split-window algorithm for estimating LST from Meteosat 9 data: Test and comparison with in situ data and MODIS LSTs, *IEEE Geoscience and Remote Sensing Letters*, 6(1):122-126, 2009.

Aubinet, M., Grelle, A., Ibrom, A., Rannik, Ü., Moncrieff, J., Foken, T., Kowalski, A. S., Martin, P. H., Berbigier, P., Bernhofer, C., Clement, R., Elbers, J., Granier, A., Grünwald, T., Morgenstern, K., Pilegaard, K., Rebmann, C., Snijders, W., Valentini, R., and Vesala, T.: Estimates of the Annual Net Carbon and Water Exchange of Forests: The EUROFLUX Methodology, in: Advances in Ecological Research, edited by: Fitter, A. H., and Raffaelli, D. G., Academic Press, 113-175, 1999.

Aubinet, M., Grelle, A., Ibrom, A., Rannik, Ü., Moncrieff, J., Foken, T., Kowalski, A., Martin, P., Berbigier, P., and Bernhofer, C.: Estimates of the annual net carbon and water exchange of forests: the EUROFLUX methodology, *Advances in Ecological Research*, 30:113-175, 2000.

Baldocchi, D., Falge, E., Gu, L., Olson, R., Hollinger, D., Running, S., Anthoni, P., Bernhofer, C., Davis, K., Evans, R., Fuentes, J., Goldstein, A., Katul, G., Law, B., Lee, X., Malhi, Y., Meyers, T., Munger, W., Oechel, W., Paw, K. T., Pilegaard, K., Schmid, H. P., Valentini, R., Verma, S., Vesala, T., Wilson, K., and Wofsy, S.: FLUXNET: A New Tool to Study the Temporal and Spatial Variability of Ecosystem– Scale Carbon Dioxide, Water Vapor, and Energy Flux Densities, *Bulletin of the American Meteorological Society*, 82(11):2415-2434, 2001.

BIBLIOGRAPHY

Baldocchi, D.: 'Breathing'of the terrestrial biosphere: lessons learned from a global network of carbon dioxide flux measurement systems, *Australian Journal of Botany*, 56(1):1-26, 2008.

Barr, A. G., van der Kamp, G., Black, T. A., McCaughey, J. H., and Nesic, Z.: Energy balance closure at the BERMS flux towers in relation to the water balance of the White Gull Creek watershed 1999–2009, *Agricultural and Forest Meteorology*, 153(0):3-13, 2012.

Bateni, S. M., Entekhabi, D., and Castelli, F.: Mapping evaporation and estimation of surface control of evaporation using remotely sensed land surface temperature from a constellation of satellites, *Water Resources Research*, 49(2):950-968, 2013.

Batra, N., Islam, S., Venturini, V., Bisht, G., and Jiang, L.: Estimation and comparison of evapotranspiration from MODIS and AVHRR sensors for clear sky days over the Southern Great Plains, *Remote Sensing of Environment*, 103(1):1-15, 2006.

Becker, F., and Li, Z.-L.: Towards a local split window method over land surfaces, *International Journal of Remote Sensing*, 11(3):369 - 393, 1990.

Berk, A., Bernstein, L. S., Anderson, G. P., Acharya, P. K., Robertson, D. C., Chetwynd, J. H., and Adler-Golden, S. M.: MODTRAN Cloud and Multiple Scattering Upgrades with Application to AVIRIS, *Remote Sensing of Environment*, 65(3):367-375, 1998.

Bhattacharya, B. K., Mallick, K., Patel, N. K., and Parihar, J. S.: Regional clear sky evapotranspiration over agricultural land using remote sensing data from Indian geostationary meteorological satellite, *Journal of Hydrology*, 387(1-2):65-80, 2010.

Bisht, G., Venturini, V., Islam, S., and Jiang, L.: Estimation of the net radiation using MODIS (Moderate Resolution Imaging Spectroradiometer) data for clear sky days, *Remote Sensing of Environment*, 97(1):52-67, 2005.

Bisht, G., and Bras, R. L.: Estimation of net radiation from the MODIS data under all sky conditions: Southern Great Plains case study, *Remote Sensing of Environment*, 114(7):1522-1534, 2010.

Bolstad, P. V., Davis, K. J., Martin, J., Cook, B. D., and Wang, W.: Component and whole-system respiration fluxes in northern deciduous forests, *Tree Physiology*,

24(5):493-504, 2004.

Brutsaert, W., and Sugita, M.: Application of self-preservation in the diurnal evolution of the surface energy budget to determine daily evaporation, *Journal of Geophysical Research*, 97(D17):18377-18382, 1992.

Caparrini, F., Castelli, F., and Entekhabi, D.: Mapping of land-atmosphere heat fluxes and surface parameters with remote sensing data, *Boundary-Layer Meteorology*, 107(3):605-633, 2003.

Caparrini, F., Castelli, F., and Entekhabi, D.: Estimation of Surface Turbulent Fluxes through Assimilation of Radiometric Surface Temperature Sequences, *Journal of Hydrometeorology*, 5(1):145-159, 2004.

Carlson, T.: An Overview of the "Triangle Method" for Estimating Surface Evapotranspiration and Soil Moisture from Satellite Imagery, *Sensors*, 7(8):1612-1629, 2007.

Carlson, T. N., Perry, E. M., and Schmugge, T. J.: Remote estimation of soil moisture availability and fractional vegetation cover for agricultural fields, *Agricultural and Forest Meteorology*, 52(1-2):45-69, 1990.

Carlson, T. N., Gillies, R. R., and Perry, E. M.: A method to make use of thermal infrared temperature and NDVI measurements to infer surface soil water content and fractional vegetation cover, *Remote Sensing Reviews*, 9(1):161 - 173, 1994.

Carlson, T. N., Gillies, R. R., and Schmugge, T. J.: An interpretation of methodologies for indirect measurement of soil water content, *Agricultural and Forest Meteorology*, 77(3-4):191-205, 1995.

Chahine, M. T.: The hydrological cycle and its influence on climate, *Nature*, 359(6394):373-380, 1992.

Chávez, J., Neale, C., Prueger, J., and Kustas, W.: Daily evapotranspiration estimates from extrapolating instantaneous airborne remote sensing ET values, *Irrigation Science*, 27(1):67-81, 2008.

Choi, M., Kustas, W. P., Anderson, M. C., Allen, R. G., Li, F., and Kjaersgaard, J. H.: An intercomparison of three remote sensing-based surface energy balance algorithms over a corn and soybean production region (Iowa, U.S.) during

SMACEX, *Agricultural and Forest Meteorology*, 149(12):2082-2097, 2009.

Cleugh, H. A., Leuning, R., Mu, Q., and Running, S. W.: Regional evaporation estimates from flux tower and MODIS satellite data, *Remote Sensing of Environment*, 106(3):285-304, 2007.

Coll, C., Caselles, V., Sobrino, J. A., and Valor, E.: On the atmospheric dependence of the split-window equation for land surface temperature, *International Journal of Remote Sensing*, 15(1):105-122, 1994.

Coll, C., Caselles, V., Galve, J. M., Valor, E., Niclòs, R., and Sánchez, J. M.: Evaluation of split-window and dual-angle correction methods for land surface temperature retrieval from Envisat/Advanced Along Track Scanning Radiometer (AATSR) data, *Journal of Geophysical Research*, 111(D12):D12105, 2006.

Coll, C., Galve, J. M., Sanchez, J. M., and Caselles, V.: Validation of Landsat-7/ETM+ Thermal-Band Calibration and Atmospheric Correction With Ground-Based Measurements, *IEEE Transactions on Geoscience and Remote Sensing*, 48(1):547-555, 2010.

Cook, B. D., Davis, K. J., Wang, W., Desai, A., Berger, B. W., Teclaw, R. M., Martin, J. G., Bolstad, P. V., Bakwin, P. S., Yi, C., and Heilman, W.: Carbon exchange and venting anomalies in an upland deciduous forest in northern Wisconsin, USA, *Agricultural and Forest Meteorology*, 126(3–4):271-295, 2004.

Courault, D., Clastre, P., Cauchi, P., and Delécolle, R.: Analysis of spatial variability of air temperature at regional scale using remote sensing data and a SVAT model, Proceedings of the First International Conference Geospatial Information in Agriculture and Forestry, Lake Buena Vista, Florida, USA, June 1-3, 1998.

Courault, D., Seguin, B., and Olioso, A.: Review on estimation of evapotranspiration from remote sensing data: From empirical to numerical modeling approaches, *Irrigation and Drainage Systems*, 19(3):223-249, 2005.

Crago, R. D., and Brutsaert, W.: Daytime evaporation and the self-preservation of the evaporative fraction and the Bowen ratio, *Journal of Hydrology*, 178(1–4):241-255, 1996.

Crago, R. D., and Brutsaert, W.: A comparison of several evaporation equations, *Water Resources Research*, 28(3):951-954, 1992.

Crago, R. D.: Conservation and variability of the evaporative fraction during the daytime, *Journal of Hydrology*, 180(1-4):173-194, 1996.

Cristóbal, J., Jiménez-Muñoz, J. C., Sobrino, J. A., Ninyerola, M., and Pons, X.: Improvements in land surface temperature retrieval from the Landsat series thermal band using water vapor and air temperature, *Journal of Geophysical Research*, 114(D8):D08103, 2009.

Curtis, P. S., Hanson, P. J., Bolstad, P., Barford, C., Randolph, J. C., Schmid, H. P., and Wilson, K. B.: Biometric and eddy-covariance based estimates of annual carbon storage in five eastern North American deciduous forests, *Agricultural and Forest Meteorology*, 113(1–4):3-19, 2002.

Dash, P., Göttsche, F.-M., Olesen, F.-S., and Fischer, H.: Land surface temperature and emissivity estimation from passive sensor data: theory and practice-current trends, *International Journal of Remote Sensing*, 23(13):2563 - 2594, 2002.

Davies, J. A., and Allen, C. D.: Equilibrium, Potential and Actual Evaporation from Cropped Surfaces in Southern Ontario, *Journal of Applied Meteorology*, 12(4):649-657, 1973.

Delogu, E., Boulet, G., Olioso, A., Coudert, B., Chirouze, J., Ceschia, E., Le Dantec, V., Marloie, O., Chehbouni, G., and Lagouarde, J. P.: Reconstruction of temporal variations of evapotranspiration using instantaneous estimates at the time of satellite overpass, *Hydrology and Earth System Sciences*, 16:2995-3010, 2012.

Dozier, J.: A method for satellite identification of surface temperature fields of subpixel resolution, *Remote Sensing of Environment*, 11:221-229, 1981.

Dugas, W., Fritschen, L., Gay, L., Held, A., Matthias, A., Reicosky, D., Steduto, P., and Steiner, J.: Bowen ratio, eddy correlation, and portable chamber measurements of sensible and latent heat flux over irrigated spring wheat, *Agricultural and Forest Meteorology*, 56(1-2):1-20, 1991.

Eichinger, W. E., Parlange, M. B., and Stricker, H.: On the Concept of Equilibrium Evaporation and the Value of the Priestley-Taylor Coefficient, *Water Resources Research*, 32(1):161-164, 1996.

Farah, H., Bastiaanssen, W., and Feddes, R.: Evaluation of the temporal variability of the evaporative fraction in a tropical watershed, *International Journal of Applied*

Earth Observation and Geoinformation, 5(2):129-140, 2004.

Farahani, H. J., Howell, T. A., Shuttleworth, W. J., and Bausch, W. C.: Evapotranspiration: Progress in measurement and modeling in agriculture, *Transactions of the Asabe*, 50(5):1627-1638, 2007.

Fischer, M. L., Billesbach, D. P., Berry, J. A., Riley, W. J., and Torn, M. S.: Spatiotemporal Variations in Growing Season Exchanges of CO2, H2O, and Sensible Heat in Agricultural Fields of the Southern Great Plains, *Earth Interactions*, 11(17):1-21, 2007.

Foken, T.: The energy balance closure problem: An overview, *Ecological Applications*, 18(6):1351-1367, 2008.

Foken, T., Aubinet, M., Finnigan, J. J., Leclerc, M. Y., Mauder, M., and Paw U, K. T.: Results Of A Panel Discussion About The Energy Balance Closure Correction For Trace Gases, *Bulletin of the American Meteorological Society*, 92(4):ES13-ES18, 2011.

Franc, G. B., and Cracknell, A. P.: Retrieval of land and sea surface temperature using NOAA-11 AVHRR· data in north-eastern Brazil, *International Journal of Remote Sensing*, 15(8):1695 - 1712, 1994.

Freitas, S. C., Trigo, I. F., Bioucas-Dias, J. M., and Gottsche, F. M.: Quantifying the Uncertainty of Land Surface Temperature Retrievals From SEVIRI/Meteosat, *IEEE Transactions on Geoscience and Remote Sensing*, 48(1):523-534, 2010.

Frey, R. A., Ackerman, S. A., Liu, Y., Strabala, K. I., Zhang, H., Key, J. R., and Wang, X.: Cloud detection with MODIS. Part I: Improvements in the MODIS cloud mask for collection 5, *Journal of Atmospheric and Oceanic Technology*, 25(7):1057-1072, 2008.

Galleguillos, M., Jacob, F., Prévot, L., French, A., and Lagacherie, P.: Comparison of two temperature differencing methods to estimate daily evapotranspiration over a Mediterranean vineyard watershed from ASTER data, *Remote Sensing of Environment*, 115(6):1326-1340, 2011.

Galve, J. A., Coll, C., Caselles, V., and Valor, E.: An atmospheric radiosounding database for generating land surface temperature algorithms, *IEEE Transactions on Geoscience and Remote Sensing*, 46(5):1547-1557, 2008.

Garatuza-Payan, J., Pinker, R. T., Shuttleworth, W. J., and Watts, C. J.: Solar radiation and evapotranspiration in northern Mexico estimated from remotely sensed measurements of cloudiness, *Hydrological Sciences Journal*, 46(3):465-478, 2001.

Gentine, P., Entekhabi, D., Chehbouni, A., Boulet, G., and Duchemin, B.: Analysis of evaporative fraction diurnal behaviour, *Agricultural and Forest Meteorology*, 143(1–2):13-29, 2007.

Gentine, P., Entekhabi, D., and Polcher, J.: The Diurnal Behavior of Evaporative Fraction in the Soil–Vegetation–Atmospheric Boundary Layer Continuum, *Journal of Hydrometeorology*, 12(6):1530-1546, 2011.

Gillies, R. R., and Carlson, T. N.: Thermal Remote Sensing of Surface Soil Water Content with Partial Vegetation Cover for Incorporation into Climate Models, *Journal of Applied Meteorology*, 34(4):745-756, 1995.

Gillies, R. R., Kustas, W. P., and Humes, K. S.: A verification of the 'triangle' method for obtaining surface soil water content and energy fluxes from remote measurements of the Normalized Difference Vegetation Index (NDVI) and surface e, *International Journal of Remote Sensing*, 18(15):3145 - 3166, 1997.

Gilmanov, T. G., Tieszen, L. L., Wylie, B. K., Flanagan, L. B., Frank, A. B., Haferkamp, M. R., Meyers, T. P., and Morgan, J. A.: Integration of CO2 flux and remotely-sensed data for primary production and ecosystem respiration analyses in the Northern Great Plains: potential for quantitative spatial extrapolation, *Global Ecology and Biogeography*, 14(3):271-292, 2005.

Gilmanov, T. G., Soussana, J. F., Aires, L., Allard, V., Ammann, C., Balzarolo, M., Barcza, Z., Bernhofer, C., Campbell, C. L., Cernusca, A., Cescatti, A., Clifton-Brown, J., Dirks, B. O. M., Dore, S., Eugster, W., Fuhrer, J., Gimeno, C., Gruenwald, T., Haszpra, L., Hensen, A., Ibrom, A., Jacobs, A. F. G., Jones, M. B., Lanigan, G., Laurila, T., Lohila, A., G.Manca, Marcolla, B., Nagy, Z., Pilegaard, K., Pinter, K., Pio, C., Raschi, A., Rogiers, N., Sanz, M. J., Stefani, P., Sutton, M., Tuba, Z., Valentini, R., Williams, M. L., and Wohlfahrt, G.: Partitioning European grassland net ecosystem CO2 exchange into gross primary productivity and ecosystem respiration using light response function analysis, *Agriculture, Ecosystems & Environment*, 121(1–2):93-120, 2007.

Glenn, E., Nagler, P., and Huete, A.: Vegetation Index Methods for Estimating

Evapotranspiration by Remote Sensing, *Surveys in Geophysics*, 31(6):531-555, 2010.

Goetz, S. J.: Multi-sensor analysis of NDVI, surface temperature and biophysical variables at a mixed grassland site, *International Journal of Remote Sensing*, 18(1):71-94, 1997.

Gómez, M., Olioso, A., Sobrino, J. A., and Jacob, F.: Retrieval of evapotranspiration over the Alpilles/ReSeDA experimental site using airborne POLDER sensor and a thermal camera, *Remote Sensing of Environment*, 96(3–4):399-408, 2005.

Gowda, P., Chavez, J., Colaizzi, P., Evett, S., Howell, T., and Tolk, J.: ET mapping for agricultural water management: present status and challenges, *Irrigation Science*, 26(3):223-237, 2008.

Guo, H., Hu, Q., and Jiang, T.: Annual and seasonal streamflow responses to climate and land-cover changes in the Poyang Lake basin, China, *Journal of Hydrology*, 355(1-4):106-122, 2008.

Hall, F. G., Huemmrich, K. F., Goetz, S. J., Sellers, P. J., and Nickeson, J. E.: Satellite Remote Sensing of Surface Energy Balance: Success, Failures, and Unresolved Issues in FIFE, *Journal of Geophysical Research*, 97(D17):19061-19089, 1992.

Han, Y., Wang, Y., and Zhao, Y.: Estimating soil moisture conditions of the greater Changbai Mountains by land surface temperature and NDVI, *IEEE Transactions on Geoscience and Remote Sensing*, 48(6):2509-2515, 2010.

Hoedjes, J., Chehbouni, A., Jacob, F., Ezzahar, J., and Boulet, G.: Deriving daily evapotranspiration from remotely sensed instantaneous evaporative fraction over olive orchard in semi-arid Morocco, *Journal of Hydrology*, 354(1-4):53-64, 2008.

Houser, P. R., Shuttleworth, W. J., Famiglietti, J. S., Gupta, H. V., Syed, K. H., and Goodrich, D. C.: Integration of soil moisture remote sensing and hydrologic modeling using data assimilation, *Water Resources Research*, 34(12):3405-3420, 1998.

Humes, K. S., Kustas, W. P., Moran, M. S., Nichols, W. D., and Weltz, M. A.: Variability of emissivity and surface temperature over a sparsely vegetated surface, *Water Resources Research*, 30(5):1299-1310, 1994.

Jia, L., Xi, G., Liu, S., Huang, C., Yan, Y., and Liu, G.: Regional estimation of daily to annual regional evapotranspiration with MODIS data in the Yellow River Delta wetland, *Hydrology and Earth System Sciences*, 13(10):1775-1787, 2009.

Jiang, L., and Islam, S.: A methodology for estimation of surface evapotranspiration over large areas using remote sensing observations, *Geophysical Research Letters*, 26(17):2773-2776, 1999.

Jiang, L., and Islam, S.: Estimation of surface evaporation map over southern Great Plains using remote sensing data, *Water Resources Research*, 37(2):329-340, 2001.

Jiang, L., and Islam, S.: An intercomparison of regional latent heat flux estimation using remote sensing data, *International Journal of Remote Sensing*, 24(11):2221-2236, 2003.

Jiang, L., Islam, S., and Carlson, T. N.: Uncertainties in latent heat flux measurement and estimation: implications for using a simplified approach with remote sensing data, *Canadian Journal of Remote Sensing*, 30(5):769-787, 2004.

Jiang, L., Islam, S., Guo, W., Singh Jutla, A., Senarath, S. U. S., Ramsay, B. H., and Eltahir, E.: A satellite-based Daily Actual Evapotranspiration estimation algorithm over South Florida, *Global and Planetary Change*, 67(1–2):62-77, 2009.

Jiménez-Muñoz, J. C., and Sobrino, J. A.: A generalized single-channel method for retrieving land surface temperature from remote sensing data, *Journal of Geophysical Research*, 108(D22):4688, 2003.

Jiménez-Muñoz, J. C., Cristobal, J., Sobrino, J. A., Soria, G., Ninyerola, M., and Pons, X.: Revision of the Single-Channel Algorithm for Land Surface Temperature Retrieval From Landsat Thermal-Infrared Data, *IEEE Transactions on Geoscience and Remote Sensing*, 47(1):339-349, 2009.

Jiménez-Muñoz, J. C., and Sobrino, J. A.: A Single-Channel Algorithm for Land-Surface Temperature Retrieval From ASTER Data, *IEEE Geoscience and Remote Sensing Letters*, 7(1):176-179, 2010.

Jiménez, C., Prigent, C., Mueller, B., Seneviratne, S. I., McCabe, M. F., Wood, E. F., Rossow, W. B., Balsamo, G., Betts, A. K., Dirmeyer, P. A., Fisher, J. B., Jung, M., Kanamitsu, M., Reichle, R. H., Reichstein, M., Rodell, M., Sheffield, J., Tu, K., and Wang, K.: Global intercomparison of 12 land surface heat flux estimates,

Journal of Geophysical Research: Atmospheres, 116(D2):D02102, 2011.

Jin, Y., Randerson, J. T., and Goulden, M. L.: Continental-scale net radiation and evapotranspiration estimated using MODIS satellite observations, *Remote Sensing of Environment*, 115(9):2302-2319, 2011.

Jung, M., Reichstein, M., Ciais, P., Seneviratne, S. I., Sheffield, J., Goulden, M. L., Bonan, G., Cescatti, A., Chen, J., and de Jeu, R.: Recent decline in the global land evapotranspiration trend due to limited moisture supply, *Nature*, 467(7318):951-954, 2010.

Kalma, J., McVicar, T., and McCabe, M.: Estimating Land Surface Evaporation: A Review of Methods Using Remotely Sensed Surface Temperature Data, *Surveys in Geophysics*, 29(4):421-469, 2008.

Kerr, Y. H., Lagouarde, J. P., and Imbernon, J.: Accurate land surface temperature retrieval from AVHRR data with use of an improved split window algorithm, *Remote Sensing of Environment*, 41(2-3):197-209, 1992.

Kim, H.-Y., and Liang, S.: Development of a hybrid method for estimating land surface shortwave net radiation from MODIS data, *Remote Sensing of Environment*, 114(11):2393-2402, 2010.

Kim, J., and Hogue, T. S.: Evaluation of a MODIS-Based Potential Evapotranspiration Product at the Point Scale, *Journal of Hydrometeorology*, 9(3):444-460, 2008.

King, M. D., Menzel, W. P., Kaufman, Y. J., Tanré, D., Gao, B. C., Platnick, S., Ackerman, S. A., Remer, L. A., Pincus, R., and Hubanks, P. A.: Cloud and aerosol properties, precipitable water, and profiles of temperature and water vapor from MODIS, *IEEE Transactions on Geoscience and Remote Sensing*, 41(2):442-458, 2003.

Komatsu, T. S.: Toward a Robust Phenomenological Expression of Evaporation Efficiency for Unsaturated Soil Surfaces, *Journal of Applied Meteorology*, 42(9):1330-1334, 2003.

Kustas, W. P., Li, F., Jackson, T. J., Prueger, J. H., MacPherson, J. I., and Wolde, M.: Effects of remote sensing pixel resolution on modeled energy flux variability of croplands in Iowa, *Remote Sensing of Environment*, 92(4):535-547, 2004.

Lambin, E. F., and Ehrlich, D.: The surface temperature-vegetation index space for land cover and land-cover change analysis, *International Journal of Remote Sensing*, 17(3):463-487, 1996.

Lettau, H.: Evapotranspiration climatonomy, *Monthly weather review*, 97(10):691-699, 1969.

Lhomme, J. P., and Elguero, E.: Examination of evaporative fraction diurnal behaviour using a soil-vegetation model coupled with a mixed-layer model, *Hydrology and Earth System Sciences Discussions*, 3(2):259-270, 1999.

Li, S., Kang, S., Li, F., Zhang, L., and Zhang, B.: Vineyard evaporative fraction based on eddy covariance in an arid desert region of Northwest China, *Agricultural Water Management*, 95(8):937-948, 2008.

Li, Z.-L., Tang, B.-H., Wu, H., Ren, H., Yan, G., Wan, Z., Trigo, I. F., and Sobrino, J. A.: Satellite-derived land surface temperature: Current status and perspectives, *Remote Sensing of Environment*, 131(0):14-37, 2013.

Liu, B., Jiang, T., Zhai, J., and Zhang, W.: New Design and Observation of Lysimeter on Actual Evapotranspiration, *Meteorological Monthly*, 36(3):112-116, 2010.

Liu, B. Y. H., and Jordan, R. C.: The interrelationship and characteristic distribution of direct, diffuse and total solar radiation, *Solar Energy*, 4(3):1-19, 1960.

Liu, Y. B., Yamaguchi, Y., and Ke, C. Q.: Reducing the discrepancy between ASTER and MODIS land surface temperature products, *Sensors*, 7(12):3043-3057, 2007.

Long, D., and Singh, V. P.: A modified surface energy balance algorithm for land (M-SEBAL) based on a trapezoidal framework, *Water Resources Research*, 48(2):W02528, 2012a.

Long, D., and Singh, V. P.: A Two-source Trapezoid Model for Evapotranspiration (TTME) from satellite imagery, *Remote Sensing of Environment*, 121(0):370-388, 2012b.

Long, D., Singh, V. P., and Scanlon, B. R.: Deriving theoretical boundaries to address scale dependencies of triangle models for evapotranspiration estimation, *Journal of Geophysical Research: Atmospheres*, 117(D05113), 2012.

Margulis, S. A., Kim, J., and Hogue, T.: A Comparison of the Triangle Retrieval and

Variational Data Assimilation Methods for Surface Turbulent Flux Estimation, *Journal of Hydrometeorology*, 6(6):1063-1072, 2005.

McCabe, M., Wood, E., Su, H., Vinukollu, R., Ferguson, C., and Su, Z.: Multisensor Global Retrievals of Evapotranspiration for Climate Studies Using the Surface Energy Budget System, in: Land Remote Sensing and Global Environmental Change, edited by: Ramachandran, B., Justice, C. O., and Abrams, M. J., Remote Sensing and Digital Image Processing, Springer New York, 747-778, 2011.

McCabe, M. F., and Wood, E. F.: Scale influences on the remote estimation of evapotranspiration using multiple satellite sensors, *Remote Sensing of Environment*, 105(4):271-285, 2006.

McVicar, T. R., and Jupp, D. L. B.: Using covariates to spatially interpolate moisture availability in the Murray–Darling Basin: A novel use of remotely sensed data, *Remote Sensing of Environment*, 79(2–3):199-212, 2002.

Menzel, W. P., Seemann, S. W., Li, J., and Gumley, L. E.: MODISatmospheric profile retrieval algorithm theoretical basis document, University of Wisconsin-Madison, 2002.

Monteith, J. L.: Evaporation and surface temperature, *Quarterly Journal of the Royal Meteorological Society*, 107(451):1-27, 1981.

Moran, M. S., Clarke, T. R., Kustas, W. P., Weltz, M., and Amer, S. A.: Evaluation of hydrologic parameters in a semiarid rangeland using remotely sensed spectral data, *Water Resources Research*, 30(5):1287-1297, 1994.

Moser, G., and Serpico, S. B.: Automatic Parameter Optimization for Support Vector Regression for Land and Sea Surface Temperature Estimation From Remote Sensing Data, *IEEE Transactions on Geoscience and Remote Sensing*, 47(3):909-921, 2009.

Nagler, P. L., Scott, R. L., Westenburg, C., Cleverly, J. R., Glenn, E. P., and Huete, A. R.: Evapotranspiration on western U.S. rivers estimated using the Enhanced Vegetation Index from MODIS and data from eddy covariance and Bowen ratio flux towers, *Remote Sensing of Environment*, 97(3):337-351, 2005.

Nemani, R., Pierce, L., Running, S., and Goward, S.: Developing satellite-derived estimates of surface moisture status, *Journal of Applied Meteorology*,

32(3):548-557, 1993.

Nemani, R. R., and Running, S. W.: Estimation of regional surface resistance to evapotranspiration from NDVI and thermal-IR AVHRR data, *Journal of Applied Meteorology*, 28(4):276-284, 1989.

Nichols, W. E., and Cuenca, R. H.: Evaluation of the evaporative fraction for parameterization of the surface energy balance, *Water Resources Research*, 29(11):3681-3690, 1993.

Nishida, K., Nemani, R. R., Running, S. W., and Glassy, J. M.: An operational remote sensing algorithm of land surface evaporation, *Journal of Geophysical Research*, 108(D9):4270, 2003.

Oki, T., and Kanae, S.: Global hydrological cycles and world water resources, *Science*, 313(5790):1068, 2006.

Okogbue, E. C., Adedokun, J. A., and Holmgren, B.: Hourly and daily clearness index and diffuse fraction at a tropical station, Ile-Ife, Nigeria, *International Journal of Climatology*, 29(8):1035-1047, 2009.

Peng, J., and Liu, Y.: Estimation of evaporative fraction from top-of-atmosphere radiance, *IAHS-AISH publication*, 343:47-52, 2011.

Peng, J., Liu, Y., and Loew, A.: Uncertainties in Estimating Normalized Difference Temperature Index From TOA Radiances, *IEEE Transactions on Geoscience and Remote Sensing*, 51(5):2487 – 2497, 2013a.

Peng, J., Borsche, M., Liu, Y., and Loew, A.: How representative are instantaneous evaporative fraction measurements of daytime fluxes?, *Hydrology and Earth System Sciences*, 17(10):3913-3919, 2013b.

Peng, J., Liu, Y., Zhao, X., and Loew, A.: Estimation of evapotranspiration from MODIS TOA radiances in the Poyang Lake basin, China, *Hydrology and Earth System Sciences*, 17(4):1431-1444, 2013c.

Penman, H. L.: Natural evaporation from open water, bare soil and grass, *Proceedings of the Royal Society of London. Series A. Mathematical and Physical Sciences*, 193(1032):120-145, 1948.

Peres, L., and DaCamara, C.: Land surface temperature and emissivity estimation

based on the two-temperature method: sensitivity analysis using simulated MSG/SEVIRI data, *Remote Sensing of Environment*, 91(3-4):377-389, 2004.

Petropoulos, G., Carlson, T., Wooster, M., and Islam, S.: A review of Ts/VI remote sensing based methods for the retrieval of land surface energy fluxes and soil surface moisture, *Progress in Physical Geography*, 33(2):224-250, 2009.

Prata, A., and Cechet, R.: An assessment of the accuracy of land surface temperature determination from the GMS-5 VISSR, *Remote Sensing of Environment*, 67(1):1-14, 1999.

Prata, A. J.: Land Surface Temperatures Derived From the Advanced Very High Resolution Radiometer and the Along-Track Scanning Radiometer 1. Theory, *Journal of Geophysical Research*, 98(D9):16689-16702, 1993.

Prata, A. J., Caselles, V., Coll, C., Sobrino, J. A., and Ottlé, C.: Thermal remote sensing of land surface temperature from satellites: Current status and future prospects, *Remote Sensing Reviews*, 12(3):175 - 224, 1995.

Price, J.: Using spatial context in satellite data to infer regional scaleevapotranspiration, *IEEE Transactions on Geoscience and Remote Sensing*, 28(5):940-948, 1990a.

Price, J. C.: Estimating surface temperatures from satellite thermal infrared data--A simple formulation for the atmospheric effect, *Remote Sensing of Environment*, 13(4):353-361, 1983.

Price, J. C.: Using spatial context in satellite data to infer regional scale evapotranspiration, *IEEE Transactions on Geoscience and Remote Sensing*, 28(5):940-948, 1990b.

Priestley, C., and Taylor, R.: On the assessment of surface heat flux and evaporation using large-scale parameters, *Monthly weather review*, 100(2):81-92, 1972.

Qin, Z., and Karnieli, A.: Progress in the remote sensing of land surface temperature and ground emissivity using NOAA-AVHRR data, *International Journal of Remote Sensing*, 20(12):2367 - 2393, 1999.

Qin, Z., Dall'Olmo, G., Karnieli, A., and Berliner, P.: Derivation of split window algorithm and its sensitivity analysis for retrieving land surface temperature from

NOAA-advanced very high resolution radiometer data, *Journal of Geophysical Research*, 106(D19):22655-22670, 2001.

Reichstein, M., Rey, A., Freibauer, A., Tenhunen, J., Valentini, R., Banza, J., Casals, P., Cheng, Y., Grünzweig, J. M., Irvine, J., Joffre, R., Law, B. E., Loustau, D., Miglietta, F., Oechel, W., Ourcival, J.-M., Pereira, J. S., Peressotti, A., Ponti, F., Qi, Y., Rambal, S., Rayment, M., Romanya, J., Rossi, F., Tedeschi, V., Tirone, G., Xu, M., and Yakir, D.: Modeling temporal and large-scale spatial variability of soil respiration from soil water availability, temperature and vegetation productivity indices, *Global Biogeochemical Cycles*, 17(4):1104, 2003.

Reichstein, M., Falge, E., Baldocchi, D., Papale, D., Aubinet, M., Berbigier, P., Bernhofer, C., Buchmann, N., Gilmanov, T., Granier, A., Grünwald, T., Havránková, K., Ilvesniemi, H., Janous, D., Knohl, A., Laurila, T., Lohila, A., Loustau, D., Matteucci, G., Meyers, T., Miglietta, F., Ourcival, J.-M., Pumpanen, J., Rambal, S., Rotenberg, E., Sanz, M., Tenhunen, J., Seufert, G., Vaccari, F., Vesala, T., Yakir, D., and Valentini, R.: On the separation of net ecosystem exchange into assimilation and ecosystem respiration: review and improved algorithm, *Global Change Biology*, 11(9):1424-1439, 2005.

Remer, L. A., Kaufman, Y. J., Tanré, D., Mattoo, S., Chu, D. A., Martins, J. V., Li, R. R., Ichoku, C., Levy, R. C., Kleidman, R. G., Eck, T. F., Vermote, E., and Holben, B. N.: The MODIS Aerosol Algorithm, Products, and Validation, *Journal of the Atmospheric Sciences*, 62(4):947-973, 2005.

Rey, A., Pegoraro, E., Tedeschi, V., De Parri, I., Jarvis, P. G., and Valentini, R.: Annual variation in soil respiration and its components in a coppice oak forest in Central Italy, *Global Change Biology*, 8(9):851-866, 2002.

Rodriguez-Iturbe, I.: Ecohydrology: A hydrologic perspective of climate-soil-vegetation dynamics, *Water Resources Research*, 36(1):3-9, 2000.

Rowntree, P. R.: Atmospheric Parameterization Schemes for Evaporation over Land: Basic Concepts and Climate Modeling Aspects, in: Land Surface Evaporation, edited by: Schmugge, T., and André, J.-C., Springer New York, 5-29, 1991.

Running, S. W., Baldocchi, D. D., Turner, D. P., Gower, S. T., Bakwin, P. S., and Hibbard, K. A.: A Global Terrestrial Monitoring Network Integrating Tower Fluxes, Flask Sampling, Ecosystem Modeling and EOS Satellite Data, *Remote Sensing of*

Environment, 70(1):108-127, 1999.

Ryu, D., Jackson, T. J., Bindlish, R., Le Vine, D. M., and Haken, M.: Soil Moisture Retrieval Using a Two-Dimensional L-Band Synthetic Aperture Radiometer in a Semiarid Environment, *IEEE Transactions on Geoscience and Remote Sensing*, 48(12):4273-4284, 2010.

Sánchez, J. M., Scavone, G., Caselles, V., Valor, E., Copertino, V. A., and Telesca, V.: Monitoring daily evapotranspiration at a regional scale from Landsat-TM and ETM+ data: Application to the Basilicata region, *Journal of Hydrology*, 351(1-2):58-70, 2008.

Sandholt, I., Rasmussen, K., and Andersen, J.: A simple interpretation of the surface temperature/vegetation index space for assessment of surface moisture status, *Remote Sensing of Environment*, 79(2–3):213-224, 2002.

Schaaf, C. B., Gao, F., Strahler, A. H., Lucht, W., Li, X., Tsang, T., Strugnell, N. C., Zhang, X., Jin, Y., and Muller, J. P.: First operational BRDF, albedo nadir reflectance products from MODIS, *Remote Sensing of Environment*, 83(1-2):135-148, 2002.

Sellers, P., Dickinson, R., Randall, D., Betts, A., Hall, F., Berry, J., Collatz, G., Denning, A., Mooney, H., and Nobre, C.: Modeling the exchanges of energy, water, and carbon between continents and the atmosphere, *Science*, 275(5299):502-509, 1997.

Seneviratne, S. I., Luthi, D., Litschi, M., and Schar, C.: Land-atmosphere coupling and climate change in Europe, *Nature*, 443(7108):205-209, 2006.

Shu, Y., Stisen, S., Jensen, K. H., and Sandholt, I.: Estimation of regional evapotranspiration over the North China Plain using geostationary satellite data, *International Journal of Applied Earth Observation and Geoinformation*, 13(2):192-206, 2011.

Shuttleworth, W., Gurney, R., Hsu, A., and Ormsby, J.: FIFE: the variation in energy partition at surface flux sites, *IAHS Publication*, 186:67-74, 1989.

Shuttleworth, W. J.: Putting the 'vap'into evaporation, *Hydrology and Earth System Sciences*, 11(1):210-244, 2007.

Sobrino, J., Coll, C., and Caselles, V.: Atmospheric correction for land surface temperature using NOAA-11 AVHRR channels 4 and 5, *Remote Sensing of Environment*, 38(1):19-34, 1991.

Sobrino, J. A., Li, Z.-L., Stoll, M. P., and Becker, F.: Multi-channel and multi-angle algorithms for estimating sea and land surface temperature with ATSR data, *International Journal of Remote Sensing*, 17(11):2089 - 2114, 1996.

Sobrino, J. A., Raissouni, N., and Li, Z.-L.: A Comparative Study of Land Surface Emissivity Retrieval from NOAA Data, *Remote Sensing of Environment*, 75(2):256-266, 2001.

Sobrino, J. A., Jiménez-Muñoz, J. C., and Paolini, L.: Land surface temperature retrieval from LANDSAT TM 5, *Remote Sensing of Environment*, 90(4):434-440, 2004a.

Sobrino, J. A., Sòria, G., and Prata, A. J.: Surface temperature retrieval from Along Track Scanning Radiometer 2 data: Algorithms and validation, *Journal of Geophysical Research*, 109(D11):D11101, 2004b.

Sòria, G., and Sobrino, J. A.: ENVISAT/AATSR derived land surface temperature over a heterogeneous region, *Remote Sensing of Environment*, 111(4):409-422, 2007.

Stisen, S., Sandholt, I., Nørgaard, A., Fensholt, R., and Jensen, K. H.: Combining the triangle method with thermal inertia to estimate regional evapotranspiration — Applied to MSG-SEVIRI data in the Senegal River basin, *Remote Sensing of Environment*, 112(3):1242-1255, 2008.

Sugita, M., and Brutsaert, W.: Daily evaporation over a region from lower boundary layer profiles measured with radiosondes, *Water Resources Research*, 27(5):747-752, 1991.

Sun, D., and Kafatos, M.: Note on the NDVI-LST relationship and the use of temperature-related drought indices over North America, *Geophysical Research Letters*, 34(24):L24406, 2007.

Tang, B., Li, Z.-L., and Zhang, R.: A direct method for estimating net surface shortwave radiation from MODIS data, *Remote Sensing of Environment*, 103(1):115-126, 2006.

Tang, R., Li, Z.-L., and Tang, B.: An application of the Ts–VI triangle method with enhanced edges determination for evapotranspiration estimation from MODIS data in arid and semi-arid regions: Implementation and validation, *Remote Sensing of Environment*, 114(3):540-551, 2010.

Tang, R., Li, Z.-L., and Chen, K.-S.: Validating MODIS-derived land surface evapotranspiration with in situ measurements at two AmeriFlux sites in a semiarid region, *Journal of Geophysical Research*, 116(D4):D04106, 2011a.

Tang, R., Li, Z.-L., Chen, K.-S., Zhu, Y., and Liu, W.: Verification of land surface evapotranspiration estimation from remote sensing spatial contextual information, *Hydrological Processes*, 26(5): 2283–2293, 2011b.

Teuling, A. J., Van Loon, A. F., Seneviratne, S. I., Lehner, I., Aubinet, M., Heinesch, B., Bernhofer, C., Grünwald, T., Prasse, H., and Spank, U.: Evapotranspiration amplifies European summer drought, *Geophysical Research Letters*, Published online, DOI: 10.1002/grl.50495, 2013.

Toller, G. N., Isaacman, A., Kuyper, J., and Salomonson, V.: MODIS Level 1B Product User's Guide, *Greenbelt, MD: NASA/Goddard Space Flight Center*, 2006.

Trenberth, K. E., Smith, L., Qian, T., Dai, A., and Fasullo, J.: Estimates of the Global Water Budget and Its Annual Cycle Using Observational and Model Data, *Journal of Hydrometeorology*, 8(4):758-769, 2007.

Trenberth, K. E., Fasullo, J. T., and Kiehl, J.: Earth's Global Energy Budget, *Bulletin of the American Meteorological Society*, 90(3):311-323, 2009.

Twine, T. E., Kustas, W., Norman, J., Cook, D., Houser, P., Meyers, T., Prueger, J., Starks, P., and Wesely, M.: Correcting eddy-covariance flux underestimates over a grassland, *Agricultural and Forest Meteorology*, 103(3):279-300, 2000.

Valor, E., and Caselles, V.: Towards the use of temperature in desertification monitoring: Results of DeMon-I Project, Remote Sensing '96 - Integrated Applications for Risk Assessment and Disaster Prevention for the Mediterranean (Proceedings of the 16th EARSel Symposium, Malta), May 1996, ISI:A1997BH19Q00040, 1996a.

Valor, E., and Caselles, V.: Mapping land surface emissivity from NDVI: Application to European, African, and South American areas, *Remote Sensing of Environment*,

57(3):167-184, 1996b.

Van De Griend, A. A., and Owe, M.: On the relationship between thermal emissivity and the normalized difference vegetation index for natural surfaces, *International Journal of Remote Sensing*, 14(6):1119 - 1131, 1993.

Van Niel, T. G., McVicar, T. R., Roderick, M. L., van Dijk, A. I. J. M., Beringer, J., Hutley, L. B., and van Gorsel, E.: Upscaling latent heat flux for thermal remote sensing studies: Comparison of alternative approaches and correction of bias, *Journal of Hydrology*, 468–469(0):35-46, 2012.

Veenendaal, E. M., Kolle, O., and Lloyd, J.: Seasonal variation in energy fluxes and carbon dioxide exchange for a broad-leaved semi-arid savanna (Mopane woodland) in Southern Africa, *Global Change Biology*, 10(3):318-328, 2004.

Venturini, V., Bisht, G., Islam, S., and Jiang, L.: Comparison of evaporative fractions estimated from AVHRR and MODIS sensors over South Florida, *Remote Sensing of Environment*, 93(1-2):77-86, 2004.

Verma, S. B., Dobermann, A., Cassman, K. G., Walters, D. T., Knops, J. M., Arkebauer, T. J., Suyker, A. E., Burba, G. G., Amos, B., Yang, H., Ginting, D., Hubbard, K. G., Gitelson, A. A., and Walter-Shea, E. A.: Annual carbon dioxide exchange in irrigated and rainfed maize-based agroecosystems, *Agricultural and Forest Meteorology*, 131(1–2):77-96, 2005.

Vermote, E. F., El Saleous, N., Justice, C. O., Kaufman, Y. J., Privette, J. L., Remer, L., Roger, J. C., and Tanré, D.: Atmospheric correction of visible to middle-infrared EOS-MODIS data over land surfaces: Background, operational algorithm and validation, *Journal of Geophysical Research: Atmospheres*, 102(D14):17131-17141, 1997.

Vermote, E. F., and Kotchenova, S.: Atmospheric correction for the monitoring of land surfaces, *Journal of Geophysical Research*, 113(D23):D23S90, 2008.

Verstraeten, W., Veroustraete, F., and Feyen, J.: Assessment of Evapotranspiration and Soil Moisture Content Across Different Scales of Observation, *Sensors*, 8(1):70-117, 2008.

Vinukollu, R. K., Wood, E. F., Ferguson, C. R., and Fisher, J. B.: Global estimates of evapotranspiration for climate studies using multi-sensor remote sensing data:

Evaluation of three process-based approaches, *Remote Sensing of Environment*, 115(3):801-823, 2011.

Wan, Z., and Li, Z.-L.: A physics-based algorithm for retrieving land-surface emissivity and temperature from EOS/MODIS data, *IEEE Transactions on Geoscience and Remote Sensing*, 35(4):980-996, 1997.

Wan, Z., Wang, P., and Li, X.: Using MODIS Land Surface Temperature and Normalized Difference Vegetation Index products for monitoring drought in the southern Great Plains, USA, *International Journal of Remote Sensing*, 25(1):61-72, 2004.

Wan, Z. M., and Dozier, J.: A generalized split-window algorithm for retrieving land-surface temperature from space, *IEEE Transactions on Geoscience and Remote Sensing*, 34(4):892-905, 1996.

Wang, K., Li, Z., and Cribb, M.: Estimation of evaporative fraction from a combination of day and night land surface temperatures and NDVI: A new method to determine the Priestley–Taylor parameter, *Remote Sensing of Environment*, 102(3-4):293-305, 2006.

Wang, K., and Dickinson, R. E.: A review of global terrestrial evapotranspiration: Observation, modeling, climatology, and climatic variability, *Reviews of Geophysics*, 50(2):RG2005, 2012.

Wang, T., Ciais, P., Piao, S., Ottlé, C., Brender, P., Maignan, F., Arain, A., Cescatti, A., Gianelle, D., and Gough, C.: Controls on winter ecosystem respiration in temperate and boreal ecosystems, *Biogeosciences*, 8:2009-2025, 2011.

Wang, W., and Liang, S.: Estimation of high-spatial resolution clear-sky longwave downward and net radiation over land surfaces from MODIS data, *Remote Sensing of Environment*, 113(4):745-754, 2009.

Wang, W., Liang, S., and Augustine, J. A.: Estimating high spatial resolution clear-sky land surface upwelling longwave radiation from MODIS data, *IEEE Transactions on Geoscience and Remote Sensing*, 47(5):1559-1570, 2009.

Wilson, K., Goldstein, A., Falge, E., Aubinet, M., Baldocchi, D., Berbigier, P., Bernhofer, C., Ceulemans, R., Dolman, H., and Field, C.: Energy balance closure at FLUXNET sites, *Agricultural and Forest Meteorology*, 113(1):223-243, 2002.

Wilson, K. B., Baldocchi, D., Falge, E., Aubinet, M., Berbigier, P., Bernhofer, C., Dolman, H., Field, C., Goldstein, A., Granier, A., Hollinger, D., Katul, G., Law, B. E., Meyers, T., Moncrieff, J., Monson, R., Tenhunen, J., Valentini, R., Verma, S., and Wofsy, S.: Diurnal centroid of ecosystem energy and carbon fluxes at FLUXNET sites, *Journal of Geophysical Research: Atmospheres*, 108(D21):4664, 2003.

Wood, E. F.: Scaling behaviour of hydrological fluxes and variables: empirical studies using a hydrological model and remote sensing data, *Hydrological Processes*, 9(3‐4):331-346, 1995.

Wu, A., and Zhong, Q.: A method for determining the sensor degradation rates of NOAA AVHRR channels 1 and 2, *Journal of Applied Meteorology*, 33(1):118-122, 1994.

Yang, F., White, M. A., Michaelis, A. R., Ichii, K., Hashimoto, H., Votava, P., Zhu, A. X., and Nemani, R. R.: Prediction of continental-scale evapotranspiration by combining MODIS and AmeriFlux data through support vector machine, *IEEE Transactions on Geoscience and Remote Sensing*, 44(11):3452-3461, 2006.

Yu, Y., Tarpley, D., Privette, J. L., Goldberg, M. D., Rama Varma Raja, M., Vinnikov, K. Y., and Xu, H.: Developing Algorithm for Operational GOES-R Land Surface Temperature Product, *IEEE Transactions on Geoscience and Remote Sensing*, 47(3):936-951, 2009.

Appendix A

Supplementary material for Chapter 4

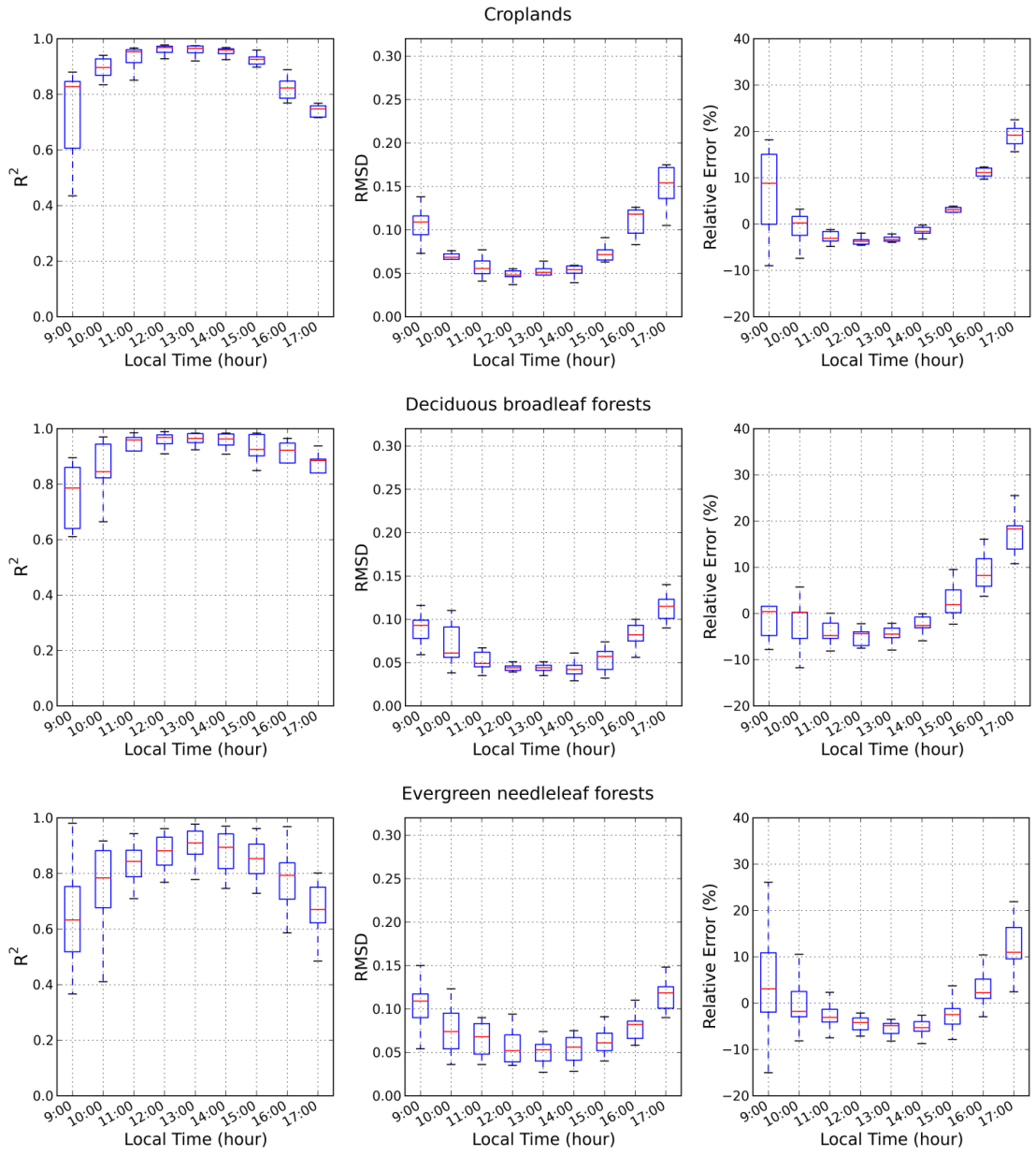

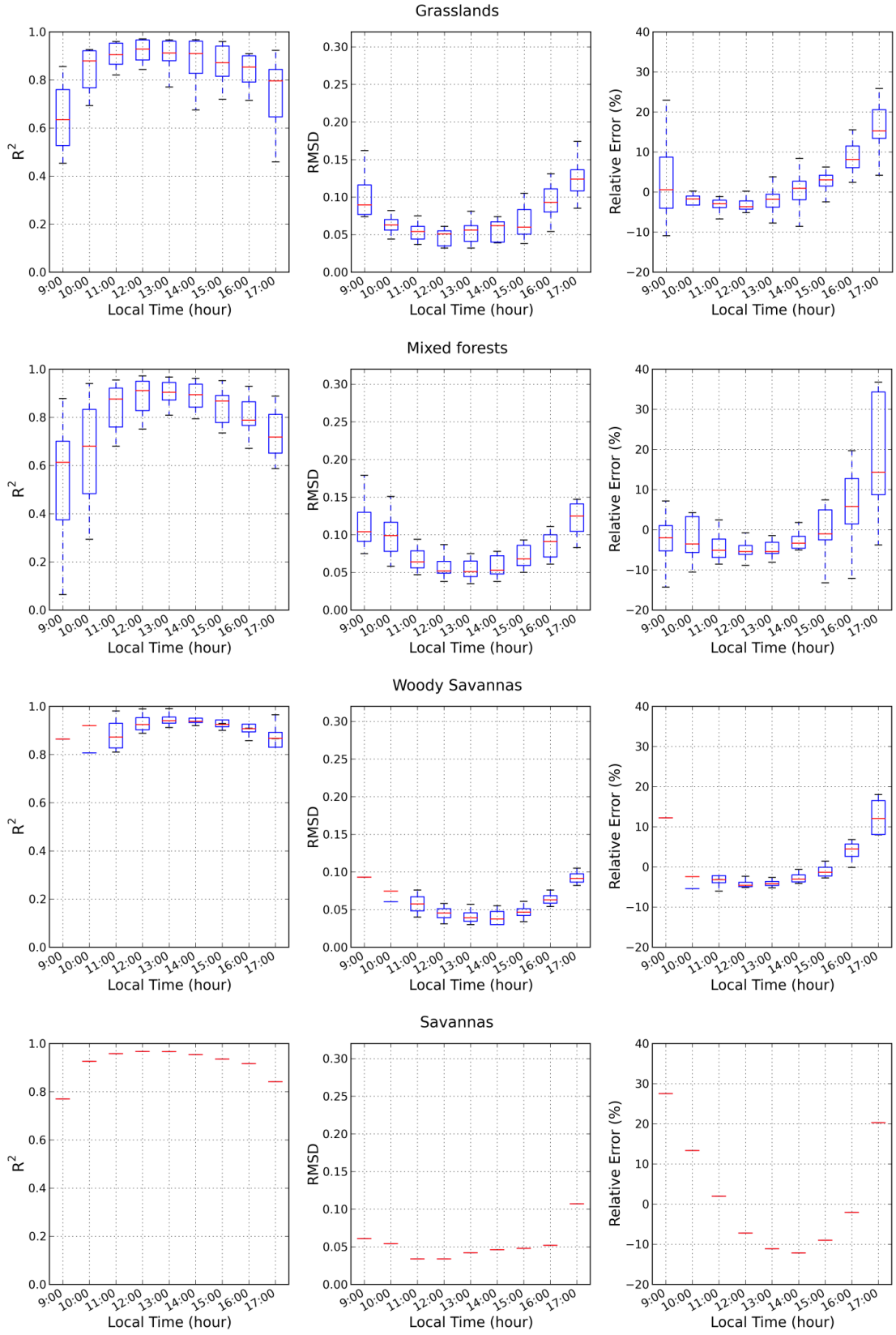
Grasslands
Mixed forests
Woody Savannas
Savannas
R2
RMSD
Relative Error (%)
Local Time (hour)
9:00
10:00
11:00
12:00
13:00
14:00
15:00
16:00
17:00

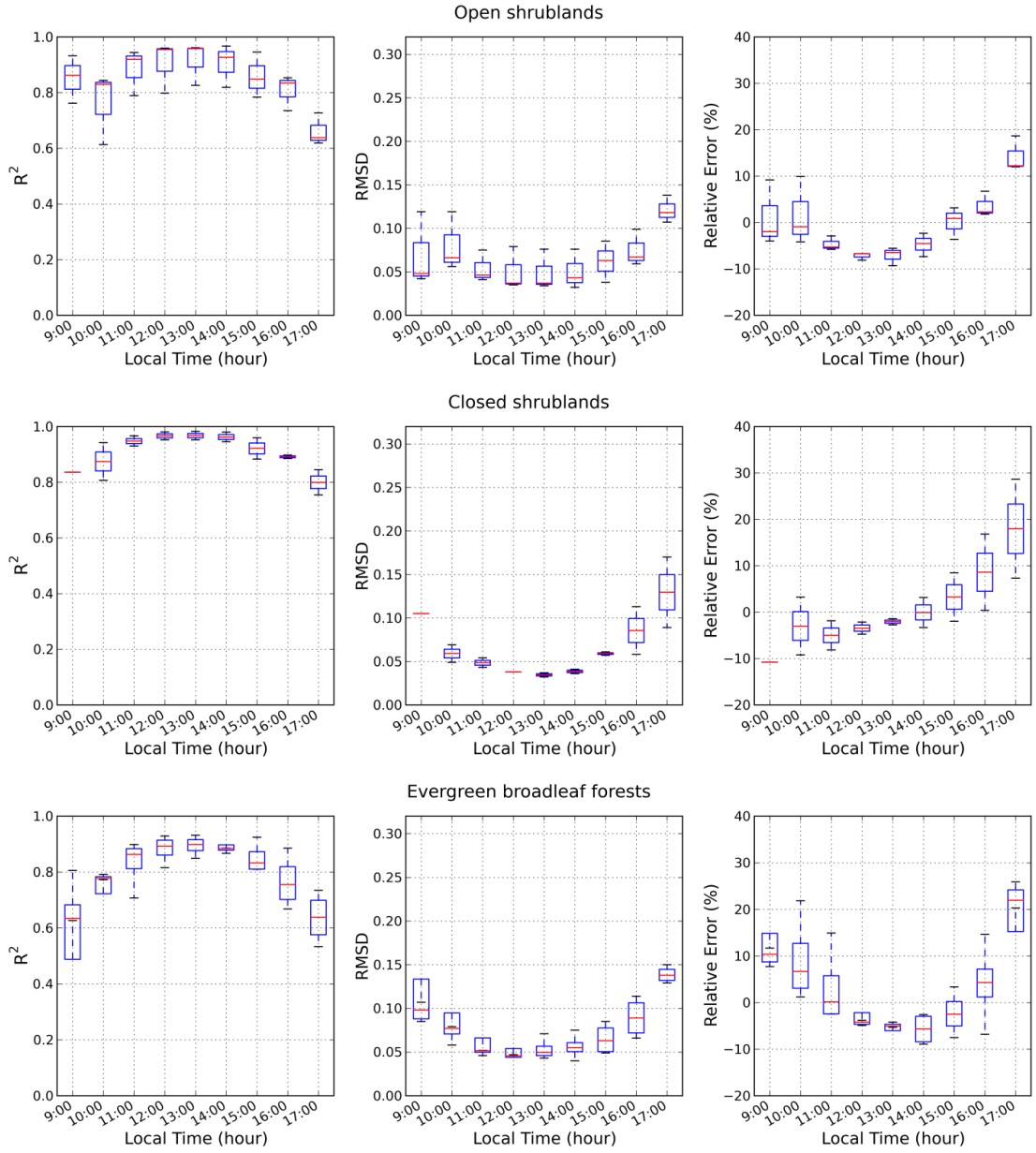

Figure A.1: Box plots of statistical results for the comparisons between instantaneous EF at different time of daytime and daytime EF for different biome types under clear sky conditions.

Appendix B

List of Publications

Peer-reviewed journal articles

- **Peng, J**., Liu, Y., and Loew, A.: Uncertainties in Estimating Normalized Difference Temperature Index From TOA Radiances, *IEEE Transactions on Geoscience and Remote Sensing*, 51(5):2487 – 2497, 2013.

- **Peng, J**., Liu, Y., Zhao, X., and Loew, A.: Estimation of evapotranspiration from MODIS TOA radiances in the Poyang Lake basin, China, *Hydrology and Earth System Sciences*, 17(4):1431-1444, 2013.

- **Peng, J**., Borsche, M., Liu, Y., and Loew, A.: How representative are instantaneous evaporative fraction measurements of daytime fluxes?, *Hydrology and Earth System Sciences*, 17(10):3913-3919, 2013.

Non peer-reviewed publications and abstracts

- **Peng, J**., Borsche, M., Loew, A.: How representative are instantaneous evaporativefraction measurements for daytime fluxes?, *Geophysical Research Abstracts*, Vol. 15, EGU2013-7265-1, 2013.

- **Peng, J**., Liu, Y., Loew, A.: Uncertaintiesin estimating Normalized DifferenceTemperature Index from TOA radiances. *Geophysical Research Abstracts*, Vol. 15, EGU2013-7368, 2013.

- **Peng, J**., Liu, Y., Zhao, X., and Loew, A.: A direct algorithm for estimating daily regional Evapotranspiration from modis TOA radiances, *2012 IEEE International Geoscience and Remote Sensing Symposium (IGARSS)*, 702-705, 2012.

- **Peng, J**., and Liu, Y.: Estimation of evaporative fraction from top-of-atmosphere radiance, *IAHS-AISH publication*, 343:47-52, 2011.

Acknowledgements

I would like to express my sincere gratitude to the people who have supported me during my PhD study. First and foremost, my deepest gratitude goes to my principal supervisor Alexander Löw for his excellent supervision, contribution and support throughout the research. I thank my co-advisor Stephan Bakan for his continuous help and advice. Also, I am grateful to Andreas Chlond for chairing my advisory panel. I thank Martin Claußen for providing me the opportunity to complete my PhD study in MPI-M (Max Planck Institute for Meteorology). I thank Michael Borsche for his scientific and technical advice. I extend sincere thanks to my former advisors Yuanbo Liu and Nan Jiang who supervised me and helped me to start my journey.

Many thanks to the IMPRS-ESM (International Max Planck Research School on Earth System Modelling), especially the coordinators Antje Weitz, Cornelia Kampmann, and Wiebke Böhm for their continuous support and kind assistance and patience. It has been my great pleasure to be part of IMPRS-ESM. I thank CAS-MPG Doctoral Promotion Programme for providing the financial support which made my PhD work possible.

I extend my sincere appreciation to CIS (Central IT Services) and library as well as administration staff for providing invaluable assistance and a great working environment. Special thanks go to Christina Rieckers from international office and Sylvia Houston from ‘Land in the Earth System’ department for their kind help and support.

I would also like to express my sincere appreciation to my fellow PhD students and friends, Jessica Engels, Victoria Naipal, Andreas Veira, Jörg Burdanowitz, Irina Petrova, Gernot Geppert, Thomas Schöngaßner, Thomas Keitzl, Zhuhua Li, Xueyuan Liu, Huan Zhang, Yuan Li, Kesheng Shu, Guoyuan Li, Shiqiang Zhang and all the others for their company and support throughout the last three years.

I warmly thank my office mates Katharina Kern, Thore Hansen and Mikhail Itkin for the nice time and interesting discussions we had together.

Last but not least I wish to express my gratitude and affection to my family for their love, understanding, support and encouragement during my endeavor to complete this work.



ISSN 1614-1199